

DISSERTATION

DEACTIVATION OF ZSM-5 DURING
CATALYTIC FAST PYROLYSIS OF BIOMASS

Submitted by

Alexander R. Stanton

Department of Chemical and Biological Engineering

In partial fulfillment of the requirements

For the Degree of Doctor of Philosophy

Colorado State University

Fort Collins, Colorado

Spring 2018

Doctoral Committee:

Advisor: Kenneth Reardon

Co-Advisor: Kristiina Iisa

David Dandy

Anthony Marchese

Gordon Smith

Copyright by Alexander R. Stanton 2018

All Rights Reserved

ABSTRACT

DEACTIVATION OF ZSM-5 DURING CATALYTIC FAST PYROLYSIS OF BIOMASS

To reduce the greenhouse gas footprint of the transportation industry and prepare for the economic impacts of global instability and oil scarcity, technologies and strategies must be developed to transition from petroleum-derived fuels to biomass-derived liquid fuels. For this transition to occur successfully in the short term, the biofuel must be a liquid hydrocarbon. Lignocellulosic biomass is an abundant, inexpensive biomass resource that does not compete with food production, making it an ideal candidate for biofuel production. Although many technologies are advancing towards this goal, catalytic fast pyrolysis (CFP) using ZSM-5 catalyst is extremely promising. During CFP, biomass is rapidly heated ($\sim 1000^{\circ}\text{C}/\text{s}$) in the absence of oxygen to a reaction temperature of $400\text{-}600^{\circ}\text{C}$ with a short residence time of 1-2 s. The resulting vapors are upgraded (deoxygenated) upon contact with a catalyst prior to condensation.

CFP, performed with ZSM-5 catalyst, allows for the direct generation of aromatic hydrocarbons (primarily: benzene, toluene, xylene, and naphthalenes) from lignocellulosic biomass, without requiring pretreatment. This conversion occurs via a two-step series of reactions, consisting of initial cracking reactions on the ZSM-5 surface followed by deoxygenation and aromatization reactions occurring within the ZSM-5 pores.

A primary hurdle for the large-scale deployment of CFP as a biofuel production method is coke formation on the catalyst. Coke is a solid, carbonaceous deposit which forms on the catalyst and causes a reversible deactivation, leading to the formation of oxygenated products. The carbon lost to coke also limits the overall conversion to desired products. The coke formation problem is exacerbated by the low hydrogen-to-carbon ratio in biomass. Despite the varied levels of deactivation experienced by individual catalyst particles within large-scale CFP reactors, little research has been conducted on ZSM-5 deactivation during CFP of biomass.

The overarching goal of this work is to advance the understanding of catalytic fast pyrolysis of biomass with ZSM-5 catalyst, in particular the process of catalyst deactivation, and guide future work towards enhancing its viability as a biofuel production process. This is accomplished by a) exploring how the products of catalytic fast pyrolysis change as the ZSM-5 catalyst progressively deactivates, b) studying the impact of catalyst properties (silica-to-alumina ratio and binder) on CFP, c) investigating the role of the two main component groups of lignocellulosic biomass (cellulose and lignin) in the deactivation of ZSM-5, and d) exploring metal modification of ZSM-5 and hydrogen addition in an effort to increase the hydrocarbon yield and improve catalyst performance.

Deactivation of ZSM-5 during CFP was studied by pyrolyzing and upgrading successive samples of biomass over a bed of catalyst and monitoring the products as the cumulative ratio of biomass pyrolyzed to catalyst bed weight (biomass:catalyst) increased, as well as characterizing and comparing fresh and post-reaction catalyst samples.

It was found that as the catalyst deactivated, the formation of fully upgraded aromatics decreased and that of primary pyrolysis vapors increased. In addition, products formed at intermediate

levels of catalyst deactivation that did not form at low or high biomass:catalyst, including phenol and alkylated phenols. These were shown to be the results of the catalytic upgrading process and not a result of partial deoxygenation of existing phenolic components in the pyrolysis vapors, as they were produced during the upgrading of cellulose vapors as well. A silica-to-alumina ratio of 30 within the ZSM-5 crystal gave the highest yield of t aromatics due to an optimal level of deoxygenation capability while not leading to excessive coke formation. The binder choice for ZSM-5 catalyst particles was also shown to be important, as alumina resulted in a significant decrease in catalyst efficacy, due to the imparted acidity from the binder leading to excessive cracking.

The study of deactivation by individual biopolymer revealed two types of coke-induced deactivation occurring during CFP of lignocellulosic biomass, one caused by the upgrading of lignin-derived pyrolysis vapors and the other caused by the upgrading of cellulose-derived pyrolysis vapors. Cellulose-induced deactivation occurs by the formation of coke resulting from an extension of the aromatization and ring-growth reactions. This coke prevents the secondary ring-growth step of upgrading, reducing the formation of aromatics, by blocking micropores and obstructing access to acid sites. Lignin-induced deactivation, caused by monomer deposition and coupling, inhibits the initial surface cracking reactions, limiting the material which can be further upgraded in the catalyst, and leading to the breakthrough of primary pyrolysis products.

However, the catalyst's acid sites remained accessible and active, allowing a stable yield of hydrocarbons to be produced. The loss of aromatic hydrocarbon formation during CFP of whole biomass is mainly the result of deactivation by the cellulosic components.

ZSM-5 catalysts modified with metals known to be active in hydrogen (Cu, Co, Ni, Pt, Ga) were prepared via incipient wetness impregnation and their deactivation was studied during CFP in

both inert and hydrogen atmospheres, with the hypothesis that coke formation would be reduced and hydrocarbon yield would be increased.

In an inert atmosphere, the formation of aromatic hydrocarbons was proportional to strong acid sites in the catalysts, and the main impact of the addition of metals was blocking acid sites responsible for aromatization. Hence, no catalyst out-performed unmodified ZSM-5 in terms of hydrocarbon yield. However, in the presence of added hydrogen, several metals reduced coke formation via hydrogenation of coke precursors, which resulted in slower deactivation. The results from CFP with Ni/ZSM-5 in hydrogen are of particular significance. The upgrading resulted in an overall oil composition with a more desirable ratio of hydrocarbons to oxygenates, compared to ZSM-5, while maintaining a comparable yield of hydrocarbons.

ACKNOWLEDGMENTS

First and foremost, I would like to acknowledge the monumental contributions to my successes made by Dr. Kristiina Iisa. Conducting my graduate research at NREL has been, at times, an alienating experience. I did not have immediate access to the graduate student peer-group or student-centric resources that are available on the CSU campus. As a result, Kristiina has taken on many roles throughout my time at NREL. She has been my day-to-day mentor, a source of personal and professional guidance, my confidant and my friend. She has invested considerable time and resources into my maturation as a scientist. She has always treated my opinions and interpretations with respect, and fostered in me the confidence to pursue independent lines of research. I will be forever grateful for her support.

Dr. Reardon has been at many key intersections during my transition into graduate studies and interest in renewable fuels, and I am grateful for his wisdom and aide. I first met Ken as an undergraduate intern through the Colorado Center for Biorefining and Biofuels research program. His passion and enthusiasm for renewable energy is palpable and inspiring. He is largely the reason that I applied to the NSF IGERT opportunity at CSU, and he became my adviser and instructor throughout that program. Ken has inspired me, and many many others, to strive for the level of mastery and breadth of understanding that he shows.

I would like to thank Dr. Anthony Marchese for the part he has played in my career path and for his advice and support as my committee member. Anthony was my first research adviser. I remember my summer interning at the Engines Lab fondly, and it ended up being a pivotal time in deciding my future path. He spoke frankly about the challenges and rewards of a career in

research and academia, and my time with him played a significant role in my decision to pursue graduate studies.

I would also like to thank Dr. Gordon Smith and Dr. David Dandy. As my committee members they have provided insight into my work and direction toward continued improvement. I am grateful for the time and energy they have devoted toward helping me advance.

I owe a lot to the Colorado Center for Biorefining and Biofuels undergraduate research internship. It is a wonderful program that introduced me, and many others, to the substantial research occurring at Colorado's research institutions, as well as providing a first opportunity to engage in meaningful research during pivotal times in our education.

My time at the National Renewable Energy Lab has been full of friendly, intelligent, and helpful people. I am particularly thankful for the members of the core team advised by Kristiina, during much of my tenure there: Dr. Rick French, Kellene Orton, Jim Stunkle, Michelle Myers, and Dr. Luc Moens. We were rarely working directly on the same projects, but our weekly meetings and brainstorming sessions were a valuable lesson in collaboration and the power of diverse perspectives when approaching a difficult issue. I always felt welcome, and that my insights were valued. I was very saddened to learn of Luc's passing, and I will always remember him as a kind and thoughtful man.

Additionally, I would like to thank my parents, Rob and Fran. Growing up, they indulged my endless curiosity and, in a time before Google, worked to find answers to my unrelenting questions. They have been the solid foundation upon which my life has been built.

Finally (and most importantly), I would like to thank my wife, Katie. She is my high school sweetheart, my most fierce supporter, and my best friend. She has been a source of unwavering

optimism, bad puns, and companionship. She has shouldered much of the burden of my prolonged graduate education, and done so with a smile and commendable grace. I would truly be lost without her.

I am extremely grateful for this team of people surrounding me, and am thankful for the roles they each have played in my personal and professional development.

TABLE OF CONTENTS

ABSTRACT.....	ii
ACKNOWLEDGMENTS	vi
1 Introduction	1
1.1 Biomass Feedstocks	1
1.2 Components of the Plant Cell Wall and General Conversion Pathways	4
1.3 Thermochemical Conversion and Fast Pyrolysis of Biomass	6
1.4 ZSM-5	8
1.5 Catalytic Fast Pyrolysis of Biomass with ZSM-5	12
1.6 Upgrading Mechanism of ZSM-5 during CFP of Biomass	15
1.7 Coke	17
1.8 Catalytic fast pyrolysis of individual biomass components	21
1.9 ZSM-5 Modification with Metals	23
2 Motivation for this work.....	26
2.1 Objectives.....	26
3 Experimental Methods and Materials.....	28
3.1 Catalyst Deactivation Experiments/ <i>ex situ</i> CFP.....	28
3.2 Reactors.....	29
3.2.1 Pyroprobe Reactor System.....	30
3.2.2 Tandem μ -Reactor System.....	34
3.2.3 Horizontal Packed-bed Reactor	38
3.3 Calibrations for Reactor Systems.....	39
3.4 Catalyst Characterization Techniques	41
3.4.1 Thermogravimetric Analysis	41
3.4.2 Ammonia Temperature Programmed Desorption.....	42
3.4.3 Nitrogen Physisorption	42
3.5 Biomass	43
3.6 Catalysts	43
3.6.1 Commercially-Available ZSM-5 Catalysts.....	43

3.6.2	Catalyst Modification.....	44
4	Deactivation Trend of ZSM-5 during CFP of Pine and Observation of Intermediate Pyrolysis Products.....	46
4.1	Products from the CFP of Pine with ZSM-5 Catalyst.....	46
4.2	Deactivation Trend of ZSM-5 during CFP of Pine.....	50
4.3	Observation of Intermediate Products.....	56
4.4	Section Conclusions.....	57
5	Impact of Silica-to-Alumina Ratio and Binder Type on the Efficacy of Upgrading During CFP of Pine with ZSM-5.....	59
5.1	Comparison of ZSM-5 Catalysts with a Variety of Silica-to-Alumina Ratios.....	59
5.2	Evaluation of ZSM-5 SAR30 Catalysts with Clay, Silica, and Alumina Binders.....	65
5.3	Section Conclusions.....	68
6	Qualitative Discussion of Products from the Catalytic and non-Catalytic Pyrolysis of Cellulose, Lignin, and Pine.....	70
6.1	Qualitative Comparison of the uncatalyzed pyrolysis of cellulose, lignin, and pine.....	70
6.2	Qualitative Comparison of the CFP of cellulose, lignin, and pine.....	75
6.3	Section Conclusions.....	78
7	Deactivation of ZSM-5 by Pine and Individual Biopolymers.....	79
7.1	Deactivation of ZSM-5 by cellulose.....	80
7.2	Deactivation of ZSM-5 by lignin.....	85
7.3	Deactivation of ZSM-5 by Pine.....	88
7.4	Deactivation trends during CFP of pine and individual biopolymers.....	91
7.5	Post-reaction catalyst analysis.....	96
7.6	Section Conclusions.....	102
8	CFP with metal-modified ZSM-5 in inert and hydrogen atmospheres.....	103
8.1	Fresh Metal-modified Catalyst Properties.....	105
8.2	Catalytic Fast Pyrolysis Reaction Results.....	109
8.3	Post-reaction Catalyst Characterization and Analysis.....	115
8.4	Section Conclusions.....	121

9	Conclusions and Future Work	123
9.1	Conclusions	123
9.2	Future Work	125
10	References	128

1 Introduction

To mitigate greenhouse gas emissions and prepare for the economic impacts of shrinking oil reserves and global instability, technologies and strategies are being developed to transition from petroleum-derived fuels to biomass-derived liquid fuels on a large scale [1] [2] [3]. For this transition to occur successfully in the short term, the biofuel product must be extensively compatible with the existing refinery, transportation, and end-use infrastructure [4]. To satisfy this requirement, the biofuel must be a liquid hydrocarbon [5] [6].

1.1 Biomass Feedstocks

Biomass is a general term applied to organic matter derived from living plants. In terms of potential biofuel feedstock, there are two broad groups: biomass which is grown and harvested specifically for biofuel production, and biomass that is collected as a byproduct or waste stream and used as a feedstock [7] [8] [9]. A graphic representation of potential biomass streams, produced by Naik et al., is shown in Figure 1.1 [7].

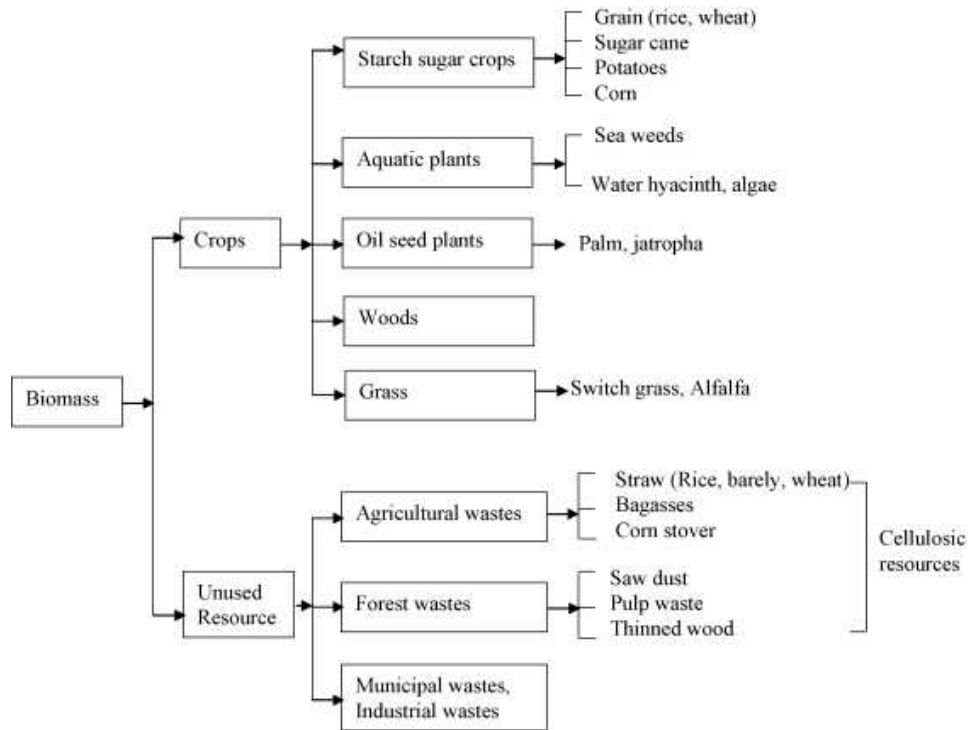


Figure 1.1 Potential sources of biomass feedstocks [7]

Of particular interest is cellulosic biomass, sometimes referred to “lignocellulosic” biomass. Cellulosic biomass encompasses feedstocks such as the non-edible parts of agricultural crops, wood and woody residues, and grasses [9]. The amount of energy available from cellulosic biomass is substantial and, if converted to liquid transportation fuel, it is estimated that it could replace 30% of the fuel demand in the United States [10]. A 2009 study by the National Academy of Science (NAS) gives a breakdown of available cellulosic biomass in the U.S. by the year 2020. Their study focused on biomass sources that would be available without substantial negative impacts to the environment or food production. This data is shown in Table 1.1 [11].

Table 1.1 Estimated cellulosic biomass available in the U.S. by year 2020 [11].

Cellulosic Biomass Feedstock	Dry Tons (millions)
Corn Stover	112
Wheat and Grass Straw	18
Hay	18
Dedicated Energy Crops	164
Woody	124
Animal Manure	12
Municipal Solid Waste	100
Total	548

Additionally, the biomass resources in the U.S. have been estimated to increase to over one billion tons per year by 2030, as shown in Figure 1.2 from the Billion Ton Report Update [12].

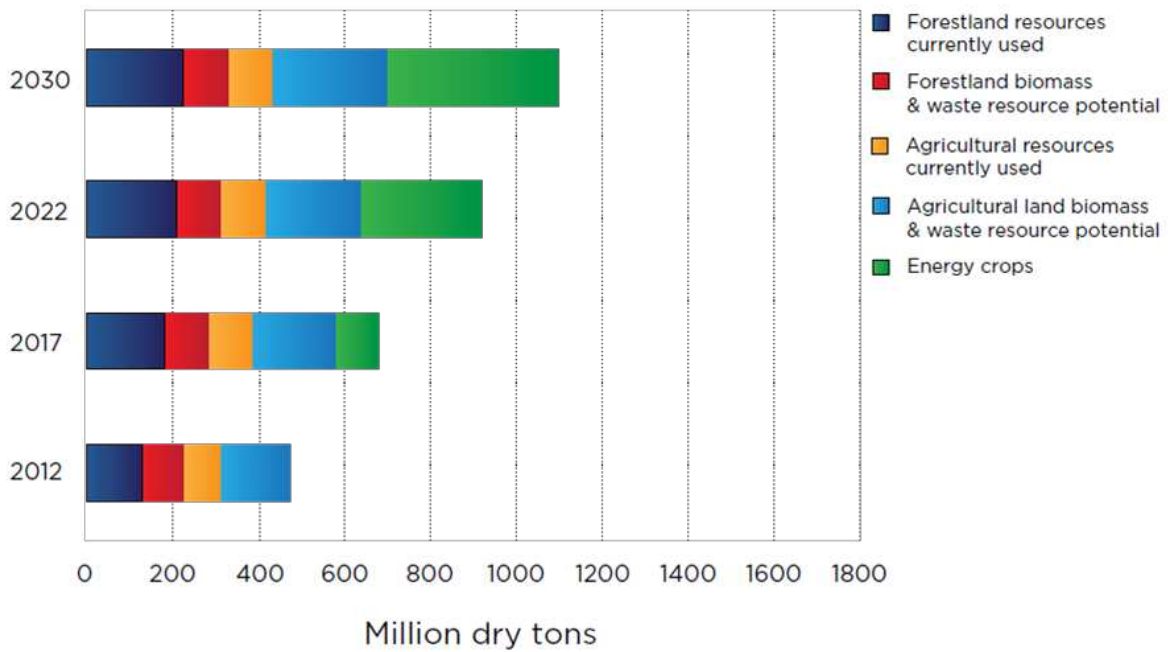


Figure 1.2: Estimated availability of cellulosic biomass, in millions of tons on a dry basis, as reported in the Billion Ton Report Update [12].

While the specifics of the assumptions made for each of these calculations can be debated, it is clear that there exists, and will exist, a sufficient domestic supply of cellulosic biomass to generate a meaningful supply of biofuel [11] [12] [13].

The primary component of cellulosic/lignocellulosic biomass is the plant cell wall, and those terms are a reference to the primary components of plant cell walls, lignin and cellulose.

Understanding the components of biomass is vital to understanding the processes by which it can be converted to a fuel.

1.2 Components of the Plant Cell Wall and General Conversion Pathways

The plant cell wall is composed of two classes of structural polymers: the polysaccharide-based polymers, cellulose and hemicellulose, and the phenolic-based polymer, lignin [14]. Cellulose is a linear, semi-crystalline polymer of glucose, while hemicellulose is a branched, amorphous polymer formed of 5- and 6-carbon sugars. Lignin is a complex, amorphous polyaromatic polymer, composed of extensively cross-linked phenolic monomers, and gives rigidity to plant structures. Together, cellulose, hemicellulose, and lignin form the cell walls of plants, as illustrated in Figure 1.3, and comprise the bulk of cellulosic biomass [15] [9].

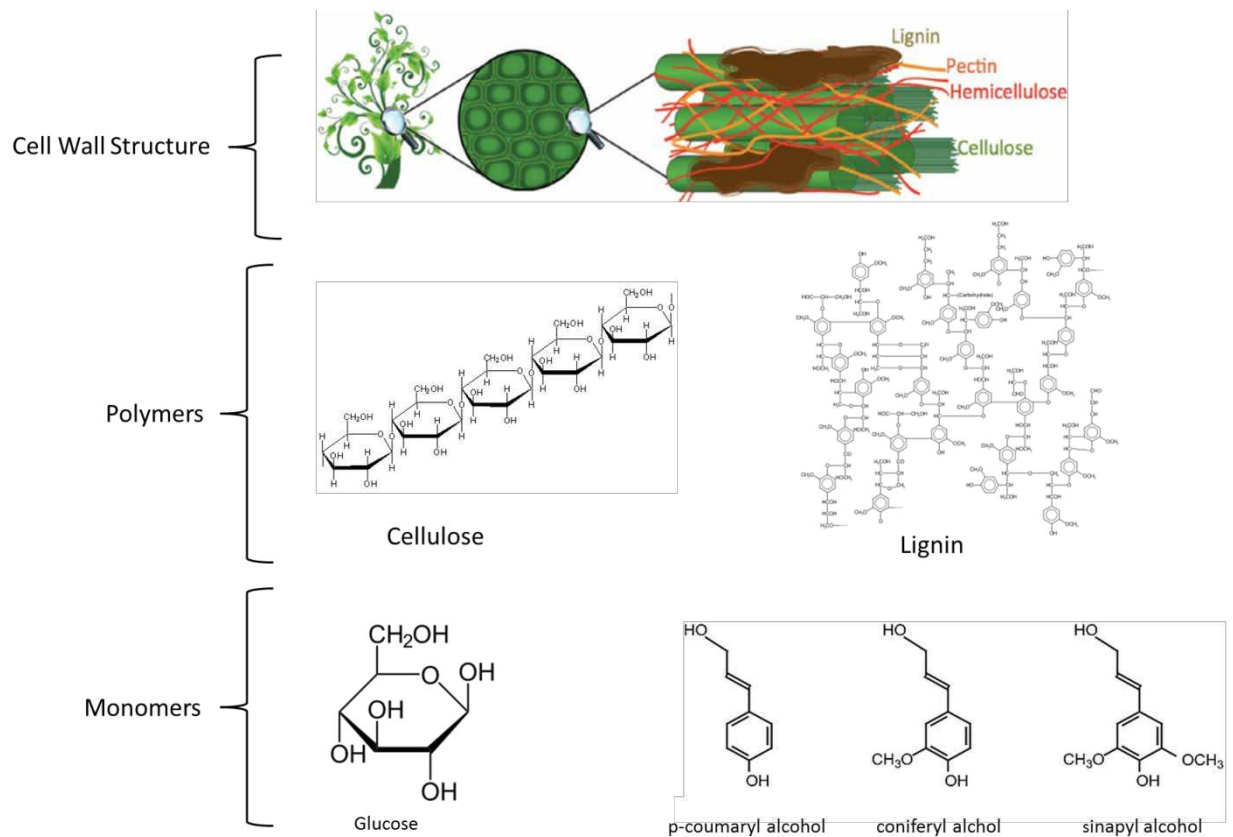


Figure 1.3 Structure and components of biomass from macro to micro structure [16].

There are two general pathways to convert biomass into biofuel. The first is “biological conversion,” which utilizes microorganisms such as yeast and genetically-modified *E. coli* to facilitate the conversion [7]. The second is “thermochemical conversion,” which uses heat, pressure, and catalysts to accomplish the conversion [7]. There are advantages and disadvantages to each general pathway. Biological conversion methods tend to be very selective; both in what feedstocks they can consume, as well as the product molecules they produce [3]. Additionally, biological conversion methods often require less severe operating conditions due to the fragility of the organisms. This can limit the throughput and enlarge the footprint of these systems [17]. Thermochemical conversion pathways have higher throughput than biological conversion

methods, but they require harsh processing conditions and struggle to achieve the high selectivity seen in biological conversion [17]. However, a significant advantage of thermochemical conversion methods, such as pyrolysis and gasification, is their ability to process the entirety of the biomass, whereas many microorganisms used in biological conversion methods cannot process the lignin component [7] [17].

1.3 Thermochemical Conversion and Fast Pyrolysis of Biomass

Of the two primary thermochemical conversion techniques, pyrolysis and gasification, gasification has historically received the most attention as a biofuel production method. This is due to the application of an analogous process in coal-to-diesel processing during WWII and later in South Africa [18]. The biomass gasification to fuels pathway consists of gasifying the biomass to form synthesis gas ($\text{CO} + \text{H}_2$), by heating the feedstock to temperatures $>800^\circ\text{C}$ [19]. Gasification can then be followed by a variety of reactions to form desired products, including the Fischer-Tropsch reaction to create aliphatic hydrocarbons [19], the water-gas shift reaction to generate hydrogen [20], or the conversion to methanol [21]. However, attention and research into fast pyrolysis is increasing, in part because it is generally a less energy-intensive process compared to gasification, and therefore has the potential to be more economic [22].

During fast pyrolysis, biomass is rapidly heated ($\sim 1000^\circ\text{C}/\text{s}$) to a reaction temperature of 400-600°C, with a residence time of 1-2 s. This process is conducted in the absence of oxygen, which results in thermal degradation of the biopolymers which compose the biomass [9] [23]. Fast pyrolysis of biomass results in the generation of a vapor product, consisting of light gases and larger vapor-phase molecules, while leaving behind char, a solid [24] [23]. At the conclusion of the fast pyrolysis reaction, the product vapors are condensed to form a liquid product referred to

as “bio-oil” or “pyrolysis oil.” Fast pyrolysis can achieve a mass-based conversion to pyrolysis oil of up to 75% [25]. The properties and composition of pyrolysis oil differ significantly from that of petroleum-derived, liquid fuels. A comparison of the properties of pyrolysis oil and those of heavy fuel oil is listed in Table 1.2.

Table 1.2 Comparison of the physical properties of typical pyrolysis oil from wood with those of heavy fuel oil [23].

Physical Property	Pyrolysis Oil	Heavy Fuel Oil
Water, wt%	15-30	0.1
pH	2.5	-
Specific Gravity	1.2	0.94
Elemental composition, wt%		
C	54-58	85
H	5.5-7.0	11
O	35-40	1
N	0-0.2	0.3
Ash	0-0.2	0.1
HHV (MJ/kg)	16-19	40
Viscosity (at 50 C), cP	40-100	180
Solids, wt%	0.2-1	1
Distillation Residue, wt%	up to 50	1

Due to the high oxygen content of biomass (~40%), the vapor-phase products and the condensed pyrolysis oil are highly oxygenated as well [15] [26]. Direct utilization of the products is impractical due to the acidity, corrosiveness, and storage instability of the resulting bio-oil [23] [24] [26]. For these reasons, fast pyrolysis needs to be coupled with a technology to produce a more stable, deoxygenated product. The two most effective methods to achieve this are hydrotreating the pyrolysis oil, which is expensive due to the high hydrogen consumption and the high pressures required (~200 bar), and catalytic fast pyrolysis [24] [27].

In the catalytic fast pyrolysis (CFP) process, which is also commonly referred to as fast pyrolysis with catalytic vapor-phase upgrading (VPU), a catalyst is used to remove the oxygen from the

vapor-phase pyrolysis products. This results in a liquid product with increased stability and decreased oxygen content. The catalyst can either be in direct contact with the pyrolyzing biomass (*in situ* CFP) or the catalytic upgrading can take place in a separate reactor (*ex situ* CFP). It has been found that there is no significant difference between the product yields of *in situ* and *ex situ* CFP [28]. The zeolite catalyst ZSM-5 has been found to be the extremely effective at deoxygenating pyrolysis vapors from biomass [29] [30] [31] [32] [33] [34].

1.4 ZSM-5

Zeolite Socony Mobil #5, abbreviated ZSM-5, was initially synthesized and explored as a catalyst by Landolt and Argauer, while working for the Mobil™ oil company (previously known as Socony-Vacuum Oil Company), in 1965 [35]. Initial ZSM-5 research was focused on its development as a dewaxing catalyst and as a catalyst for Fluidized Catalytic Cracking (FCC) reactors [36]. However, ZSM-5 has since been found to be effective for a variety of acid-catalyzed reactions, including the conversion of methanol to gasoline [37], the polymerization and isomerization of light olefins [38], and the deoxygenation and upgrading of biomass pyrolysis vapors [9].

ZSM-5 is an aluminosilicate zeolite of the MFI type and is a solid-acid catalyst in its protonated form. ZSM-5 contains both weaker, electron pair-accepting Lewis acid sites and stronger, proton-donating Brønsted acid sites [24] [39]. The Brønsted acidity of ZSM-5 is a function of the silica-to-alumina ratio (SAR) in the catalyst's framework. From the starting point of a pure silicate, each instance of an alumina ion (Al^{+3}) replacing a silica ion (Si^{+4}) in the ZSM-5 framework results in an unbalanced charge. When an H^+ satisfies the charge balance, a Brønsted acid site is formed [40]. So as the proportion of alumina increases, i.e. the SAR decreases, the

density of Brønsted acid sites, and the total acidity of the catalyst, increases. The acidity of ZSM-5 is known to influence the function and efficacy of the catalyst [41] [42] [43] [44]. A diagram of a Brønsted acid site within the ZSM-5 framework is shown in Figure 1.4.

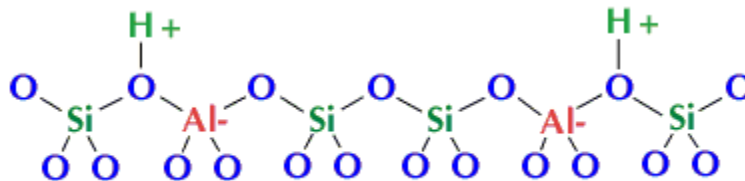


Figure 1.4 Diagram of a Brønsted acid site present in ZSM-5 framework [45].

ZSM-5 catalysts are crystalline structures, approximately 1 μm in size, with internal microchannels. The ZSM-5 zeolite belongs to the pentasil family of zeolites, which have pore structures defined by eight 5-member rings of Si and Al, with O at the vertices. A diagram of the pentasil unit of ZSM-5, as well as the catalyst's structure and framework, are shown in Figure 1.5.

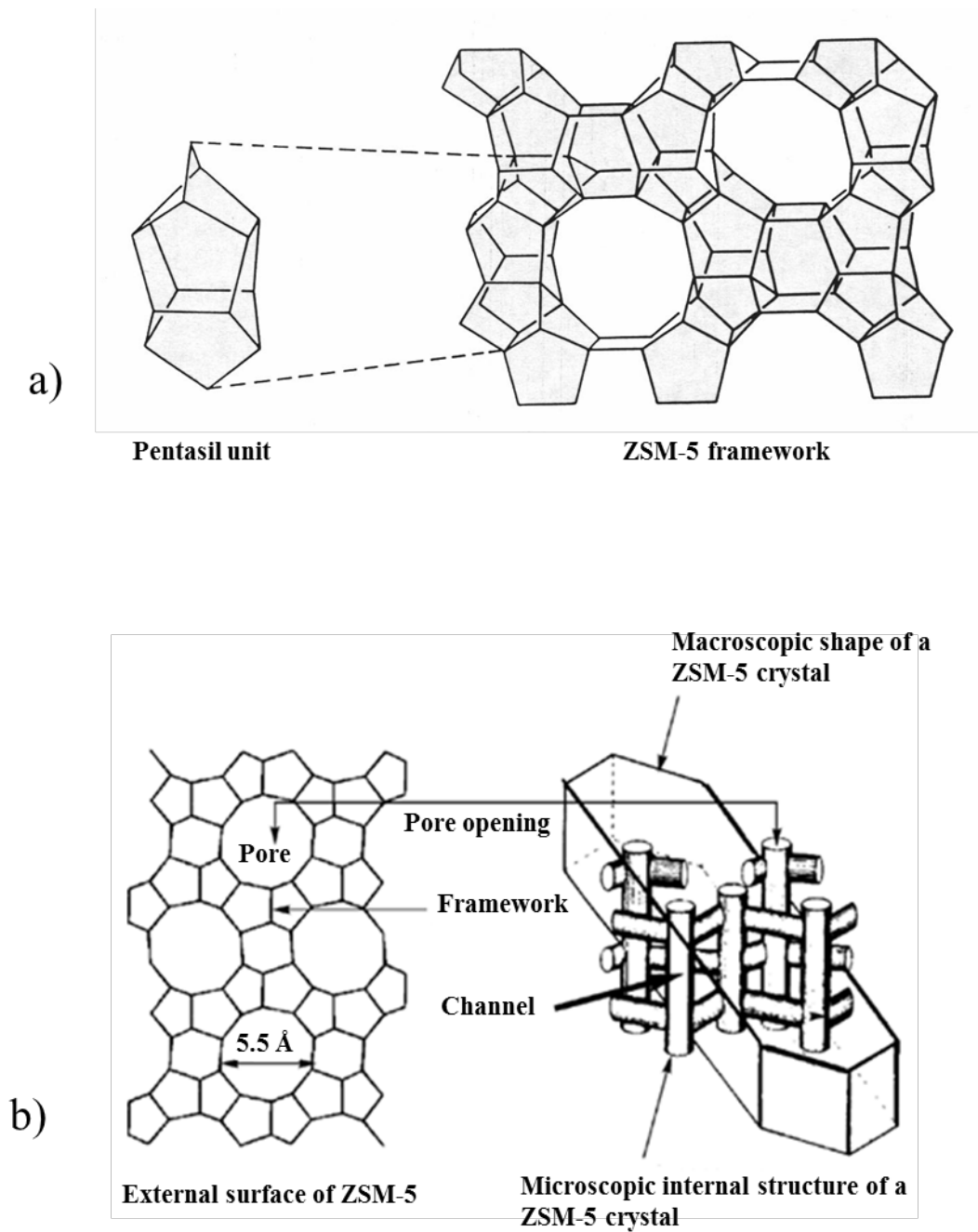


Figure 1.5 Diagram of the geometry and structures of ZSM-5, containing: a) schematic of the base pentasil unit of ZSM-5, formed by Si, Al, and O, and how those pentasil units form the ZSM-5 framework and b) schematic relating the ZSM-5 framework to the internal structure of channels within a macroscopic ZSM-5 crystal [46] .

When the pentasil units fit together to form the framework of ZSM-5, 10-ring holes are created and bounded by faces of the interlocking pentasil units, as shown in Figure 1.5 a). In the 3D structure of the catalysts, the majority of these holes are within the catalyst, forming channels. ZSM-5 contains both straight channels, shown running vertically, and zig-zag channels, shown running horizontally in Figure 1.5 b). The openings to the channels are approximately 5.5 Å, and are referred to as pore windows, while the channels themselves are called micropores [46]. Larger openings in the catalyst crystal, called mesopores, are naturally-occurring imperfections in the ZSM-5 crystal. They can also be added intentionally during the catalyst synthesis [47]. The uniformity of the pore window size results in ZSM-5, as well as other zeolite catalysts, being a shape-selective catalyst [48]. Molecules that are larger than the pore window experience a mass transfer limitation that excludes them from reacting [48]. Additionally, this shape selectivity limits the type of products which can form within the catalyst. However, surface reactions on zeolites are not affected by these constraints [49].

The small size of the zeolite crystals makes them impractical for real-world reactors, due to pressure drops which occur across fixed beds and problems with fluidization in fluidized bed reactors. In order to form a functional catalyst, binders are added to form macroscopic catalyst particles. Typical ZSM-5 binders include alumina, silica, and clay [50]. The addition of binder also forms large “macro pores” between the catalyst crystals. A schematic of a catalyst particle consisting of a zeolite crystal and binder is shown in Figure 1.6.

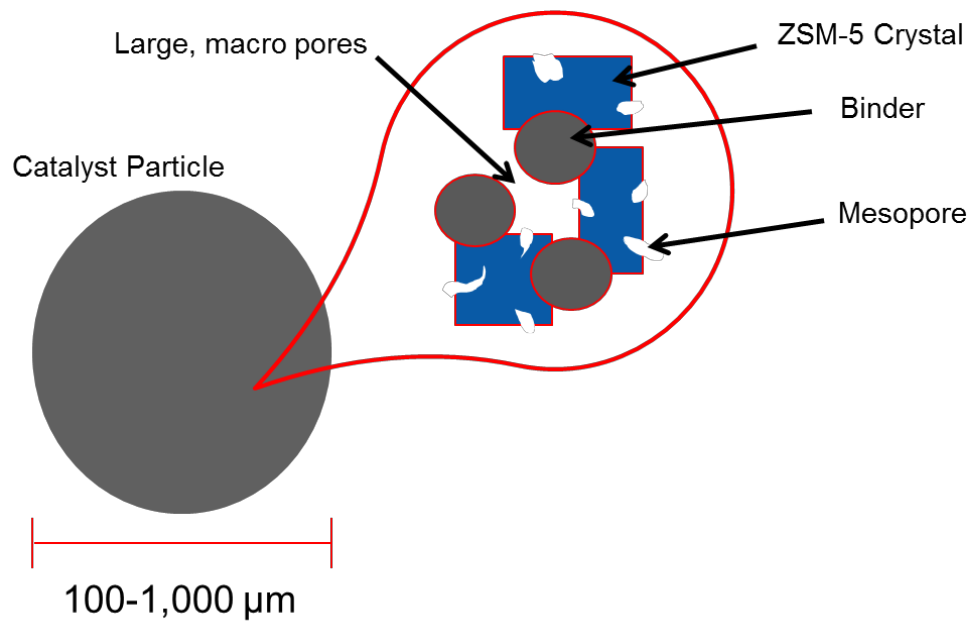


Figure 1.6 Diagram of a macroscopic catalyst particle of zeolite crystals and binder.

1.5 Catalytic Fast Pyrolysis of Biomass with ZSM-5

CFP of biomass with ZSM-5 catalyst results in the generation of solid, liquid, and gas product fractions. A diagram of the general product streams is shown in Figure 1.7.

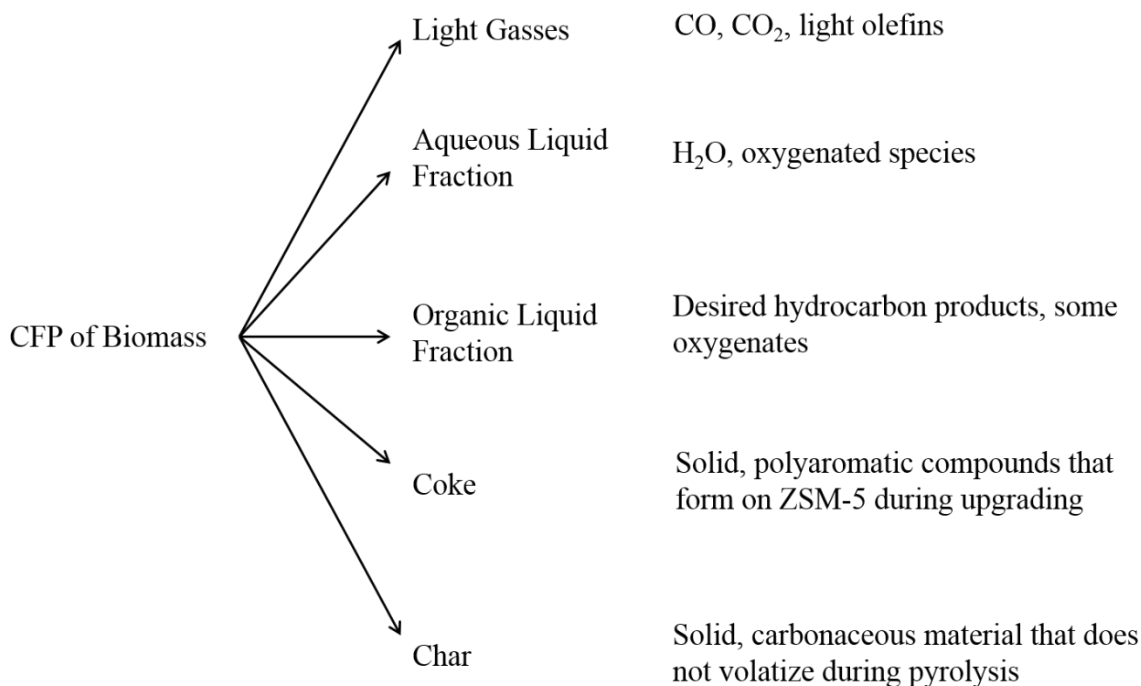


Figure 1.7: The product streams generated by the catalytic fast pyrolysis of biomass with ZSM-5 catalyst.

The organic liquid fraction is considered the desired product stream, as it contains the liquid-range hydrocarbons. The primary liquid-range products from CFP with a fully-active ZSM-5 catalyst are aromatics [24] [29] [51] [52]. Results with fresh, fully-active ZSM-5 reported in the literature have been achieved by performing CFP on small reactors with excess catalyst, and often with model compounds or fractions of biomass, such as cellulose. As an example of results from this style of experiment, the carbon yields and selectivities from the CFP of cellulose with excess ZSM-5 catalyst are listed in Table 1.3, as reported by Wang et al. [53]. Carbon yields are often reported in CFP literature, as an ideal conversion would be one that resulted in all carbon in the feed ending up in liquid-range hydrocarbons.

Table 1.3: Carbon yields and carbon selectivity reported by Wang et al. during the CFP of glucose with ZSM-5. Pyrolysis occurred at 500°C and upgrading at 600°C, with excess catalyst (biomass:catalyst=0.05). C₉ aromatics included indanes, indenenes, and alkylbenzene. C₁₀₊ aromatics include naphthalenes and higher polyaromatics [53].

Overall carbon Yield (%)	
CO	25.5
CO ₂	9.7
Coke	9.4
Aromatics	27
Olefins	17.9
Aromatic Selectivity (%)	
Benzene	24.5
Toluene	36.5
Xylene	12.5
C ₉ aromatics	11.6
C ₁₀₊ aromatics	14.9
Olefin Selectivity (%)	
Ethylene	57.2
Propene	42.8
Butane	n.d.

Although the information gathered from experiments performed with excess catalyst is not without value, it fails to give any insight into what is occurring in larger-scale, more realistic reactors.

In large-scale operations it is impractical and cost-prohibitive to operate under very low biomass:catalyst, which results in a condensed oil which contains oxygenates [54] [55] [56] [57].

A characteristic example of a mass balance from a reactor intended to simulate a full-scale implementation is shown in Figure 1.8. The figure displays data from CFP of pine with a ZSM-5 catalyst in 2-inch fluidized bed reactor, operating at 500°C, with a biomass:catalyst=2.3, as reported by Iisa et al. [58].

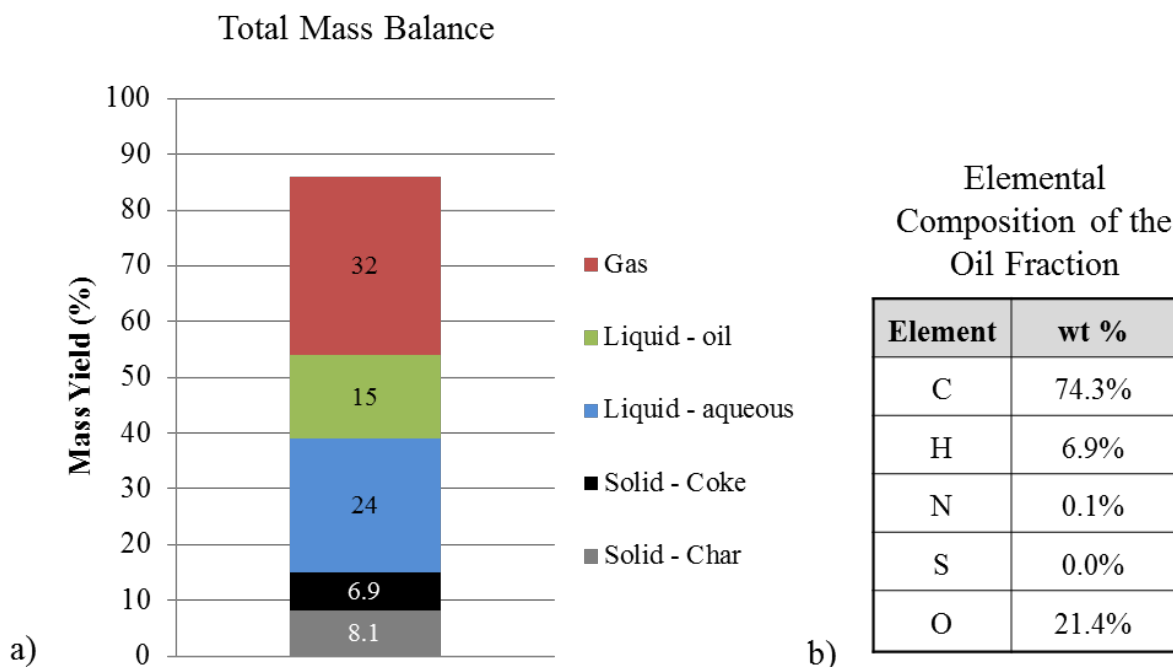


Figure 1.8: a) mass yields of the solid, liquid, and gas fractions generated during the CFP of pine at 500°C, in a 2-inch fluidized bed reactor, with a biomass:catalyst=2.3, and b) the elemental composition of the oil fraction, as reported by Iisa et al. [58].

It can be seen that the yield of desirable oil is only 15%, based on the mass of biomass fed, and the oil had an oxygen content of approximately 21 wt%. Due to the strict oxygen tolerances of petroleum refineries, a likely real-world scenario would be CFP of biomass coupled with mild hydrotreating, with the resulting stream integrated with a traditional petroleum refinery [59] [60] [61].

1.6 Upgrading Mechanism of ZSM-5 during CFP of Biomass

The mechanism of the upgrading that occurs on ZSM-5 during CFP is not well understood; however, it is known to consist of two major steps. The first step involves cracking reactions on the surface of the catalyst. The surface reactions are necessary for many of the raw pyrolysis products to enter the catalyst pores, especially those derived from lignin, due to the size-

restriction of the pore opening [52]. The surface reactions include thermal cracking, as well as the removal of oxygen functional groups by decarboxylation, decarbonylation, and dehydration [29] [52]. The second step of the upgrading process is the formation of aromatics.

Dahl and Kolboe, while studying methanol-to-olefin (MTO) reactions with zeolite catalysts, proposed a hydrocarbon pool mechanism to explain the hydrocarbon formation reactions they observed [62] [63] [64]. Their proposed reaction scheme is shown in Figure 1.9.

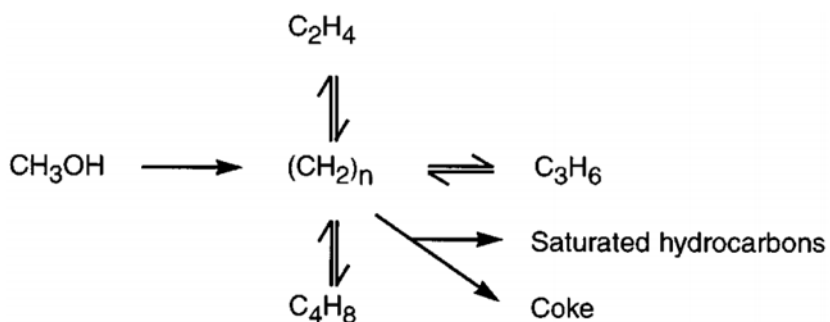


Figure 1.9: Hydrocarbon pool mechanism proposed by Dahl and Kolboe to explain hydrocarbon formation during methanol-to-olefin reactions in zeolites [64].

Subsequent research into the hydrocarbon pool during MTO has focused on side-chain and pairing mechanisms [65]. These two reaction schemes are shown in Figure 1.10.

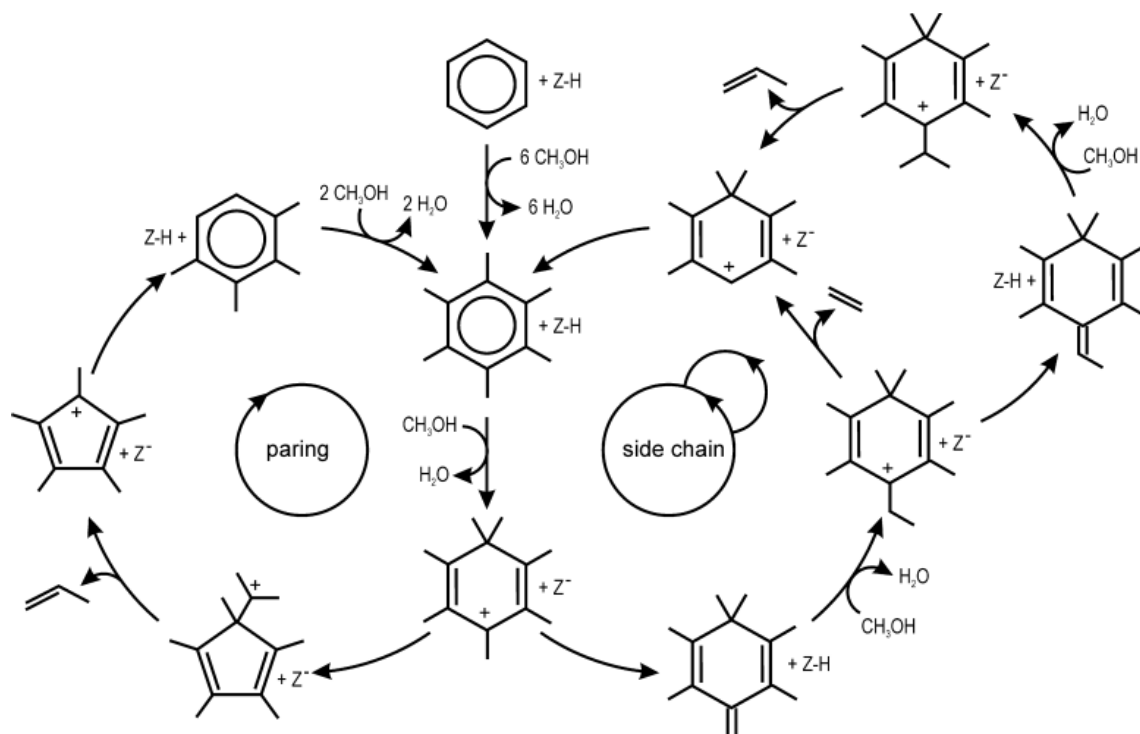


Figure 1.10: Schematic of paring (left) and side chain (right) reactions occurring in the hydrocarbon pool within zeolites during methanol-to-olefin reactions. The zeolite in its protonated form is represented by Z-H, and by Z⁻ in its deprotonated form [65].

The hydrocarbon pool and dual cycle mechanism hypotheses for MTO reactions have been extensively studied and upheld [66] [67]. The hydrocarbon pool mechanism explains the results observed from CFP with ZSM-5. The MTO hydrocarbon pool mechanism is considered analogous to what is occurring during ZSM-5 upgrading of pyrolysis vapors, wherein the hydrocarbon pool initially develops within the catalyst and acts as an intermediate step in the production of aromatics via deoxygenation, pairing, and sidechain reactions [68] [69] [70].

1.7 Coke

A significant drawback to CFP with ZSM-5 catalysts is coke formation. Coke is a general term for large polyaromatic hydrocarbons that form on catalysts during reactions [71]. Coke forms on

the surface of the ZSM-5 catalyst and in its pores, to the extent possible under the constrictions of the catalyst's shape selectivity [71] [72]. Coking results in the reversible deactivation of ZSM-5 due to the physical occlusion of active sites [71] [73] [74] [75]. The deactivation can be reversed via oxidation, allowing the catalyst to resume activity [76]. Coke is known to form on ZSM-5 during methanol-to-olefin (MTO) reactions as well as during CFP of biomass. As it is a less complex system, coke formation reactions have been studied in greater detail for MTO reactions, where it has been found that progressive ring growth reactions on the catalyst's surface results in coke [77].

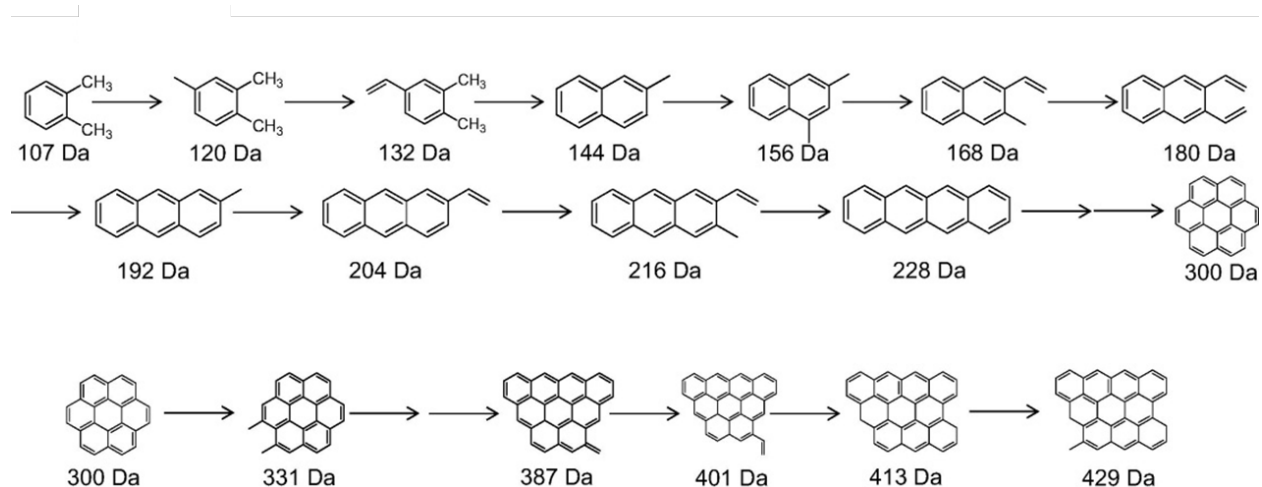


Figure 1.11: Proposed reaction scheme of the progression of coke formation on ZSM-5 surface during methanol-to-olefin conversions [77].

CFP of biomass is a much more complex reaction, with an extremely diverse collection of molecular weights and functional groups interacting with the catalyst. This has led to the formulation and proposal of multiple routes of coke formation on ZSM-5. These routes include ring-growth reactions as a result of aromatic production during deoxygenation, as observed in

MTO reactions [52] [54] [68] [78], and the condensation, deposition, and eventual coupling of lignin monomers [24] [52].

It is known that the chemical composition of the feedstock being upgraded over ZSM-5 impacts the selectivity toward coke-forming reactions [73]. A useful metric in anticipating excessive coking on ZSM-5 is the effective hydrogen index (EHI) of the feedstock. The EHI is an adjusted measure of the molar hydrogen-to-carbon ratio in a feedstock, which assumes that all oxygen will be removed as water [73] [79] [80]. The EHI is defined by Equation 1, with C, H, and O representing moles of carbon, hydrogen, and oxygen, respectively, in the feedstock [73].

Equation 1: Formula for the Effective Hydrogen Index (EHI), where C, H, and O represent moles of carbon, hydrogen, and oxygen, respectively, in the feedstock.

$$EHI = (H / C)_{eff} = \frac{(H - 2O)}{C}$$

The EHI was first proposed by Chen et al., and has become a widely-used standard for determining if a CFP feedstock has sufficient hydrogen to primarily form desired aromatics, or if the feedstock will result in excessive coke generation and rapid deactivation of ZSM-5. It has been determined that the amount of coke formed during CFP with ZSM-5 correlates strongly with the EHI, and that feedstocks with an EHI <1 coked significantly during upgrading with ZSM-5 [73] [79]. Lignocellulosic biomass has an EHI of between 0 and 0.4 [73].

The assumption that all oxygen is rejected as water is a somewhat problematic one, as we know that decarbonylation and decarboxylation reactions also occur, resulting in the generation of CO and CO₂, respectively. However, acid-catalyzed dehydration is the primary mode of oxygen rejection during CFP with ZSM-5. There also exists strong evidence supporting the use of the

EHI as a tool for feedstock assessment, as the results from Zhang et al. clearly show a correlation between EHI and coke formation [79]. The coke yields from Zhang's study have been plotted as a function of feedstock EHI in Figure 1.12 [79].

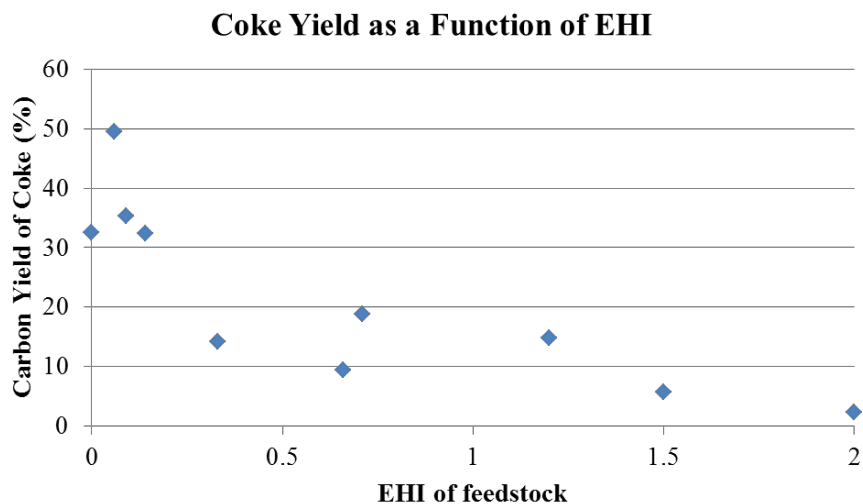


Figure 1.12: The carbon-based coke yield, as a function of the effective hydrogen index, obtained by Zhang et al. during the catalytic upgrading of ten biomass-derived feedstocks over ZSM-5 at 600°C [79].

The cumulative results from EHI studies clearly show that biomass is a hydrogen-deficient feedstock for catalytic upgrading over ZSM-5. This deficiency results in a stoichiometric limitation to the yield of liquid-range aromatics, and an increased favorability of reactions to multi-ring aromatics and coke precursors, which have a lower H/C ratio. A variety of aromatic structures and their H/C ratio is shown in Figure 1.13.

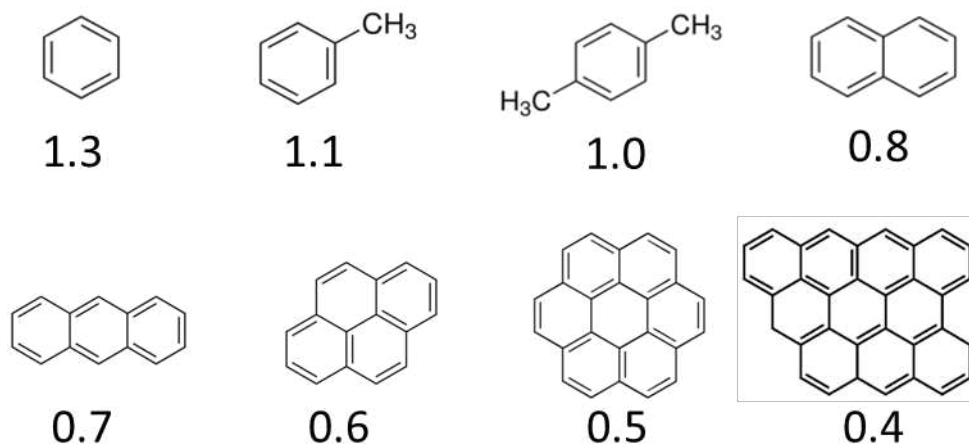


Figure 1.13: Structures and corresponding H/C ratios for CFP products, ranging from desired liquid-range aromatics to large coke-precursors. The limited availability of hydrogen in biomass leads to the stoichiometric favorability of products with lower H/C ratios.

1.8 Catalytic fast pyrolysis of individual biomass components

Non-catalytic fast pyrolysis of cellulose and lignin generate very different, oxygenated products [81] [82] [83] [84]. A diagram from Talmadge et al. beautifully illustrates the contributions from the polysaccharide component and the phenolic component of biomass to the overall composition of uncatalyzed pyrolysis vapor, shown in Figure 1.14 [84].

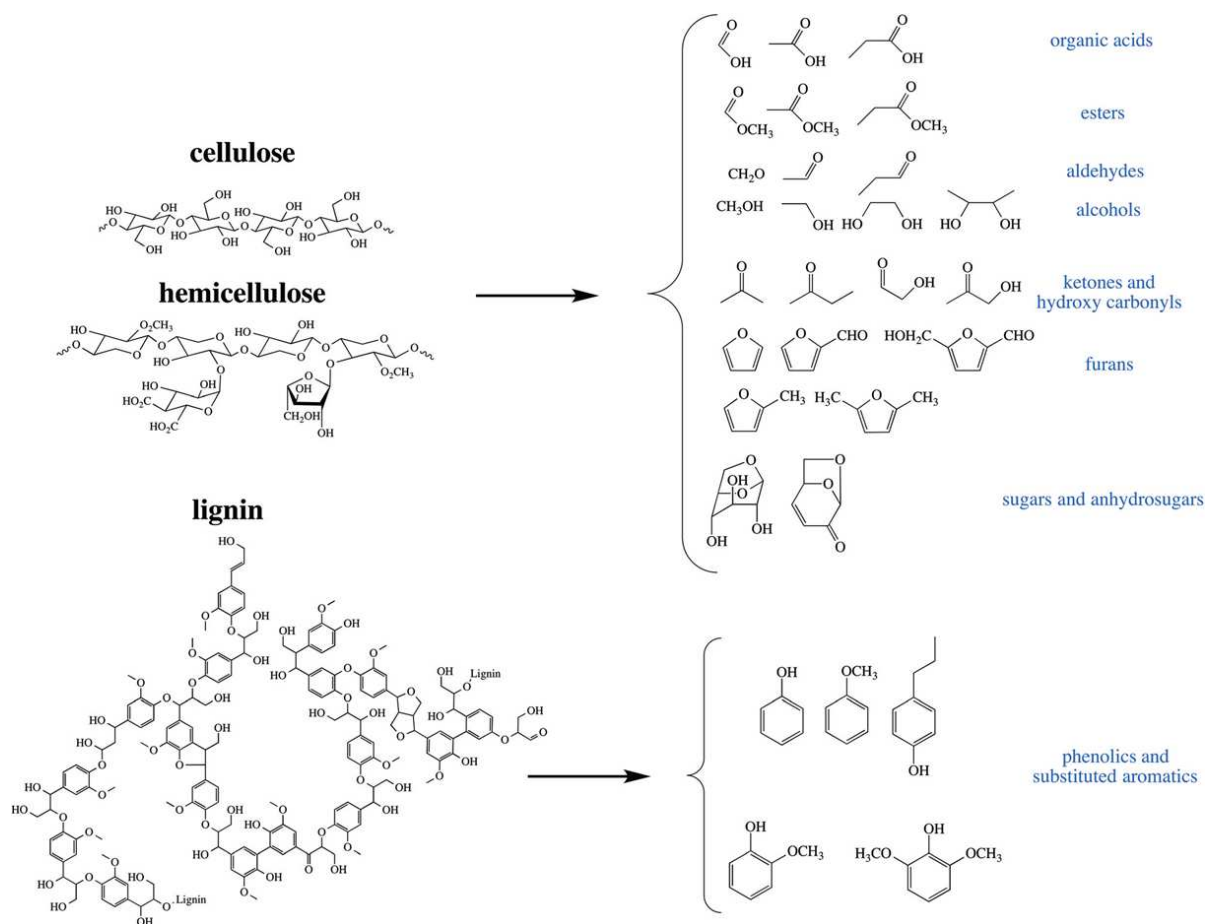


Figure 1.14 contributions from the polysaccharide component (cellulose and hemicellulose) and the phenolic component (lignin) of biomass to the overall product composition of uncatalyzed pyrolysis vapor [84].

Despite the different compounds generated by the non-catalytic pyrolysis of biomass fractions, during CFP they all yield the same aromatic hydrocarbon products, when upgrading is performed with ZSM-5 [31] [52] [85]. Carlson et al. found that the fractions of biomass not only produced the same products, but also that the selectivity towards key aromatic hydrocarbons was very similar for a variety of biomass components and surrogates, as shown in Figure 1.15 [85].

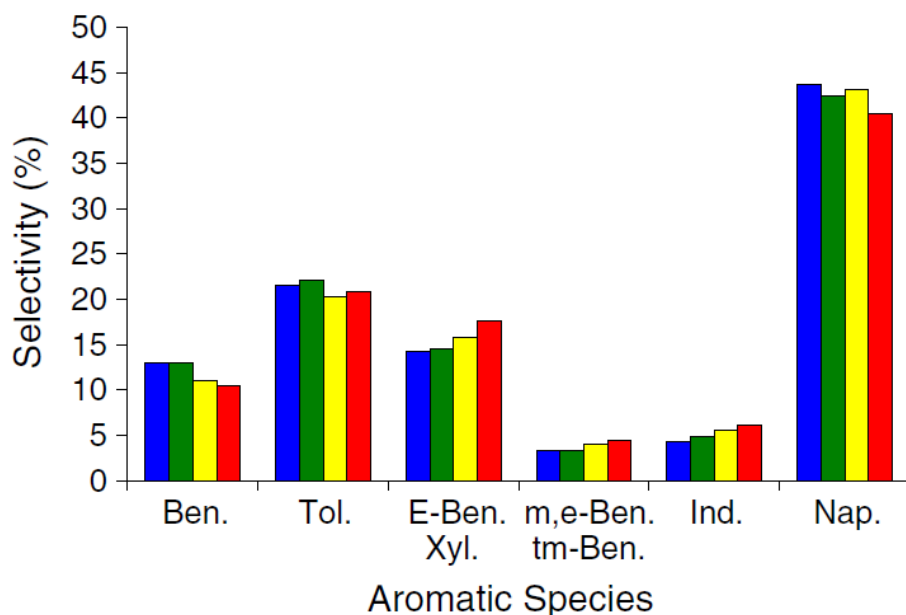


Figure 1.15: The selectivity towards benzene, toluene, ethyl-benzene and xylenes, methyl-ethyl-benzene and trimethyl-benzene, indanes, and naphthalenes, during CFP of biomass fractions and related compounds at 600°C in a Pyroprobe reactor, with a biomass:catalyst=0.05. Blue: glucose, green: cellobiose, yellow: cellulose, red: xylitol. As reported by Carlson et al. [85].

Despite the growing body of work analyzing the CFP of individual biomass components, the contributions of the biopolymers to the deactivation of ZSM-5 during upgrading have not been widely studied.

1.9 ZSM-5 Modification with Metals

As discussed in Section 1.7, the CFP of biomass is a hydrogen-deficient system, and it follows that providing hydrogen to the reaction environment may have a favorable impact. However, molecular hydrogen is quite unreactive without a catalyzing metal surface. Having a metal surface present allows for the adsorption of molecular hydrogen, and facilitates the breaking of the strong sigma bond between the two hydrogen atoms [86]. This step is commonly referred to

as “activating” the hydrogen, as the adsorbed hydrogen reacts much more readily after the sigma bond cleavage. A diagram of hydrogen being activated is shown in Figure 1.16.

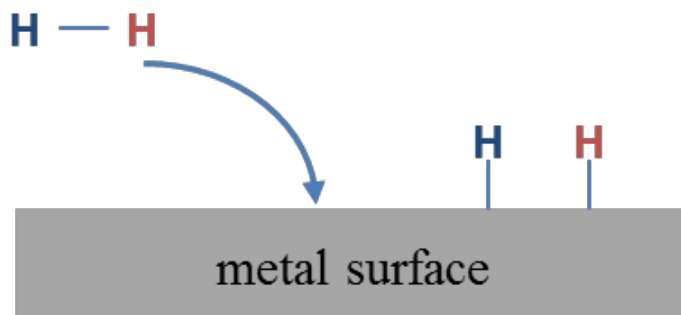


Figure 1.16: Diagram of the activation of hydrogen by a metal surface. Molecular hydrogen adsorbs to the surface of the metal, breaking the H-H bond and forming H-metal bonds. In this form, hydrogen participates in hydrogenation reactions much more readily.

ZSM-5 is not a sufficient surface to activate molecular hydrogen, and the addition of hydrogen as a carrier gas has been shown to have no impact on CFP with unmodified ZSM-5 catalyst [87]. In an attempt to decrease the amount of carbon being lost to coke, and increase the liquid-range hydrocarbon yield from CFP, many research groups have modified ZSM-5 to include metals [29] [54] [56] [88] [89] [90] [91] [92] [93] [94] [95]. It is generally hypothesized that the metals will utilize hydrogen generated *in situ* during pyrolysis, or provided externally, to hydrogenate coke precursors [90]. However, the efficacy of metal-modification is not clear from the literature, due both to conflicting results and the absence of catalyst deactivation data.

Park [88], Cheng [54], and Kelkar et al. [89] reported that the incorporation of Ga to ZSM-5 resulted in an increased aromatic yield and a decrease in coke formation. However, the effect was lost or reversed at loadings above 1% [89], and other studies were unable to reproduce the enhanced aromatic yields over Ga/ZSM-5 in a bench-scale reactor [76]. Iliopoulou et al. found

that the addition of Ni and Co resulted in less coke formation, as well as oils that were of lower oxygen content, but in lower yield [56]. The team later saw similar results with Co at the pilot scale [90]. However, Vichaphund et al. [91] and Melligan et al. [92] found that the incorporation of Ni, Ga, and Cu all gave lower hydrocarbon yields and higher oxygenate yields than their respective unmodified catalysts.

Others have reported that the addition of Co, Ni, and Pt to ZSM-5, during CFP under hydrogen resulted in reduced hydrocarbon yield at atmospheric pressure, but enhanced yield at 400 psi [93].

2 Motivation for this work

Despite the surge of interest in CFP in recent years, a complete understanding of the process is lacking in one major area: the deactivation of the ZSM-5 catalyst. Bench scale and pilot scale experiments, which are most representative of real-world applications and allow for the condensation and collection of CFP product oil, are limited. From these experiments, however, it is known that the product oil includes aromatic hydrocarbons and a variety of oxygenates, including phenol and alkylated phenols [30] [96].

The majority of experimental data from CFP experiments are collected with micro-scale reactors (biomass samples ≤ 15 mg), and often with model compounds or cellulose. The gap in knowledge arises from the fact that most of the micro-scale experiments are conducted with very high catalyst-to-biomass ratios, meaning that the catalyst remains very active for the duration of the experiment [29] [52] [85] [97]. Although this gives insight into part of the catalytic process, it is not representative of the conditions in large-scale reactors, and it gives no insight into how the catalyst's functionality changes during the coking and deactivation process. If CFP of biomass is to be scaled from the laboratory to the production level, there is an urgent need for laboratory results which can give applicable, practical information on catalyst behavior. This work focuses on furthering the understanding of ZSM-5 deactivation during CFP of biomass.

2.1 Objectives

The overarching goal of this work is to advance the understanding of catalytic fast pyrolysis with ZSM-5, and guide future endeavors towards enhancing its viability as a biofuel production method. This is achieved by studying a key obstacle and under-researched component of

catalytic fast pyrolysis: the deactivation of ZSM-5 during upgrading. This dissertation is formed by work towards four specific objectives:

1. Determine how the products of catalytic fast pyrolysis change as the ZSM-5 catalyst progressively deactivates.
2. Study the impact of the silica-to-alumina ratio in the base zeolite crystal, as well as the material used as binder, on the catalytic performance of ZSM-5 during CFP of biomass to inform the selection of catalysts for further study.
3. Elucidate the role of the two component groups of biomass, polysaccharide biopolymers and phenolic biopolymers, in the deactivation of ZSM-5.
4. Create advanced catalysts by modifying ZSM-5 such that ambient hydrogen can be utilized, and evaluate the impact of the metal-modified catalysts on the hydrocarbon yield and catalyst deactivation during CFP of biomass in inert and hydrogen atmospheres.

3 Experimental Methods and Materials

3.1 Catalyst Deactivation Experiments/*ex situ* CFP

The majority of experiments reported in this work are examples of *ex situ* CFP, and they are designed to give insight during the deactivation of the upgrading catalyst as it is exposed to successive pulses of pyrolysis vapors. These experiments were carried out on a variety of reactors, detailed in Table 3.1. Although the detectors, heating methods, and biomass delivery systems varied, all reactors used for the *ex situ* catalyst deactivation experiments were fixed bed reactors with a similar flow path. Figure 3.1 is a diagram of the general, shared flow path of the reactors used for these experiments.



Figure 3.1 Common flow path for the reactors used in these experiments

Each of the catalyst deactivation experiments was performed in a similar fashion. Successive samples of biomass were pyrolyzed and upgraded over a single packed bed of catalyst. This allowed for the products to be assessed as a function of the ratio of “total weight of biomass pyrolyzed”-to-“weight of the catalyst bed” (biomass:catalyst). Plotting the CFP products as a function of the biomass:catalyst enables one to observe the change in products as the catalyst bed becomes deactivated. The specific reactors used for these experiments are detailed in the following section.

3.2 Reactors

The pyrolysis experiments reported in this document fall into two classes: 1) those performed for the analysis of pyrolysis products and 2) those performed for the generation of post-reaction catalyst samples. The experiments for the identification and quantification of pyrolysis products were performed in either the Tandem μ -Reactor or the Pyroprobe reactor system, detailed in Sections 3.2.1 and 3.2.2, respectively. These reactors are powerful analytic tools when coupled with analyzers and their low materials consumption and out-of-the-box readiness makes them valuable additions to any pyrolysis lab. However, the drawback to these small reactors is that their 10 mg catalyst bed is insufficient for collection and post-reaction characterization. For this reason, a third reactor was employed specifically for the generation of post-reaction catalyst samples. The Horizontal Reactor, detailed in Section 3.2.3, was selected for these supplemental experiments because its 50 mg catalyst bed is capable of generating sufficient post-reaction catalyst to perform multiple characterizations. Table 3.1 summarizes some of the specifics of the reactors.

Table 3.1 General parameters of reactors and analyzers used in the experiments presented in this document.

Reactor	Catalyst Bed Size	Biomass Sample Size	Analyzer	Advantages
Pyroprobe	10 mg	1 mg	GC-MS	Detailed species information and quantification; reactant-gas capable
Tandem μ -Reactor	10 mg	0.5 mg	GC-MS/FID	Detailed species information and quantification; detects light gasses
Horizontal Reactor	500 mg	50 mg	N/A	Generates sufficient post-reaction catalyst to perform characterizations

3.2.1 Pyroprobe Reactor System

3.2.1.1 Pyroprobe Flow Path and Components

The Pyroprobe reactor system is comprised of a commercially-available analytical pyrolyzer, the Pyroprobe model 5200 from CDS Analytical Inc., coupled with a gas chromatogram-mass spectrometer (GC-MS) for quantitative catalytic pyrolysis experiments. A diagram of the Pyroprobe reactor and analyzer configuration is shown in Figure 3.2.

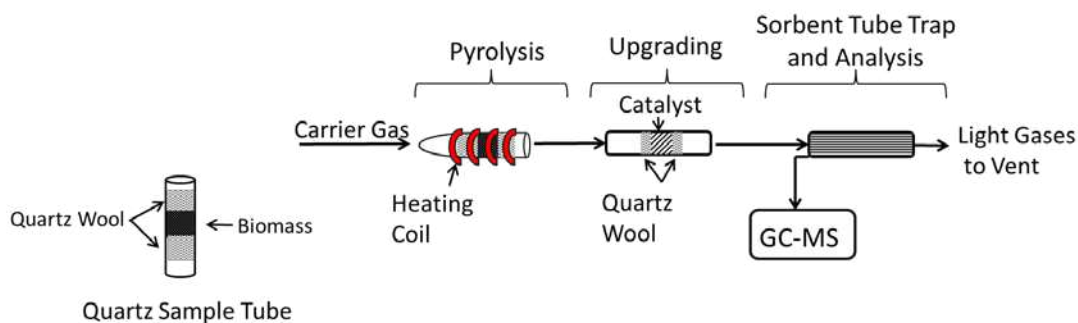


Figure 3.2 Diagram of the Pyroprobe reactor system and biomass sample tube.

The Pyroprobe system utilizes a computer-controlled, resistively-heated coil for sample pyrolysis, and a constantly-heated fixed bed for catalytic upgrading. The catalyst bed contained 10 mg of catalyst, and each quartz sample tube contained 1 mg of biomass. A sorbent tube trap, filled with Tenax-TA™ [poly (2,6 diphenyl-p-phenylene oxide)], was in-line with the flow path, following the upgrading zone. The use of the trap separates a CFP experiment on the Pyroprobe into two phases: the reaction phase and the analysis phase.

During the reaction phase, reactor carrier gas (54 mL of helium or 54 mL of hydrogen) carries the pyrolysis vapors from the pyrolyzing zone, through the upgrading zone, and finally to the

trap. The trap adsorbs the condensable components of the upgraded pyrolysis vapors and allows the non-condensable gases to be vented. At the conclusion of each reaction phase, the analysis phase of the experiment begins. An automated 8-port valve activates, which switches the active carrier stream from the reactor's carrier gas to the GC's carrier gas (54 mL/min of He), flowing in the reverse direction through the trap and to the GC inlet. This allows the Pyroprobe lines to be purged with GC carrier gas. Following this, the trap is heated to 400°C in order to desorb the trapped pyrolysis products, which are then carried to the GC-MS for analysis.

The sorbent trap is a powerful addition to the Pyroprobe, and sets it apart from other small-scale reactor systems. Although it is not ideal to have an imposed step between pyrolysis and analysis, the sorbent tube trap allows the Pyroprobe to use reactant and/or corrosive gasses (e.g. hydrogen, H₂S, butane, etc.) and elevated pressures (up to 500 psi) that other Py/GC-MS systems cannot. It achieves this by switching carrier gas streams after the pyrolysis products have been adsorbed onto the trap, allowing for conditions in the reactor that the GC interface could not tolerate if the reactor's exit flow was plumbed directly to GC-MS.

An additional benefit of the sorbent tube trap is that it prevents large polyaromatic tars, which are formed from CFP but are too heavy for detection by GC-MS, from accumulating in the GC-MS, as they have boiling points higher than the 400°C desorption temperature. The reduction in heavy tars entering the analysis systems results in the MS signal staying extremely constant, compared to other Py/GC-MS systems, and reduces the frequency at which calibrations and maintenance on the GC and MS must be performed.

3.2.1.2 Pyroprobe GC-MS Analyzer

For product identification and quantification in the Pyroprobe reactor system, an Agilent G1530A gas chromatograph was used, coupled with an HP 5973 mass spectrometer.

Condensable products were desorbed from the trap and carried directly to the GC-MS. The GC contained a 30 meter capillary column (Agilent 190915-433) with a 5% phenyl and 95% dimethyl polysiloxane stationary phase, operated at a constant volumetric flow of 2 mL/min. The GC interface was held at 300°C, with a 50:1 split ratio. During analysis, the oven temperature was held at 40°C for 3 minutes before ramping to 240°C at 6°C/min, followed by a 10°C/min ramp to 300°C. The NIST98 MS library was used for product identification. For product quantification, the GC-MS was calibrated as described in Section 3.3.

3.2.1.3 Temperature Calibration of the Pyroprobe Heating Coil

The temperature reached inside the quartz sample tube, suspended in the heating coil of the Pyroprobe, is not directly measured in the base Pyroprobe configuration. Instead, to achieve the set-point entered into the Pyroprobe software, a calculated amperage is applied to the coil based on the manufacturer's measurements of the coil's resistance. A known discrepancy exists between the temperature set-point of the Pyroprobe and the actual temperature reached inside the quartz sample tube. CDS, the manufacturer of the Pyroprobe system, estimates the offset to be 100°C. To determine the temperature off-set independently, a series of calibration experiments was performed using a special Pyroprobe arm which was equipped with a thermocouple inserted into the heating coil. The experimental set-up, shown in Figure 3.3, allowed the thermocouple to sit inside a quartz sample tube which was loaded into the heating coil. This arrangement allowed

for an accurate measurement of the temperature achieved in the sample tube. The results of the calibration experiments are shown in Figure 3.4.

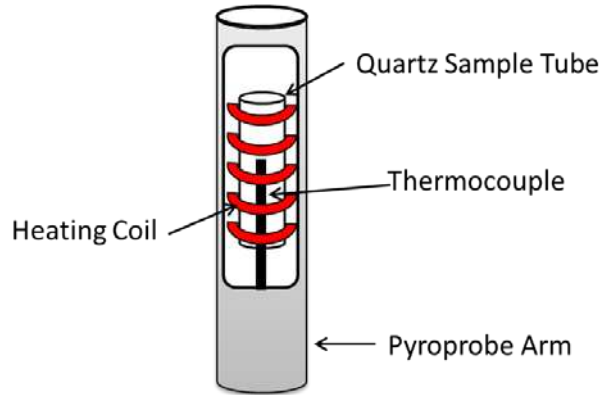


Figure 3.3 Diagram of a Pyroprobe arm equipped with a thermocouple to measure the temperature reached within the sample tube.

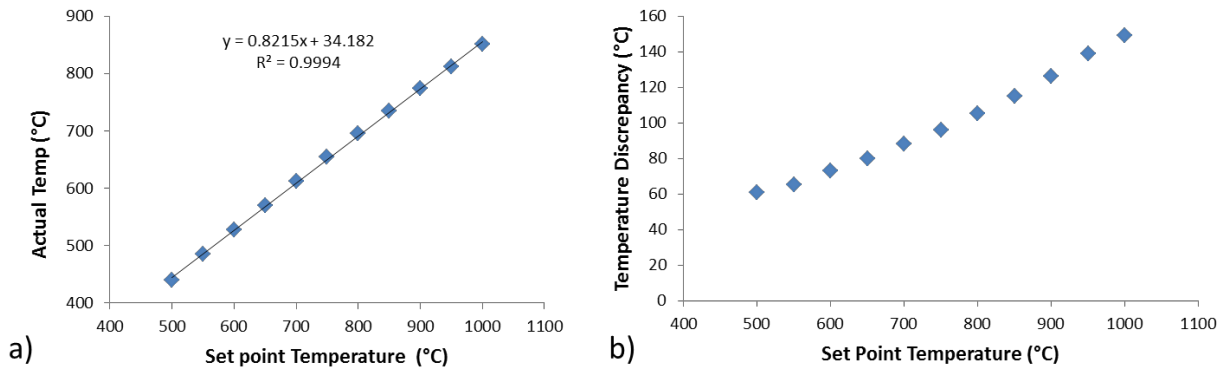


Figure 3.4 Pyroprobe temperature calibration a) Correlation between set point and measured temperature and b) Temperature off-set as a function of set point temperature.

It was found that the discrepancy varied between 60°C and 150°C, depending on the set point used. For all experiments reported here, a set point of 567°C was used to achieve a pyrolysis temperature of 500°C.

3.2.2 Tandem μ -Reactor System

3.2.2.1 Tandem μ -Reactor Flow Path and Components

The Tandem μ -Reactor system was composed of a Tandem μ -Reactor (Rx-3050 TR, Frontier Laboratories), coupled with a GC-MS/FID to obtain detailed product information. The system was equipped with an autosampler (AS-1020E, Frontier Laboratories) with a 40 cup capacity.

The Tandem μ -Reactor consists of two vertically-stacked continuously-heated zones: a pyrolysis zone and zone which can either be a transfer zone or a catalytic upgrading zone, depending on the configuration of the reactor. In either scenario, GC carrier gas flows through both zones, and carries all products to the inlet of the GC-MS/FID. The Tandem μ -Reactor can be set up into either the *ex situ* configuration or the *in situ* configuration. More detailed schematics and operational descriptions can be found elsewhere [98].

3.2.2.2 Tandem μ -Reactor Ex Situ Configuration

In the *ex situ* configuration, the second heated zone of the reactor is the upgrading zone, and contains a 10 mg catalyst bed, suspended between two plugs of quartz wool. A diagram of the Frontier Tandem μ -Reactor in the *ex situ* configuration is shown in Figure 3.5.

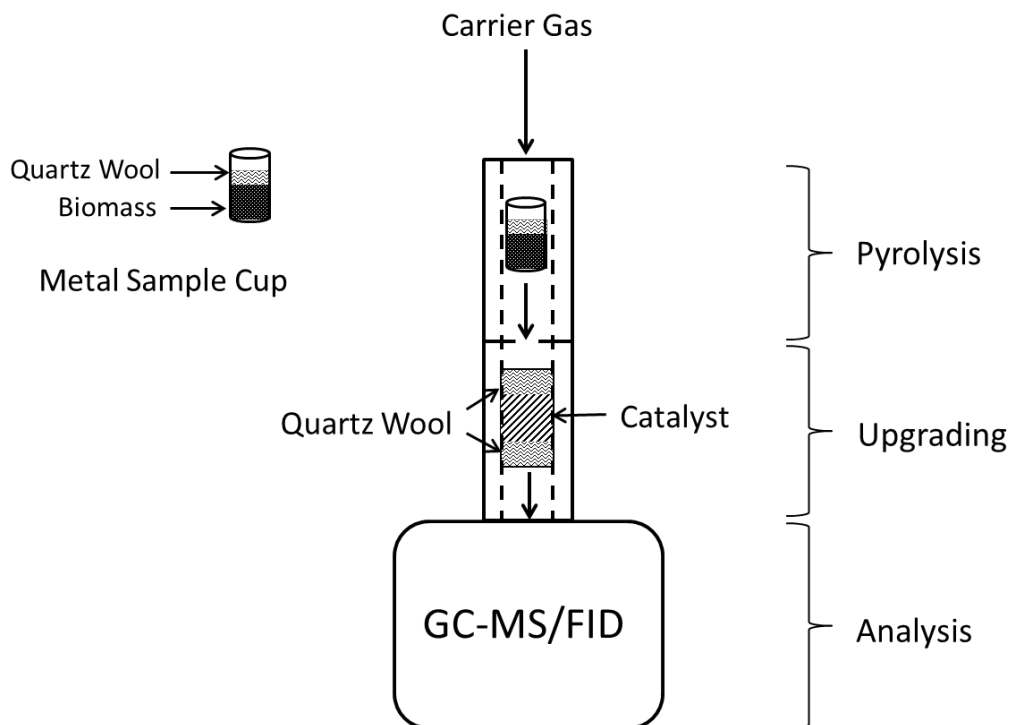


Figure 3.5 Diagram of the Tandem μ -Reactor system in the *ex situ* configuration. This is the configuration used for catalyst deactivation experiments.

During an *ex situ* CFP experiment on the Tandem μ -Reactor, a sample cup containing 0.5 mg of biomass is dropped into the pyrolysis zone. The pyrolysis products are then carried through upgrading zone by GC carrier gas, and finally to the inlet of the GC-MS/FID detection system. In the experiments presented in this work, both the pyrolysis zone and the upgrading zone were held at 500°C.

3.2.2.3 Tandem μ -Reactor *in situ* Configuration

When the Tandem μ -Reactor is set up in the *in situ* configuration, the second heated zone of the reactor is a transfer zone, and consists of an empty quartz transfer line. A diagram of the reactor in the *in situ* configuration is shown in Figure 3.6

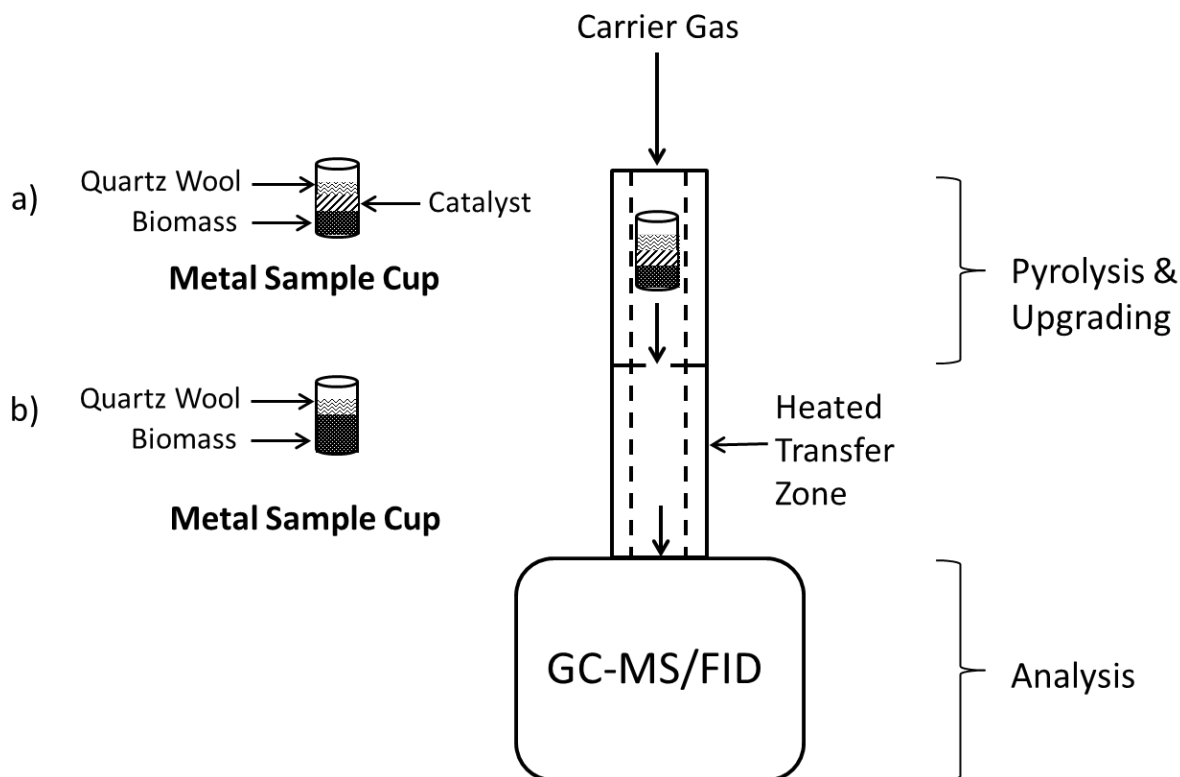


Figure 3.6 Diagram of the Tandem μ -Reactor in the *in situ* configuration for a) *in situ* CFP for catalyst screening experiments or b) non-catalytic pyrolysis

When set up in the *in situ* configuration, the Tandem μ -Reactor can be used for either *in situ* CFP experiments or for non-catalytic pyrolysis experiments. During an *in situ* CFP experiment, the sample cup is loaded with a 0.5 mg layer of biomass, and then covered with the desired weight of catalyst, as shown in Figure 3.6 a). When dropped into the first heated zone, both pyrolysis and catalytic upgrading occur in the sample cup, and the upgraded products are then carried through

the transfer zone to the GC-MS/FID. During a non-catalytic pyrolysis experiment, the sample cup would be loaded with biomass only, as depicted in Figure 3.6 b). After the sample cup is dropped into the first heated zone, pyrolysis occurs and the raw pyrolysis vapors are carried through the transfer zone to the GC-MS/FID for analysis.

3.2.2.4 Tandem μ -Reactor GC-MS/FID Analyzers

After exiting the second heated zone of the Tandem μ -Reactor, products are carried to the GC-MS/FID (7890B / 5977A, Agilent Technologies). The vapors first arrive at the front of the GC, where they are trapped at -196°C in a liquid nitrogen microjet cryo-trap (MJT-1030Ex, Frontier Laboratories). The cryo-trap is located in-line with UA-5 columns for both the MS and FID. The GC oven program used for these experiments started from an oven rest temperature of 40°C , followed by a $15^{\circ}\text{C}/\text{min}$ ramp to 300°C . The cryo-trap allowed for greater product stratification than could be achieved by GC alone. CFP products and their retention times were identified by MS signal, using the NIST98 MS library. The FID signal, matched by retention time, was used for quantification, and was calibrated as described in Section 3.3.

A drawback of the Tandem μ -Reactor is that the attached MS has a high rate of tar accumulation, which results in both the need for more frequent cleaning and maintenance of the MS source, as well as a less consistent MS signal. The tar accumulation is a result of the direct flow path from the reactor to the GC inlet. Large polyaromatic compounds, which are formed during CFP but are too large to be detected by the GC, accumulate in the system. The FID, however, has a much more stable response factor and was added to the system to decrease the frequency with which the system needed to be calibrated.

3.2.3 Horizontal Packed-bed Reactor

3.2.3.1 Horizontal Packed-bed Reactor Flow Path and Components

The primary advantage of the Horizontal Packed-bed Reactor is that it can generate sufficient post-reaction catalyst to be characterized. The reactor consists of a quartz tube, with a sample insertion port located perpendicular to the flow path. 500 mg of catalyst was placed in the reactor, suspended between two plugs of quartz wool. Quartz sample boats, which contained 50 mg of biomass, are inserted into the flow path of the reactor, where pyrolysis occurs. The pyrolysis vapors were then carried by 54 mL/min of carrier gas (helium or hydrogen) over the catalyst bed. A diagram of the horizontal reactor is shown in Figure 3.7.

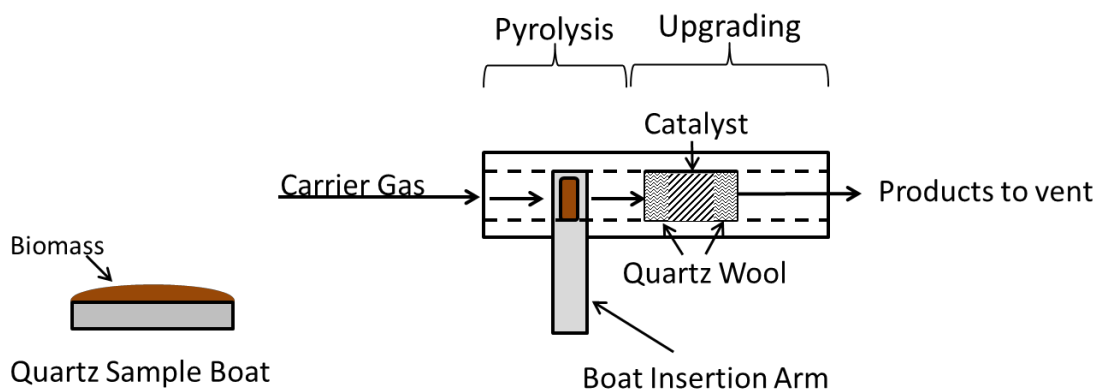


Figure 3.7 Diagram of the horizontal reactor used for catalyst sample generation

Following each experiment on the Horizontal Packed-bed Reactor, the catalyst bed was cooled under helium until the catalyst bed was $<200^{\circ}\text{C}$, to ensure no oxidation of coke occurred. The post-reaction catalyst was then portioned for subsequent catalyst characterization techniques.

3.3 Calibrations for Reactor Systems

For both the Tandem μ -Reactor and Pyroprobe reactor systems, a thorough calibration was performed on the GC-MS and GC-MS/FID, respectively. For quantification, the systems were calibrated for 40 of the most common products identified during the CFP of biomass. A list of these compounds can be found in Table 3.2.

Table 3.2 Hydrocarbon and oxygenate compounds for which the vapor product analysis systems were calibrated.

Hydrocarbons	Oxygenates
1,2,3-trimethyl benzene	1,2-benzenediol
1H-Indene, 1-methyl-	1,2-benzenediol, 4-methyl-
benzene	1,2-cyclopentanedione
ethyl benzene	1H-indenol
indane	1-naphthalenol
indene	2-cyclopenten-1-one
naphthalene	2-cyclopenten-1-one, 2-hydroxy-3-methyl-
naphthalene, 1,5-dimethyl-	2-cyclopenten-1-one, 2-methyl-
naphthalene, 1-methyl-	2-methoxy-4-vinylphenol
naphthalene, 2-methyl-	3-buten-2-one
o-xylene	4-hydroxy-3-methoxybenzaldehyde
phenanthrene	acetaldehyde
phenanthrene, 1-methyl-	acetic acid
p-xylene	acetone
toluene	benzofuran
	benzofuran, 2-methyl
	furan
	furan, 2,5-dimethyl-
	furan, 2-methyl-
	furfural
	phenol
	phenol, 2,3-dimethyl-
	phenol, 2,4,6-trimethyl-
	phenol, 2,4-dimethyl-
	phenol, 2-methoxy-
	phenol, 2-methoxy-4-(1-propenyl)-
	phenol, 2-methoxy-4-methyl-
	phenol, 2-methyl-
	phenol, 3-methyl-
	phenol, 4-ethyl-2-methoxy-
	phenol, 4-methyl-

The 40 compounds were contained in two separate calibration solutions, prepared by Accustandard Labs. The oxygenated compounds, along with toluene, were in the oxygenate standard with methylene chloride as a solvent, and the hydrocarbons were contained in a second standard solution, with toluene as a solvent. The calibration mixtures were serially diluted with

their native solvent, at ratios of 1:2, 1:4, 1:8, 1:16, and 1:32. For both systems, the calibration procedure was to manually inject 1 μL of calibration solution from each dilution into the front inlet of the GC. In the case of the Pyroprobe GC-MS system, a correlation between MS area and the known concentration of the analytes in the calibration solution was created. For the Tandem μ -Reactor GC-MS/FID, a correlation between FID area and the known concentration of the analytes in the calibration solution was created. This procedure was performed approximately monthly, or at the beginning of a new experimental set.

For compounds which the analysis systems were not specifically calibrated, functional group matching and molecule size were used. This provided a best approximation of the response factors for the un-calibrated compounds.

3.4 Catalyst Characterization Techniques

3.4.1 Thermogravimetric Analysis

Thermogravimetric analysis (TGA) was performed, using Setaram's Setsys Evolution TGA-DSC instrument, on the post-reaction catalysts to determine the mass of coke present. Prior to the TGA characterization, catalyst samples (~20 mg) were stabilized in a 50 mL/min flow of zero air for seven minutes at ambient temperature. Following the stabilization, TGA analysis began, and the post-reaction catalyst samples were heated at a rate of 20°C/min to a final temperature of 780°C, in the same flow of zero air.

3.4.2 Ammonia Temperature Programmed Desorption

To determine the number of acid sites accessible on the fresh and post-reaction catalysts, temperature programmed desorption of ammonia (NH₃TPD) was performed on an Altamira AMI-390 system. In preparation for NH₃TPD, the catalyst samples were pretreated. Unmodified, fresh catalysts were pretreated at 500°C for 30 minutes in a flow of 10% O₂ in Ar. Metal-modified, fresh catalysts (used in Section 8) were pretreated at 500°C for 30 min in a stream of 10% H₂/Ar for reduction to occur. All post-reaction catalysts were pretreated at 500°C for 30 min in helium. Following pretreatment, all samples were cooled to 120°C to begin the NH₃TPD analysis.

Initially, samples were held at 120°C for 30 minutes while being flushed with 100% helium. NH₃ adsorption was then performed using a flow of 25 sccm of 10%NH₃/He for 30 min, also at 120°C. Following adsorption, the samples purged for 10 min in a flow of helium to remove any stray NH₃ prior to temperature programmed desorption. The TPD was performed by heating the samples to 500°C, at a rate of 30°C/min, followed by a hold for 30 minutes at 500°C. The desorbing ammonia was tracked by a thermal conductivity detector (TCD), which allowed for the quantification of desorbed ammonia.

3.4.3 Nitrogen Physisorption

Catalyst characterisation for surface area, micropore surface area, and pore volume was performed via nitrogen physisorption. The characterization was performed on a Quadrasorb SI from Quantachrome Instruments. In preparation for physisorption, samples were held under vacuum at 350°C overnight (approximately 16 hours), to ensure sufficient time for outgassing of any physisorbed species. The samples were then cooled to 77 K, by immersion in liquid nitrogen,

for the characterization. The physisorption data was used to calculate each sample's total surface area using the multi-point Brunauer-Emmett-Teller (BET) method, and used to calculate the surface area contribution from the pores and the pore volume using the Barrett-Joyner-Halenda (BJH) method. Additionally, the contribution from the micropores (<2 nm) to the total catalyst surface area was calculated via the DeBoer t-plot method.

3.5 Biomass

For all experiments performed with whole biomass, pinewood provided from Idaho National Laboratory was used. For experiments with individual biopolymers (Sections 6 and 7), several representative, purified samples were used. To represent cellulose, Avicell cellulose was obtained from Sigma Aldrich. To represent lignin, organosolv lignin from mixed hardwoods was produced in-house at the National Renewable Energy Laboratory (NREL). Detailed process information can be found elsewhere [99]. All biomasses were milled to a fine powder (approximate particle size <1 μm) for the experiments reported here.

3.6 Catalysts

3.6.1 Commercially-Available ZSM-5 Catalysts

Table 3.3 lists the ZSM-5 catalysts which were used for the experiments described in this document, as well as their manufacturers, properties, and the sections in which they are used.

Table 3.3 Name, manufacturer, and properties of the unmodified ZSM-5 catalysts used in the experiments described in this document.

ZSM-5 Catalyst Name	Manufacturer	SAR	Binder	Used in Sections
UPV-2	Albemarle	proprietary	proprietary	4
Alfa Aesar-23	Alfa Aesar	23	none	5.1
Alfa Aesar-30	Alfa Aesar	30	none	5.1
Alfa Aesar-50	Alfa Aesar	50	none	5.1
Alfa Aesar-80	Alfa Aesar	80	none	5.1
Alfa Aesar-280	Alfa Aesar	280	none	5.1
Nexceris-alumina	Nexceris	30	alumina	5.2
Nexceris-clay	Nexceris	30	clay	5.2, 7
Nexceris-SiO ₂	Nexceris	30	SiO ₂	5.2, 8

3.6.2 Catalyst Modification

In addition to the catalysts which were used in the condition that the manufactures provided, a series of catalysts was generated in-house by modifying the Nexceris-SiO₂ catalyst.

The metal-modified catalysts were prepared via incipient wetness impregnation. This was performed using an aqueous solution containing the nitrate precursors of the desired metals (Cu, Ga, Ni, Co, or Pt) obtained from Sigma Aldrich. An equimolar quantity of metal was added to each catalyst, which corresponded to a 2:1 molar ratio of aluminum in the catalyst to metal being added. Basing the modification loadings on a molar ratio resulted in varied weight loadings on the catalysts, as detailed in Table 3.4.

Table 3.4: Metal loadings of the modified catalysts.

Catalyst	Metal Loading
Cu/ZSM-5	3.3 wt%
Ga/ZSM-5	3.7 wt%
Ni/ZSM-5	3.1 wt%
Co/ZSM-5	3.1 wt%
Pt/ZSM-5	10.3 wt%

Following the impregnation, the modified catalysts were dried at 110°C in air for three hours and then calcined by heating at a rate of 2°C/min up to 550°C, and holding at 550°C for three hours.

4 Deactivation Trend of ZSM-5 during CFP of Pine and Observation of Intermediate Pyrolysis Products

The *ex situ* catalytic fast pyrolysis (CFP) experiments described in this section were performed on the Pyroprobe reactor (detailed in Section 3.2.1), to study the deactivation of ZSM-5 during CFP of pine. The experimental design was structured so that product observations could be made at multiple points as the catalyst deactivated. To achieve this, a 10 mg catalyst bed of UPV-2 ZSM-5 catalyst was loaded in the upgrading zone and held at 500°C. This catalyst was selected due to its superior upgrading ability in a prior screening [100]. Successive 1 mg samples of pine were then pyrolyzed and upgraded over the catalyst until a cumulative biomass:catalyst ~2 was achieved. Following the pyrolysis and upgrading of each sample, detailed species information was collected via gas chromatography and mass spectroscopy (GC-MS).

4.1 Products from the CFP of Pine with ZSM-5 Catalyst

A GC chromatogram from the first pyrolyzed and upgraded sample, with select structural IDs, is shown in Figure 4.1.

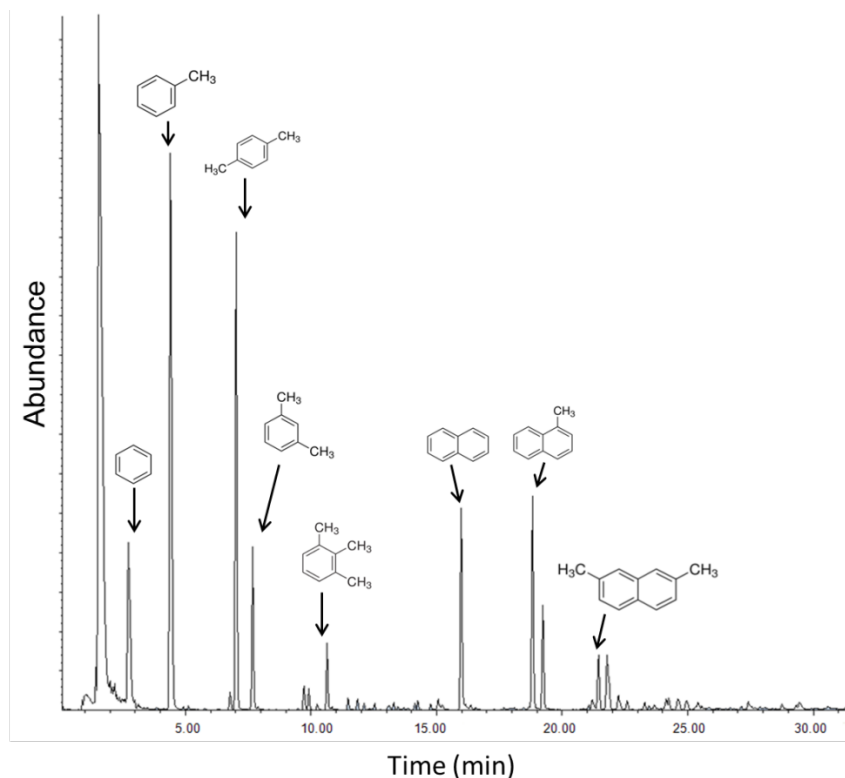


Figure 4.1 GC Chromatogram, with compound structure labels, from CFP of pine over a fresh ZSM-5 catalyst (biomass:catalyst = 0.1). The Y-axis shows MS area count abundance from the compound(s) eluting from the GC column at the specified retention time, shown on the X-axis.

In Figure 4.1, the total ion MS area abundance (Y-axis) is shown for the compound eluting from the GC column at a given retention time (X-axis). At retention time ~2 minutes, there is a large unlabeled peak in the chromatogram. This peak is formed by the coelution of light compounds (<C₅ hydrocarbons) that are not sufficiently separated by the GC configuration to identify. The primary, liquid-range products begin with benzene at a retention time of 3.0 minutes. As the GC method progresses and the oven temperature increases, higher boiling-point products, and products with increasing strong column interactions, exit the GC column and are analyzed by the MS. The specifics of the GC temperature program are detailed in Section 3.2.1.2. The compound designation is a result of matching the MS ion scattering pattern of the compound eluting from

the GC column with a library of fragmentation patterns compiled by the National Institute of Standards and Technology (NIST).

The information gathered from the GC-MS analysis, as well the product grouping, from the chromatogram in Figure 4.1 is detailed in Table 4.1.

Table 4.1 Product list, GC retention time, quality of NIST library match, compound group designations, and area counts for the first pine sample pyrolyzed and upgraded over ZSM-5 (biomass:catalyst= 0.1). The sample was pyrolyzed and upgraded at 500°C, on the Pyroprobe reactor.

Compound	Retention Time	Quality	Group	Sub Group	Area Counts
Benzene	3.0	94	HC	Benzene	147,128
Toluene	4.7	95	HC	Toluene	423,753
Ethylbenzene	7.0	91	HC	other 1-ring Aromatics	23,894
p-Xylene	7.2	97	HC	p-Xylene	301,013
Benzene, 1,2-dimethyl-	7.8	87	HC	other 1-ring Aromatics	51,131
Benzene, 1-ethyl-3-methyl-	9.9	95	HC	other 1-ring Aromatics	8,972
Benzene, 1,2,3-trimethyl-	10.7	97	HC	other 1-ring Aromatics	17,069
Indane	11.9	87	HC	other 1-ring Aromatics	31,447
Indene	12.2	95	HC	other 1-ring Aromatics	21,470
Indane, 1-methyl-	14.8	93	HC	other 1-ring Aromatics	12,216
Indane, 2-methyl-	15.1	96	HC	other 1-ring Aromatics	15,741
2-Methylindene	15.3	90	HC	other 1-ring Aromatics	22,865
Naphthalene	16.0	94	HC	2-Ring Aromatics	61,179
Naphthalene, 2-methyl-	18.9	91	HC	2-Ring Aromatics	82,086
Naphthalene, 2-methyl-	19.3	94	HC	2-Ring Aromatics	24,553
Naphthalene, 2,6-dimethyl-	21.5	97	HC	2-Ring Aromatics	24,637
Naphthalene, 2,6-dimethyl-	21.8	97	HC	2-Ring Aromatics	7,555

In Table 4.1, the primary products from the first biomass sample pyrolyzed and upgraded are shown in the order of their GC retention time. The third column in the table is the percent match (quality) of the MS signal when compared to the NIST library entries for the compound. Following the identification of each primary peak, the compounds are grouped for a broader analysis of the products. The simplest grouping of the liquid-range products is through designation as either hydrocarbon (HC) or oxygenated (OX) species. The products are then sub-grouped by other characteristics, such as number of aromatic rings for hydrocarbons, and by functional groups for oxygenates. Indane and indene are grouped as 1-ring aromatics, rather than in a separate category, in part because of the ambiguity of the MS structural matches. It is often very difficult to determine which structural isomer is present without running a known standard. This becomes particularly apparent with indenenes and indanes, as the open and the closed-ring forms are nearly indistinguishable.

The upgraded products from the first pulse of pine vapors are entirely aromatic hydrocarbons, and are primarily 1-ring aromatics. Benzene, toluene, and p-xylene account for the majority of all product area counts, together accounting for ~70% of the total area counts.

The described method of grouping similar compounds allows for trends in the products to be visualized easily over the course of the deactivation experiment. The broadest grouping, separating products into hydrocarbons and oxygenates, allows for observation of the overall deactivation trend of the catalyst.

4.2 Deactivation Trend of ZSM-5 during CFP of Pine

The grouping of all products as either HC or OX, for each of the successive pine samples pyrolyzed and upgraded over the ZSM-5 catalyst bed, is shown in Figure 4.2.

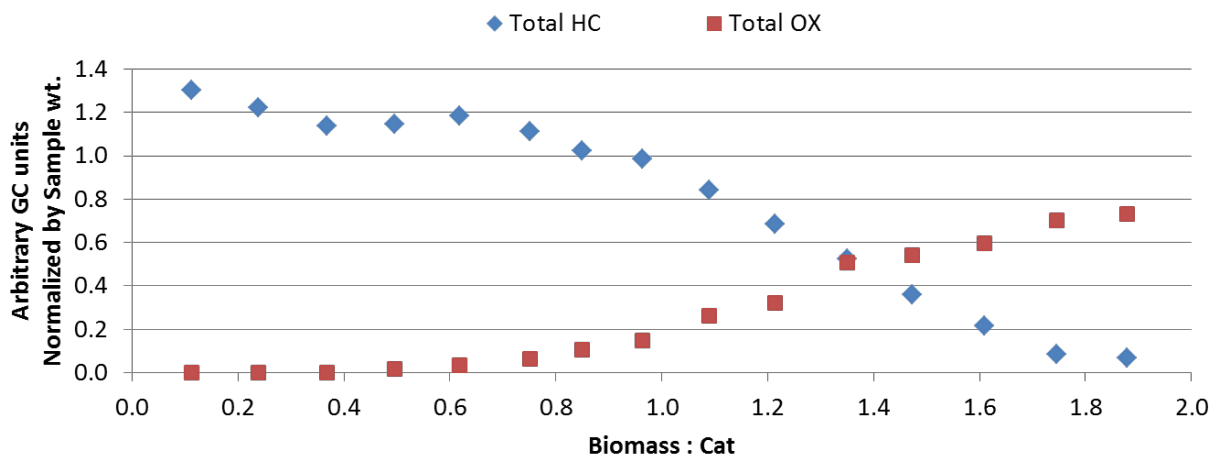


Figure 4.2 Deactivation trend of ZSM-5 during CFP of pine. The blue markers represent the total GC area counts of hydrocarbon species, while the red markers represent the total area counts of oxygenated species. The cumulative ratio of biomass pyrolyzed –to- catalyst bed weight (biomass:catalyst) is shown on the X-axis.

The X-axis of Figure 4.2 shows the cumulative ratio of biomass pyrolyzed to catalyst bed weight. At the beginning of the experiment, at low biomass:catalyst, the products are all hydrocarbons and no oxygenates are produced. As an increasing number of pine samples are pyrolyzed and upgraded over the ZSM-5, the catalyst bed’s efficacy at deoxygenating the pyrolysis vapors decreases, and a progressive amount of GC area counts are attributed to oxygenated compounds. At the end of the experiment, biomass:catalyst= 1.9, the products are overwhelmingly oxygenates.

Table 4.2 and Table 4.3 give detailed product information for the data points at biomass:catalyst of 1 and 1.9, respectively.

Table 4.2 Product list, GC retention time, quality of NIST library match, compound group designations, and area counts for the first sample upgraded, biomass:catalyst= 1.0

Compound	Retention Time	Quality	Group	Sub Group	Area Counts
Furan, 2-methyl-	2.5	96	OX	Furans	68,449
1,3-Cyclohexadiene	2.9	92	HC	Cyclohexadiene	36,611
Benzene	3.1	91	HC	Benzene	91,904
Toluene	4.7	95	HC	Toluene	286,247
Ethylbenzene	7.0	91	HC	other 1-ring Aromatics	29,114
p-Xylene	7.2	97	HC	p-Xylene	258,961
Styrene	7.8	96	HC	other 1-ring Aromatics	14,844
Benzene, 1-ethyl-4-methyl-	9.9	95	HC	other 1-ring Aromatics	15,113
Phenol	10.8	86	OX	Phenol	26,732
Indane	11.9	87	HC	other 1-ring Aromatics	15,980
Indene	12.2	95	HC	other 1-ring Aromatics	35,455
Phenol, 2-methyl-	12.7	95	OX	Alkylated Phenols	16,062
Phenol, 3-methyl-	13.4	93	OX	Alkylated Phenols	9,727
Phenol, 2-methoxy-	13.6	93	OX	Methoxy Phenols	7,281
Benzofuran, 2-methyl-	14.0	92	OX	Benzofurans	5,651
Indane, 2-methyl-	15.1	96	HC	other 1-ring Aromatics	17,848
2-Methylindene	15.3	97	HC	other 1-ring Aromatics	32,742
Naphthalene	16.0	97	HC	2-Ring Aromatics	60,300
Phenol, 2-methoxy-4-methyl-	16.4	96	OX	Methoxy Phenols	12,501
Naphthalene, 2-methyl-	18.9	94	HC	2-Ring Aromatics	68,030
Naphthalene, 2,7-dimethyl-	21.5	98	HC	2-Ring Aromatics	21,015

Table 4.3 Product list and grouping information for biomass:catalyst 1.9

Compound	Retention Time	Quality	Group	Sub Group	Area Counts
Furan, 2-methyl-	2.5	94	OX	Furans	100,259
Acetic acid	2.7	91	OX	Acids	34,178
Toluene	4.6	93	HC	Toluene	28,359
2-Cyclopenten-1-one	6.2	90	OX	Cyclopentanones	31,381
Furfural	6.3	93	OX	Furans	47,019
p-Xylene	7.1	95	HC	p-Xylene	27,116
2-Cyclopenten-1-one, 2-methyl-	8.2	90	OX	Cyclopentanones	6,633
2-Furancarboxaldehyde, 5-methyl-	9.9	93	OX	Furans	34,880
Phenol	10.7	94	OX	Phenol	2,259
1,2-Cyclopentanedione, 3-methyl-	11.9	93	OX	Cyclopentanones	9,802
Phenol, 2-methyl-	12.7	97	OX	Alkylated Phenols	10,859
Phenol, 2-methoxy-	13.5	97	OX	Methoxy Phenols	94,358
Naphthalene	16.0	93	HC	2-Ring Aromatics	12,538
Phenol, 2-methoxy-4-methyl-	16.3	97	OX	Methoxy Phenols	87,485
Phenol, 4-ethyl-2-methoxy-	18.5	91	OX	Methoxy Phenols	38,427
2-Methoxy-4-vinylphenol	19.3	91	OX	Methoxy Phenols	90,395
Phenol, 2-methoxy-3-(2-propenyl)-	20.4	98	OX	Methoxy Phenols	48,327
Phenol, 2-methoxy-4-(1-propenyl)-	21.5	96	OX	Methoxy Phenols	36,834
Phenol, 2-methoxy-4-(1-propenyl)-	22.5	97	OX	Methoxy Phenols	112,629

In Table 4.2, which lists the product details for the biomass:catalyst= 1.0 results, it can be seen that several of the major products are oxygenates. The furans group, and specifically 2-methylfuran, is the most dominant oxygenated product, followed by phenol, alkylated phenols and alkylated benzofuran. Methoxy phenols are also present, indicating breakthrough of primary pyrolysis vapors. The methoxy functional group, $-OCH_3$, is prevalent in the phenolic monomers which comprise lignin, and is seen in abundance during uncatalyzed pyrolysis of pine. Despite the presence of oxygenated species, the product list is still dominated by hydrocarbons, both in number of products and area counts.

At the end of the deactivation experiment, at biomass:catalyst= 1.9, the products, detailed in Table 4.3, are almost entirely oxygenates. The three hydrocarbon products still produced (toluene, xylene, and naphthalene), account for only a small fraction of the total area counts. Also of note, the methoxy phenol compounds have shifted from singularly-alkylated methoxy phenols to larger branched methoxy phenols, more closely resembling lignin monomers. This indicates that very little catalytic functionality remains. The furan products have increased in area counts at biomass:catalyst=1.9, compared to biomass:catalyst= 1, along with methoxy phenols. However, phenol, alkylated phenols, and benzofurans, have decreased in the later stages of the deactivation experiment.

At biomass:catalyst=1.9, Table 4.3, several compounds are seen that were not present at biomass:catalyst=1.0, such as acetic acid, furfural, 5-methyl-2-Furancarboxaldehyde, and cyclopentenones. To better visualize the concurrent changes in product group distribution as the catalyst deactivates, the area counts attributed to all groups have been plotted in Figure 4.3.

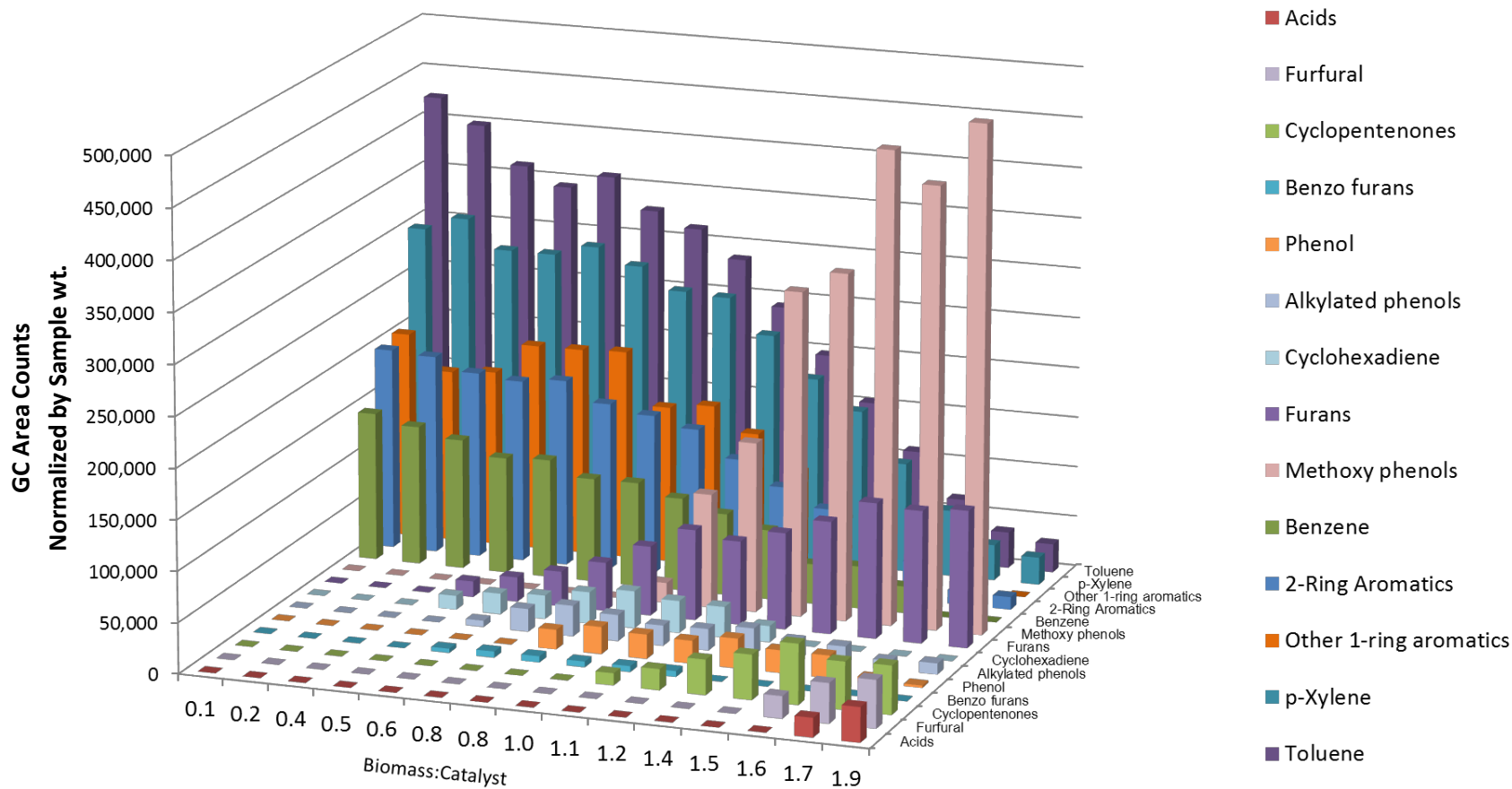


Figure 4.3 A detailed view of the area counts attributed to each product grouping throughout the duration of the *ex situ* CFP experiment, as a function of the cumulative ratio of biomass pyrolyzed –to- catalyst bed weight (biomass:catalyst) is shown on the X-axis.

In Figure 4.3, at low biomass:catalyst, the only products produced are 1- and 2-ring aromatics, with area counts contributed to toluene and p-xylene being the most dominant. As successive samples of pine are pyrolyzed and upgraded, the levels of hydrocarbons steadily decrease, and the types of products being formed become more diverse. At biomass:catalyst ~ 0.6 , furans, benzofurans, and phenols are detected as the first oxygenated species. However, a non-aromatic hydrocarbon group that is not present at low biomass:catalyst, cyclohexadiene, is also observed.

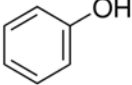
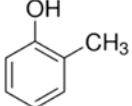
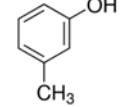
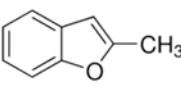
As the ZSM-5 continues to deactivate, methoxy phenols and furans become the prominent product groups formed. At high biomass:catalyst there are very few hydrocarbons produced, and late stage oxygenated products, such as acids, furfural, and cyclopentenones are formed.

4.3 Observation of Intermediate Products

Most product groups were observed to have a singular, overarching yield trend. The product group either formed in largest quantities with fresh catalyst and steadily decreased to a minimum (e.g. benzene, toluene, and naphthalene), or formed at higher biomass:catalyst and steadily increased to a maximum at the end of the experiment (e.g. furans and methoxy phenols).

However, there was a third category of product groups that did not conform to either of these trends. A group of “intermediate products” was observed that were neither produced in great abundance at very low nor very high biomass:catalyst, and they reached their greatest abundance during intermediate levels of catalyst deactivation. The intermediate products observed are listed in Table 4.4.

Table 4.4 List of intermediate compounds, and their structures and grouping, formed during *ex situ* CFP of pine with ZSM-5. These products were produced in greatest abundance at intermediate biomass:catalyst.

Compound Name	Structure	Grouping
Phenol		Phenol
2-methylphenol		Alkylated Phenols
3-methylphenol		Alkylated Phenols
2-methylbenzofuran		Benzofurans
1,3-cyclohexadiene		Cyclohexadiene

The intermediate species, with the exception of 1,3-cyclohexadiene, are all oxygenated and aromatic. This observation suggests that the intermediates may be the result of the partial or incomplete deoxygenation of lignin pyrolysis vapors, which are aromatic oxygenates. This hypothesis is further discussed in Section 7.

4.4 Section Conclusions

The deactivation trend of ZSM-5 and changes in product slate during *ex situ* CFP of pine have been observed as successive samples of pine were pyrolyzed and upgraded over a fixed catalyst bed of UPV-2 ZSM-5. At low biomass:catalyst, the ZSM-5 was fresh and fully active,

generating only aromatic hydrocarbons. The yield of these hydrocarbons steadily decreased throughout the experiment as the catalyst deactivated, presumably due to coke formation. At biomass:catalyst=0.5 the first oxygenated products, furans, were formed. As the cumulative mass of pine pyrolyzed and upgraded over the catalyst increased, deactivation became more severe and more complex oxygenates and primary pyrolysis products, such as methoxy phenols, were seen in the products.

Of particular note were several products formed at intermediate levels of catalyst deactivation at biomass:catalyst= ~0.6 -1.7. The intermediate species, with the exception of 1,3-cyclohexadiene, are all oxygenated and aromatic, including phenol and alkylated phenols. This observation led to the hypothesis that the intermediate products are the result of incomplete deoxygenation of the aromatic oxygenates formed by the non-catalytic pyrolysis of lignin. This is further explored in Section 7.

5 Impact of Silica-to-Alumina Ratio and Binder Type on the Efficacy of Upgrading During CFP of Pine with ZSM-5

Two important parameters of zeolite catalyst composition are the silica-to-alumina ratio (SAR) within the zeolite crystal and the binder material which is used to form macro catalyst particles. Although little has been reported on the influence of SAR and binder on CFP of biomass, both parameters are known to play a role on the upgrading capability of ZSM-5 during other reactions [42]. In order to conduct research with the authorization to characterize the catalysts, it was essential to select a commercially-available catalyst. A screening study was performed to determine the impact of these two parameters on the efficacy of ZSM-5 during CFP of pine, and to inform the selection of appropriate catalysts for further study.

The screenings, for both the SAR and binder type, were performed as *in situ* CFP experiments in the Tandem μ -Reactor. The experiments were performed at 500°C, and with a biomass:catalyst=0.2. The *in situ* configuration of the reactor is detailed in Section 3.2.2.3, and the specific preparation for an *in situ* CFP experiment is shown in Figure 3.6 b). The pine used is detailed in Section 3.5.

5.1 Comparison of ZSM-5 Catalysts with a Variety of Silica-to-Alumina Ratios

The Brønsted acidity of ZSM-5 is a function of the silica-to-alumina ratio (SAR) in the catalyst. Each instance of an aluminum (Al^{+3}) ion replacing a silica (Si^{+4}) ion in the ZSM-5 framework requires a +1 cation to satisfy the charge balance. When the substituting cation is H^+ , it forms a Brønsted acid site [40]. This creates an inversely proportional relationship between the SAR of the catalyst and its acidity. The Brønsted sites are thought to facilitate the desirable upgrading

reactions which occur during CFP with ZSM-5, due to their role in the hydrocarbon pool mechanism established for MTO reactions [65].

To determine the strength of the correlation between the SAR of a ZSM-5 and its quality as an upgrading catalyst for CFP of biomass, a screening of a wide variety of SARs was conducted. Samples of pure (no binder) ZSM-5 catalysts with SARs of 23, 30, 50, 80, and 280 were procured from Alfa Aesar. A series of *in situ* catalytic fast pyrolysis experiments was conducted using a 1:5 biomass:catalyst ratio. The total GC area counts, normalized by sample weight, attributed to hydrocarbons and oxygenates are shown in Figure 5.1. Although the summation of GC area counts is qualitative and cannot be tied to a specific yield, confidence can be had in the observable trends.

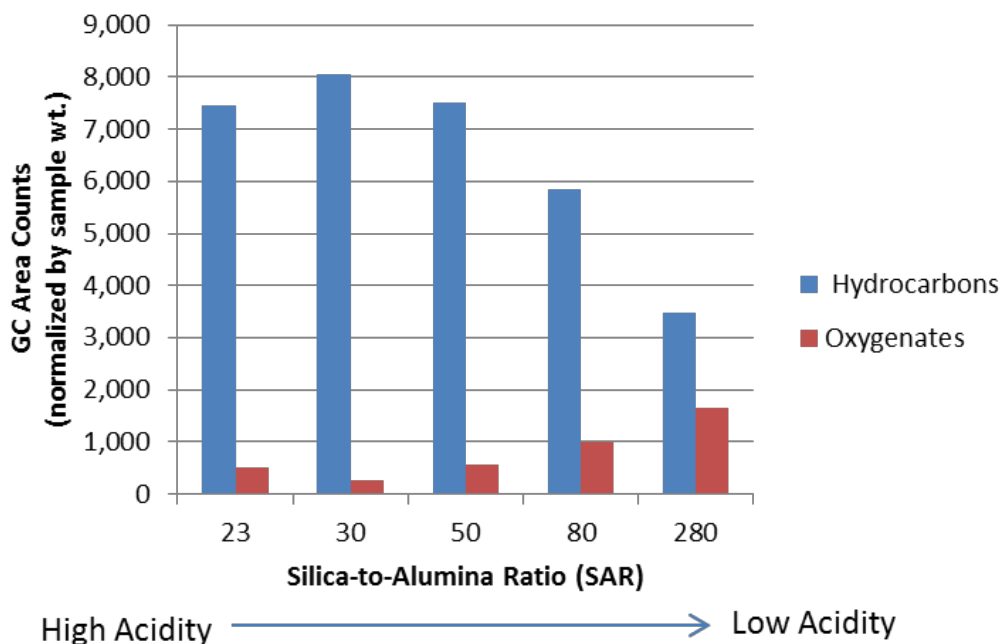


Figure 5.1 Impact of SiO₂-to-Al₂O₃ ratio on total GC area counts attributed to hydrocarbons (blue) and oxygenates (red) during *in situ* catalytic pyrolysis with pine.

From Figure 5.1, the low-SAR, and therefore more acidic, catalysts yielded a higher amount of hydrocarbon area counts during CFP, compared to the higher-SAR, less acidic catalysts. The ZSM-5 with SAR30 generated the highest hydrocarbon area counts, while the SAR280 ZSM-5 generated the least. The trend of oxygenate area counts was inversely proportional to that of the hydrocarbon yield. ZSM-5 SAR30 yielded the least area counts of oxygenates, while CFP with the higher and lower SAR catalysts resulted in more oxygenate area counts.

The acid sites of ZSM-5 are responsible for catalyzing the dehydration/aromatization reactions that result in the aromatic hydrocarbons which compose the overwhelming majority of hydrocarbon products formed during CFP with ZSM-5. Pérez-Uriarte et al., found during upgrading reactions with dimethyl ether over ZSM-5 that the rate of catalyst deactivation was inversely proportional to SAR, due to the slower rate of coke precursor formation in the less acidic catalysts [42]. Similarly, Wan et al. found that aromatic yield, coke formation, and deactivation rate were inversely proportional to SAR during methanol-to-gasoline reactions over ZSM-5 [44]. It is therefore hypothesized that the reason that ZSM-5 SAR30 performed the strongest as an upgrading catalyst, in that it resulted in the highest counts of hydrocarbons and the lowest counts of oxygenates, is that it is at the optimal point in these two concurrent trends:

- 1) Efficacy of deoxygenation increases with acidity
- 2) Coke formation, and the associated decrease in catalyst longevity, increases with acidity

These trends are sketched in Figure 5.2.

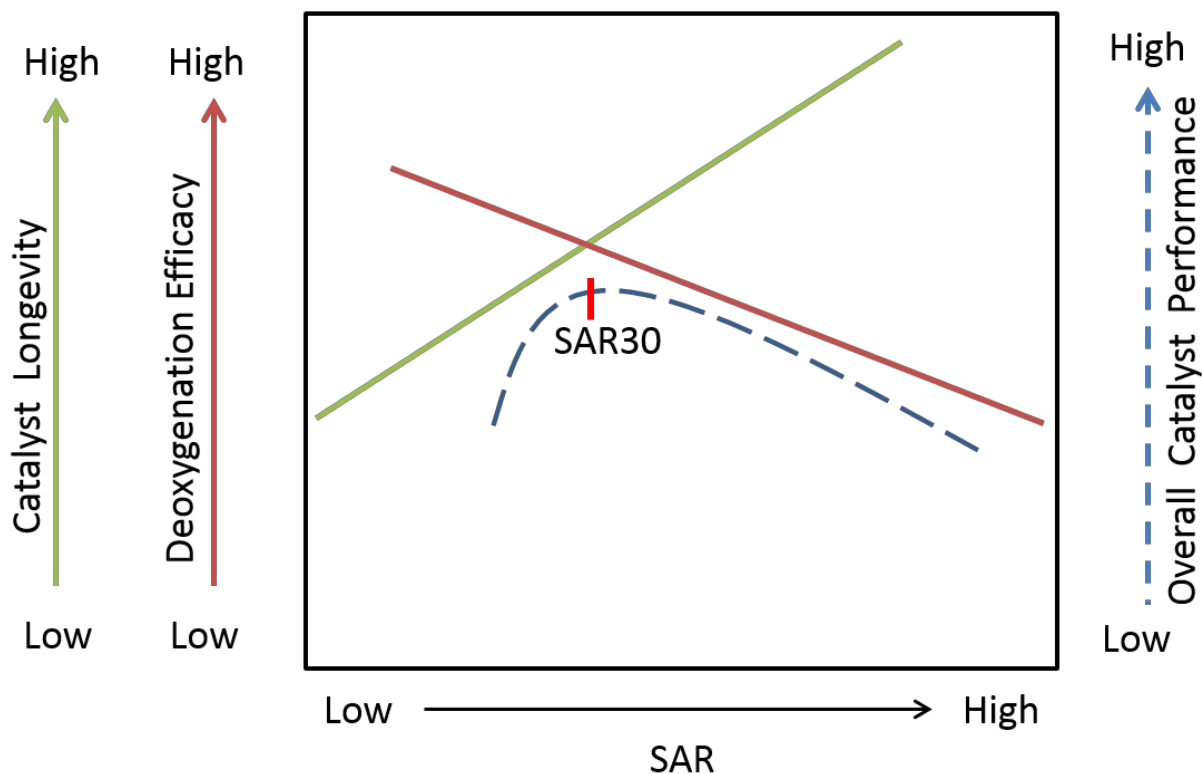


Figure 5.2 Graphic representation of the impact of ZSM-5 Silica-to-Alumina Ratio (SAR) on overall upgrading performance during CFP of biomass.

Considering these trends also gives insight into the amount of oxygenates produced, shown in red in Figure 5.1. At very low SAR, the high acidity results in the rapid formation of coke and catalyst deactivation. This resulted in oxygenated, raw pyrolysis products passing through unreacted. At high SAR, the low-acidity catalysts do not have sufficient acid sites to fully deoxygenate the pyrolysis vapors.

The selectivity seen within the hydrocarbon products is detailed in Figure 5.3.

Selectivity of Aromatic Hydrocarbons

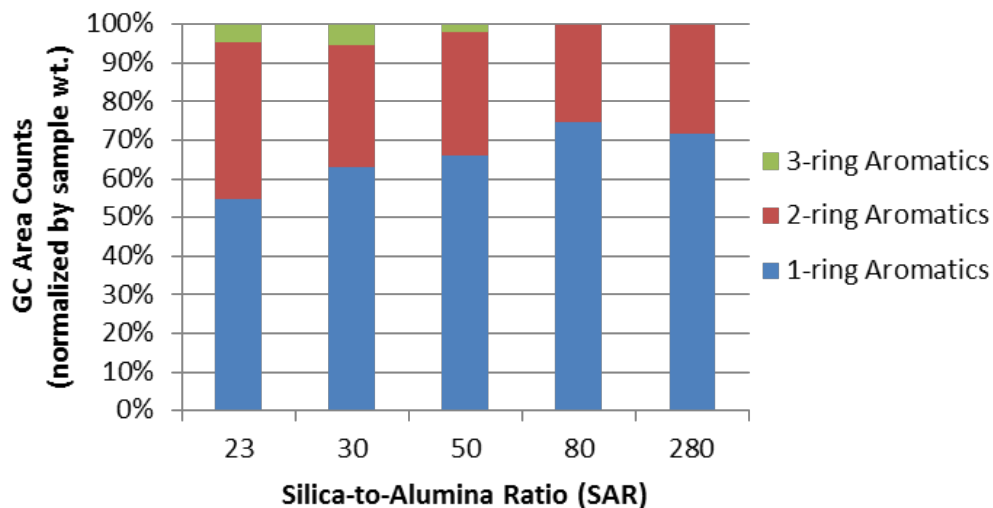


Figure 5.3 Selectivity towards 1-, 2-, and 3-ring aromatics during *in situ* catalytic fast pyrolysis of pine at 500°C and a biomass:catalyst=0.2, with ZSM-5 catalysts of varying silica-to-alumina ratios.

In Figure 5.3, which shows the selectivity of aromatic hydrocarbons, several trends can be observed. The selectivity to 1-ring aromatics increases with SAR, likely as a result of the decreasing ability to generate multi-ring aromatics as the number of acid sites decreases with the rising SAR. For the same reason, the selectivity towards 2-ring aromatics decreases with SAR. The catalysts with the lowest acidity, SAR80 and SAR280, did not form any detectable 3-ring aromatics. The 3-ring aromatic selectivity trends with a maximum at SAR30, possibly indicating that the most acidic catalyst, SAR23, is resulting in an increase in continued aromatization reactions to larger polyaromatic compounds that are not detectable by GC.

In addition to liquid-range aromatics, area counts from light hydrocarbons (compounds with less than six carbons) were collected.

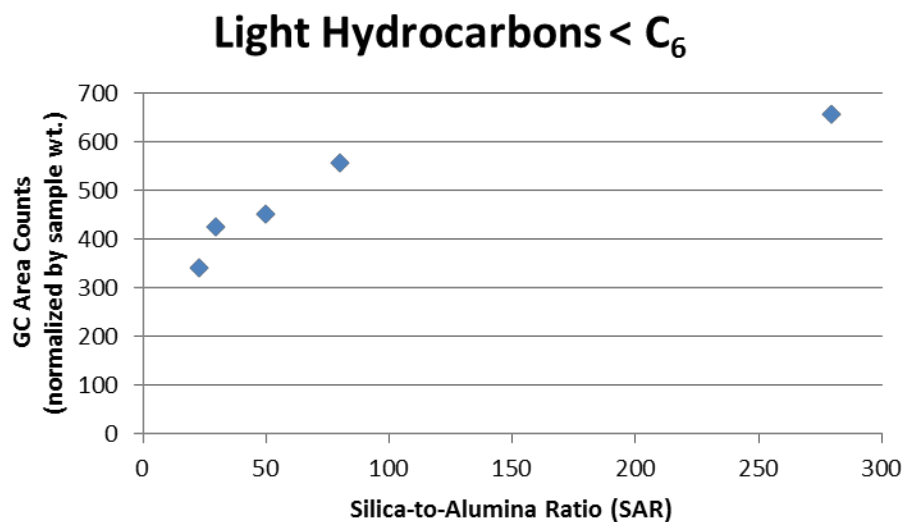


Figure 5.4 Area count contributions from light hydrocarbon (<C₆) gasses during catalytic fast pyrolysis with ZSM-5 catalysts with varying silica-to-alumina ratios

The GC area counts that are attributed to light hydrocarbons are detailed in Figure 5.4. The light hydrocarbons observed were entirely alkenes, and primarily propenes and butenes. They trend upward with SAR, and plateau at the lowest acidities. The observed trend within the olefin yield was also observed by Wan et al. during methanol conversions of ZSM-5 [44]. However, the team also noted many aliphatic hydrocarbons that were not observed during the upgrading experiments reported here [44]. It is likely that at lower acidities, the olefins are consumed by aromatization reactions, explaining the upward trend with SAR. However, at high SAR, the acid sites are overwhelmed and cannot deoxygenate sufficiently to continue the trend.

Due to its superior performance in hydrocarbon production and oxygenate elimination, SAR30 was determined to be the optimal silica-to-alumina upgrading for CFP of biomass, and it was used to inform the selection of catalysts to be studied for the impact of binder type, as detailed in Section 5.2.

5.2 Evaluation of ZSM-5 SAR30 Catalysts with Clay, Silica, and Alumina Binders

The catalysts investigated in Section 5.1, although scientifically interesting, were impractical as a CFP catalyst due to their small size. Without the addition of a binder, ZSM-5 crystals pack tightly together, resulting in severe practical limitations. However, the insight gained was applied to selecting a commercially-available ZSM-5 catalyst for further study. Three ZSM-5 catalysts with SAR30, with different binder materials, were procured from Nexceris. The binders used were: alumina, silica, and bentonite clay. A series of *in situ* screening experiments were performed, using biomass:catalyst=0.2, following the same procedure described in Section 5.1. The mass yield of hydrocarbons and oxygenates from these experiments is shown in Figure 5.5.

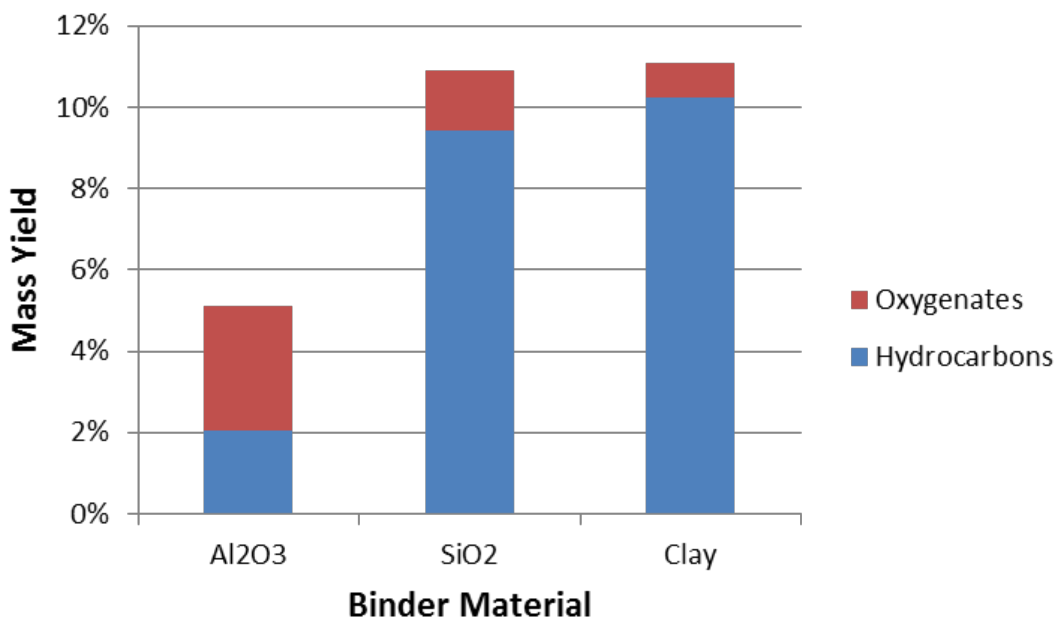


Figure 5.5 Mass yield of hydrocarbons and oxygenates during *in situ* screening of ZSM-5 catalysts with different binder materials.

The ZSM-5 catalysts with clay and SiO₂ binder performed comparably, each yielding ~10% hydrocarbons and ~1% oxygenates. The alumina catalyst performed poorly as an upgrading

catalyst, yielding only 2% hydrocarbons and 3% oxygenates. The alumina binder lends additional Lewis acidity to the catalysts, and is thought to have shifted the acidity of the catalysts beyond the optimal range, leading to poor upgrading ability. Although Lewis acid sites do not participate in the aromatization reactions as predicted by the study of methanol-to-olefin studies on ZSM-5 [65], the presence of extra-framework alumina in ZSM-5 have been known to improve zeolite activity, likely due to a synergistic effect between Brønsted and Lewis acid sites [101]. The selectivity among the aromatic hydrocarbons produced during the *in situ* CFP experiments is shown in Figure 5.6.

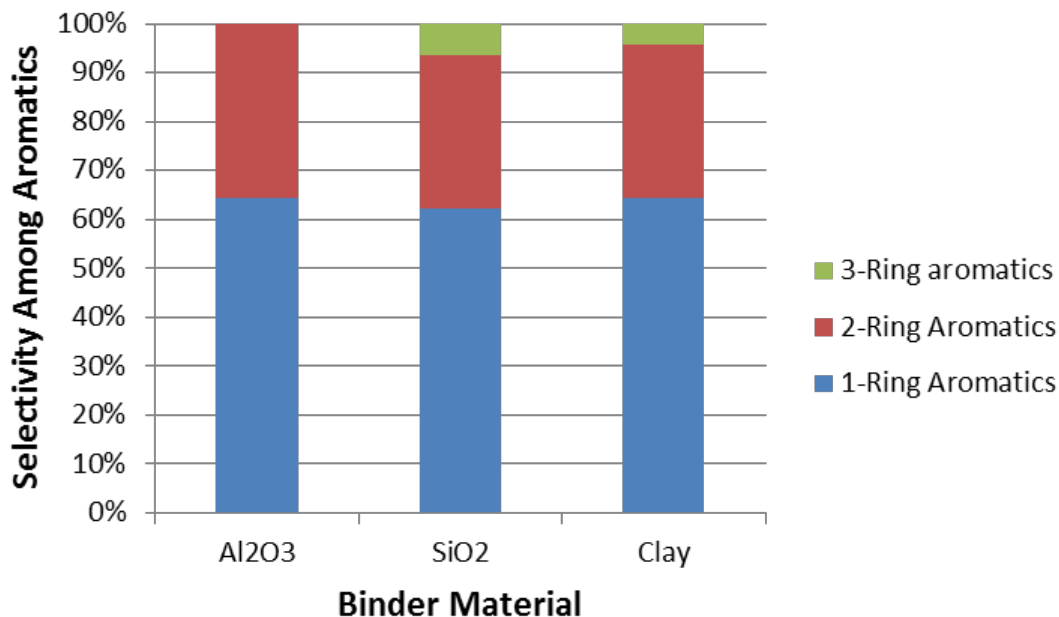


Figure 5.6 Selectivity among aromatic hydrocarbons during *in situ* screening of ZSM-5 catalysts with different binder materials.

Despite the differences in yield among the catalysts, the selectivity to 1-ring aromatics is quite similar with all three binder types at ~63%. The primary difference between the binders is that ZSM-5 catalysts with silica and clay binders produce 1-,2-,and 3-ring aromatics, while the ZSM-5 with alumina binder produces no 3-ring aromatics. As seen in Section 5.1, after reaching an optimal level, increased acidity leads to a decrease in 3-ring aromatic production; this is likely due to the intensified aromatization reactions leading to polyaromatic coke precursors. Analysis of the selectivity among the oxygenated species formed during upgrading, shown in Figure 5.7, supports the hypothesis that added acidity from the alumina binder is the cause of the poor performance of the $\text{Al}_2\text{O}_3/\text{ZSM-5}$ catalyst.

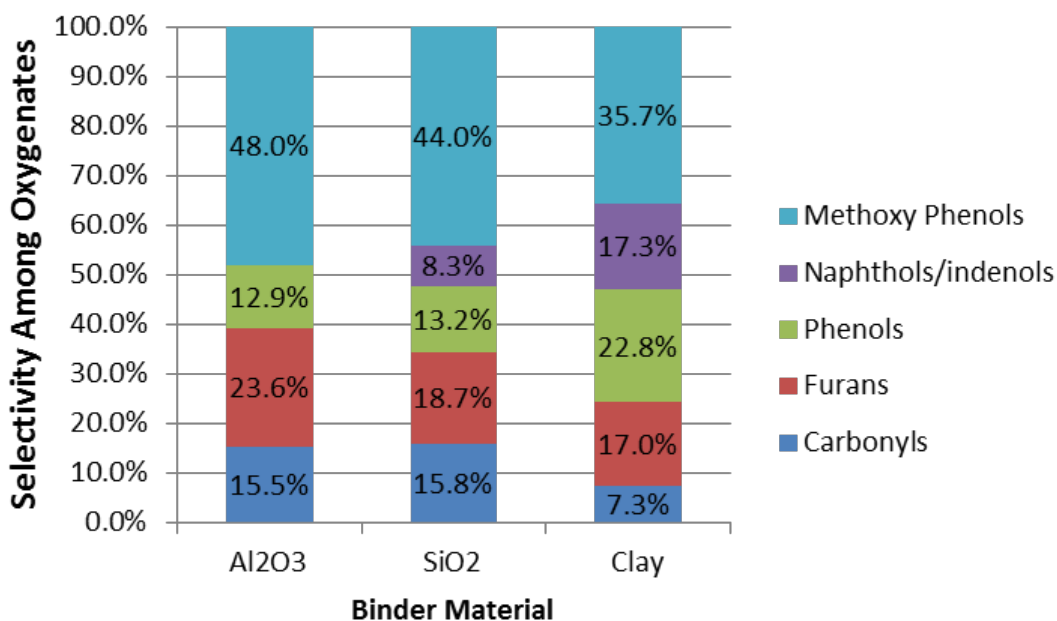


Figure 5.7 Selectivity among oxygenates during *in situ* screening of ZSM-5 catalysts with different binder materials.

The primary component of the oxygenates formed by all three catalysts were methoxy phenols. These are primary pyrolysis products and are found in CFP oil as the catalyst becomes

deactivated. The $\text{Al}_2\text{O}_3/\text{ZSM-5}$ catalyst had the lowest selectivity towards phenols, which are known to form during the intermediate stages of catalyst deactivation, and produced no indenols/naphthols. This information, coupled with the low hydrocarbon yield and high oxygenate yield of $\text{Al}_2\text{O}_3/\text{ZSM-5}$, as shown in Figure 5.5, indicates a rapid deactivation of the catalyst.

It is likely that the additional Lewis acidity from the alumina binder impacts the upgrading characteristics of the catalyst in a similar way to that of additional Brønsted acid sites, resulting in the catalyst being effectively outside the optimal range of acidity. In Section 5.1 it was found that increasing acidity beyond that achieved with a zeolite of SAR30, decreased the catalyst's efficacy during CFP.

The results presented here laid the groundwork for a larger-scale experiment on the impact of binder, conducted on a 2-inch fluidized bed reactor, which validated these experimental results [58].

5.3 Section Conclusions

Through a series of *in situ* CFP experiments with ZSM-5 catalysts of different silica-to-alumina (SAR) ratios and binder types, two catalysts were selected as adequate for additional study. At very low and very high SARs, ZSM-5 performs poorly as an upgrading catalyst for CFP of biomass. At high SAR, there are insufficient acid sites to deoxygenate the pyrolysis vapors effectively. At very low SAR, the high acidity leads to excessive aromatization and rapid deactivation. The pure ZSM-5 with an SAR of 30 was found to be the most effective at upgrading pyrolysis vapors.

Of the three catalysts tested for the impact of their binder, clay/ZSM-5 SAR30, silica/ZSM-5 SAR30, and alumina/ZSM-5 SAR30, clay/ZSM-5 and silica/ZSM-5 performed well, and comparably. It is thought that the added acidity from the alumina binder caused a net effect similar to that of increased Brønsted acidity, and resulted in a catalyst particle that was too acidic for effective upgrading. It would, perhaps, be a better binder choice for a base catalyst with a higher SAR.

Due to their superior performance, clay/ZSM-5 SAR30 and silica/ZSM-5 SAR30 were selected to be used for future CFP experiments.

6 Qualitative Discussion of Products from the Catalytic and non-Catalytic Pyrolysis of Cellulose, Lignin, and Pine

Before discussing the catalyst deactivation and product spectrum changes that occur during extensive upgrading with pine and its individual biopolymers, it is advantageous to have a general, qualitative discussion of the uncatalyzed and catalyzed pyrolysis of these biomasses.

6.1 Qualitative Comparison of the uncatalyzed pyrolysis of cellulose, lignin, and pine

To better understand the contributions of the polysaccharide and polyphenolic components of biomass to the composition of uncatalyzed pyrolysis vapors generated from whole biomass, a short series of Py/GC-MS experiments was performed on cellulose, lignin, and pine. A quantity of 0.5 mg of each biomass was loaded into a sample cup, and pyrolyzed at 500°C in the Tandem μ -Reactor without any catalyst. The Tandem μ -Reactor was in the *in situ* configuration, detailed in Section 3.2.2.3. These contributions are illustrated in a side-by-side comparison of the chromatograms from the uncatalyzed pyrolysis of the three biomasses, shown in Figure 6.1.

Select peaks, which are shared between the chromatogram of uncatalyzed pyrolysis of pine and that of either the uncatalyzed pyrolysis cellulose or lignin, have been labeled. The labeled peaks are identified and tabulated, along with their structures, in Table 6.1.

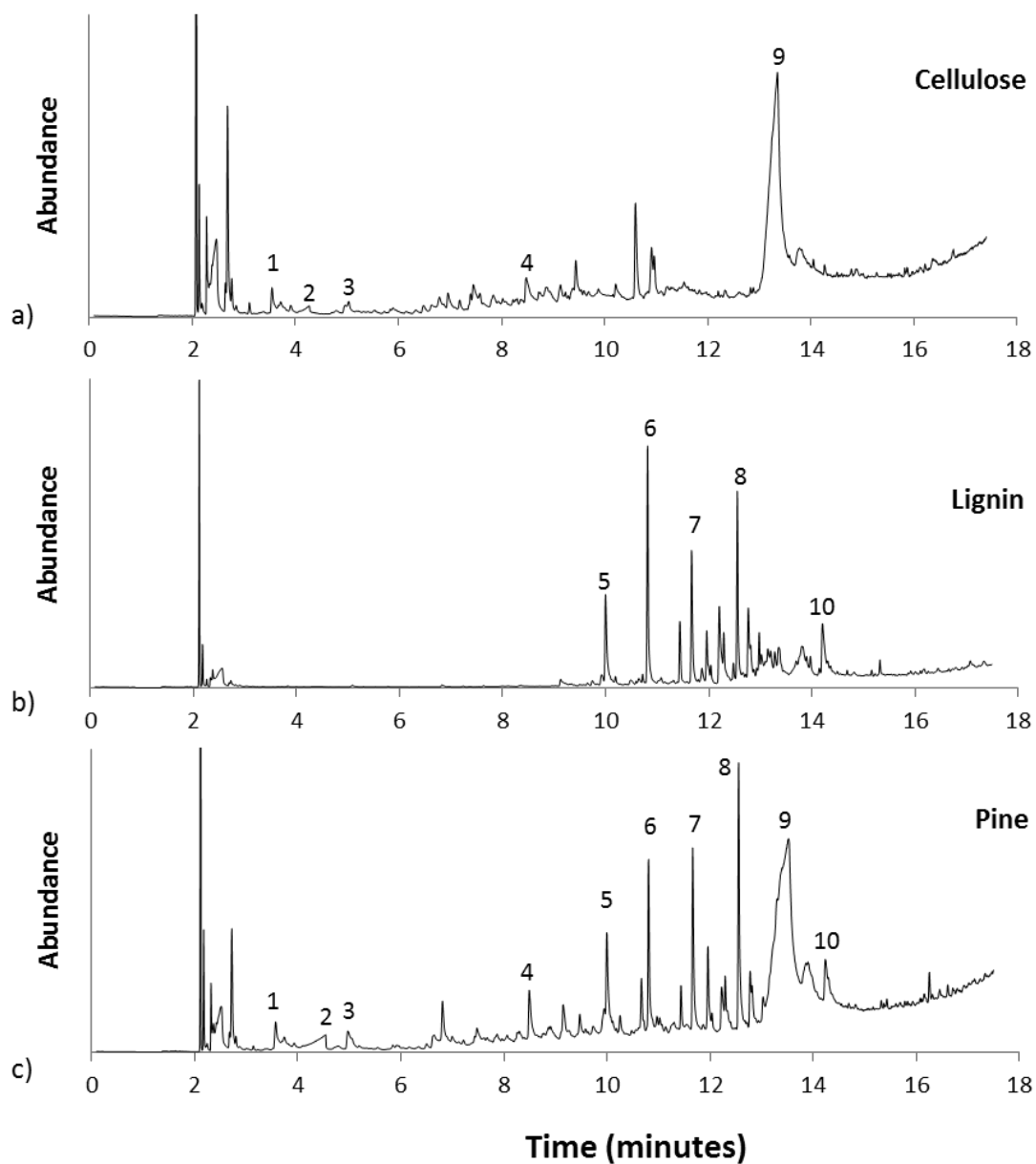
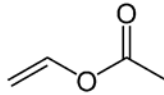
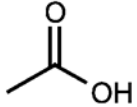
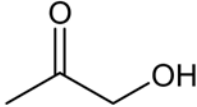
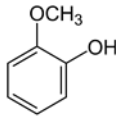
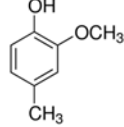
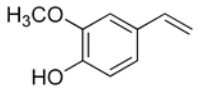
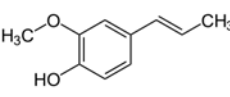
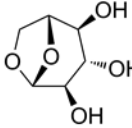
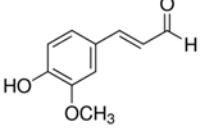


Figure 6.1: GC chromatograms from the uncatalyzed pyrolysis of a) cellulose, b) lignin, and c) pine at 500°C. The peaks of several compounds, which are shared between the chromatogram of pine pyrolysis and that of cellulose or lignin, have been labeled. The corresponding peak identification and structures are listed in Table 6.1.

Table 6.1: GC peak labels shown in Figure 6.1, and the corresponding compound identification and structures.

#	RT (min)	Compound Name	Structure
1	3.6	vinyl acetate	
2	4.4	Acetic Acid	
3	5.0	2-Propanone, 1-hydroxy-	
4	8.4	2-Cyclopenten-1-one, 2-hydroxy-	
5	10.0	Phenol, 2-methoxy-	
6	10.8	Phenol, 2-methoxy-4-methyl-	
7	11.7	2-Methoxy-4-vinylphenol	
8	12.6	Phenol, 2-methoxy-4-(1-propenyl)-	
9	13.3	levoglucosan	
10	14.2	4-Hydroxy-3-methoxycinnamaldehyde	

The chromatogram for non-catalytic pyrolysis of cellulose is shown in Figure 6.1 a). The spectrum contains only oxygenated species, and five peaks of particular interest are labeled. The raw pyrolysis of cellulose produced many of the low molecular weight oxygenates that are common in raw pyrolysis oil. Of particular note is acetic acid, which contributes largely to the acidity of raw pyrolysis oil and, by extension, its poor fuel quality. Dominating the GC chromatogram of the uncatalyzed pyrolysis of cellulose is levoglucosan, which is peak label #9 in Figure 6.1. Levoglucosan is an anhydrous sugar which is formed in abundance during non-catalytic pyrolysis of cellulose and materials which contain cellulose. The dehydration reaction that occurs when glucose (the monomer of cellulose) converts to levoglucosan is depicted in Figure 6.2.

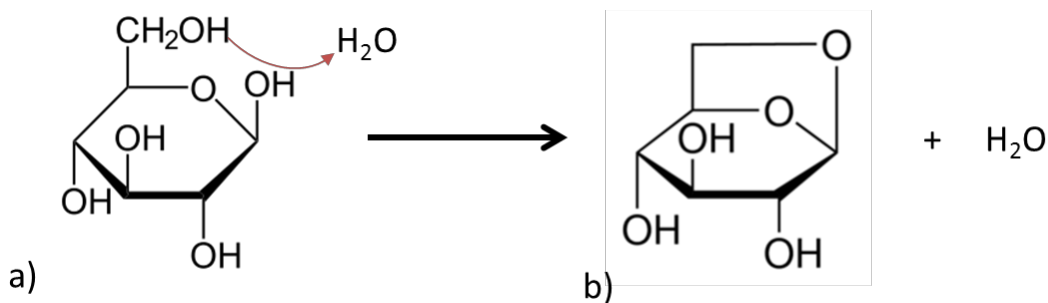


Figure 6.2 Dehydration reaction of a) glucose, the monomer of the cellulose biopolymer, converting to b) levoglucosan, an anhydrous sugar formed in abundance during uncatalyzed pyrolysis of cellulose.

Levoglucosan further reacts to form the remainder of the cellulose pyrolysis products. More detailed product analysis of the uncatalyzed pyrolysis of cellulose can be found elsewhere [102] [81] [103].

In Figure 6.1 b), a chromatogram from non-catalytic pyrolysis of lignin is shown. The chromatogram shows that the uncatalyzed pyrolysis produces very few low molecular weight compounds. Most of the compounds are aromatic oxygenates, with the overwhelming majority of them being methoxy phenols. A methoxy functional group is an R–OCH₃ group. Methoxy phenol compounds are generated from the thermal depolymerization of lignin, which is composed of phenolic monomers. The three monomers of lignin are shown in Figure 6.3 and provide insight into the products formed during the non-catalytic pyrolysis of lignin. A more comprehensive discussion of the products from the uncatalyzed pyrolysis of lignin can be found elsewhere [83].

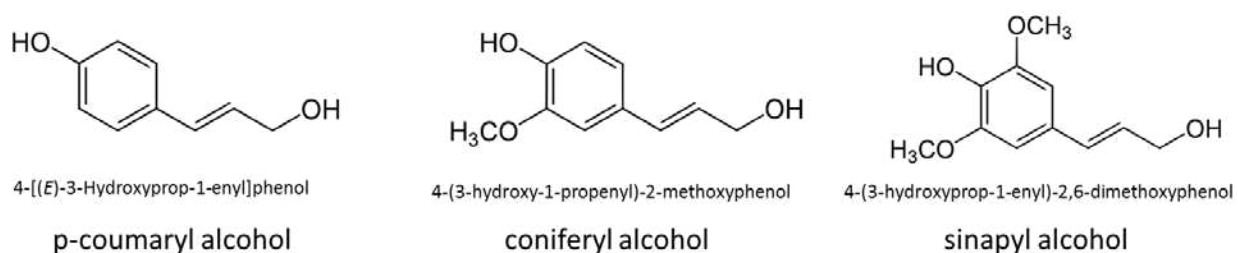


Figure 6.3 The three primary monomers of lignin, labeled by their IUPAC names as well as the common names. All three of the monomers are phenolics, and coniferyl and sinapyl alcohol both contain the R–OCH₃ methoxy group, putting them in the category of “methoxy phenols.”

The GC chromatogram from the uncatalyzed pyrolysis of pine is shown in Figure 6.1 c). From comparing the three sections of Figure 6.1, one can observe that the chromatogram from the uncatalyzed pyrolysis of pine is largely the summation of the chromatograms generated by cellulose and lignin. This is the foundation of the work presented in Section 7, in that it validates the assumption that pyrolyzing lignin and cellulose separately isolates their components from the profile of whole biomass, allowing conclusions to be drawn about their individual impacts.

6.2 Qualitative Comparison of the CFP of cellulose, lignin, and pine

A series of *ex situ* CFP experiments with cellulose, lignin, and pine were performed in the Tandem μ -Reactor, in the *ex situ* configuration, as detailed in Section 3.2.2.2. Pyrolysis and upgrading occurred at 500°C, with Nexceris ZSM-5 catalyst with clay binder, at a biomass:catalyst=0.1. The chromatograms from these experiments are shown in Figure 6.4. Several notable peaks, which were found on all three chromatograms, have been labeled and the corresponding compound identifications and structures from those peaks are shown in Table 6.2.

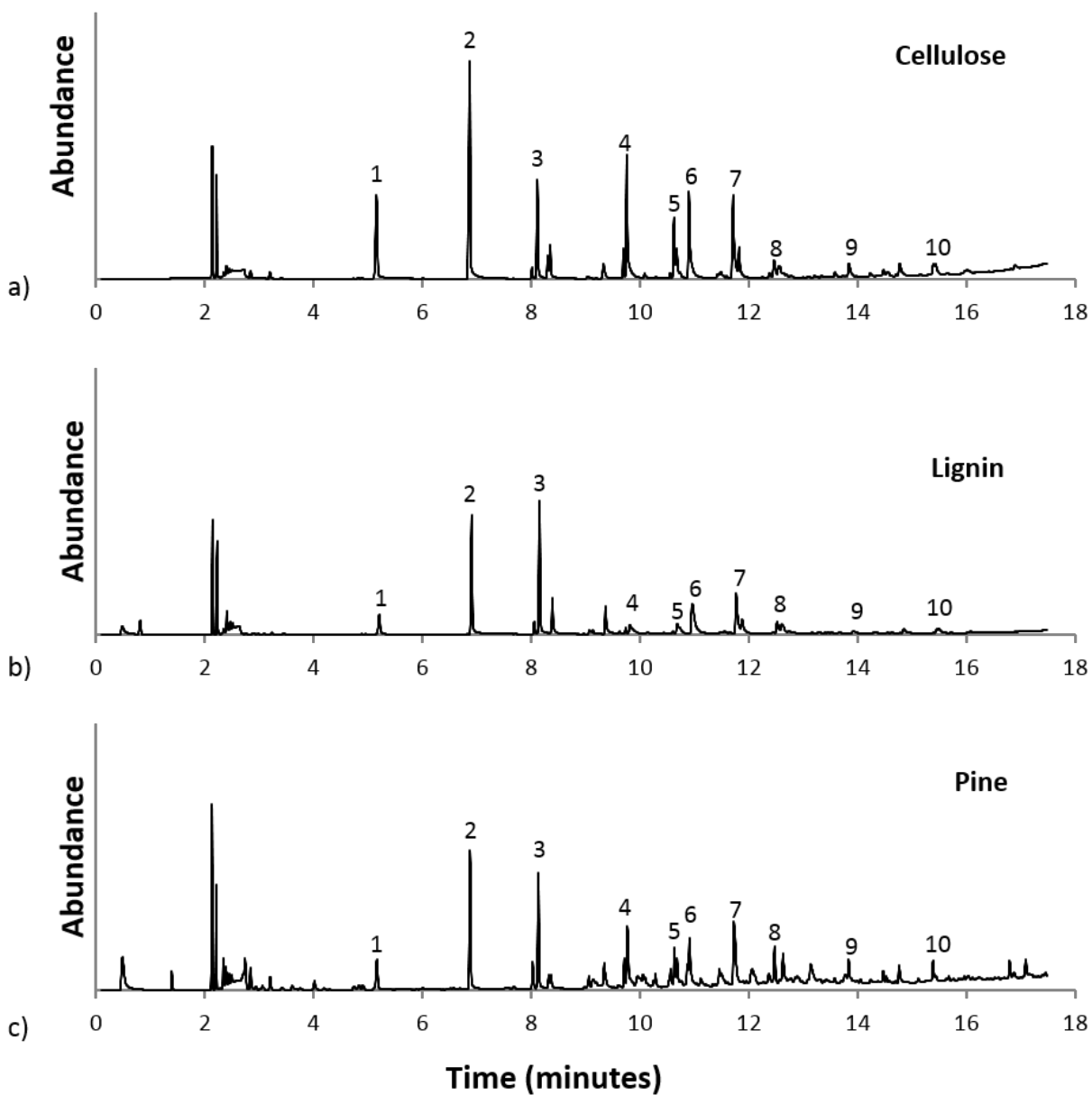
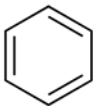
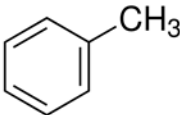
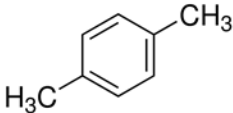
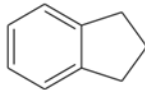
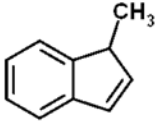
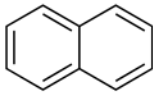
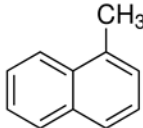
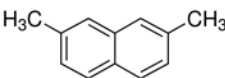
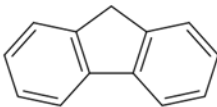
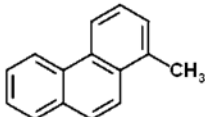


Figure 6.4: GC chromatograms from the CFP of a) cellulose, b) lignin, and c) pine at 500°C, with ZSM-5 catalyst, at a biomass:catalyst=0.1 Ten notable peaks, which are products from the CFP of all three biomasses, are labeled. The corresponding peak identification and structures are listed in Table 6.2.

Table 6.2: GC peak label numbers from Figure 6.4 and the corresponding compound identification and structures.

#	RT (min)	Compound Name	Structure
1	5.2	benzene	
2	6.9	toluene	
3	8.2	p-xylene	
4	9.7	indane	
5	10.6	indene, 1-methyl-	
6	10.9	naphthalene	
7	11.8	naphthalene, 1-methyl-	
8	12.5	naphthalene, 2,7-dimethyl	
9	13.8	fluorene	
10	15.4	phenanthrene, 1-methyl	

Despite the fact that cellulose and lignin have starkly different compositions, and yield very different products during uncatalyzed pyrolysis, it has been found that they yield nearly identical products, compared to each other and to pine, during CFP with fresh ZSM-5. All products identified were hydrocarbons, and all of the liquid-range hydrocarbons were aromatics. This result is possible due to the extensive cracking and aromatization reactions that occur during catalytic upgrading with ZSM-5. There were no products found during CFP of cellulose, lignin, and pine that were shared with the products from non-catalytic pyrolysis.

6.3 Section Conclusions

This observation has been noted before, and the CFP of biomass and its fractions has been studied in some detail with fresh catalyst and at low biomass-to-catalyst ratios [52] [31].

However, the role of cellulose and lignin in the deactivation of ZSM-5 during upgrading is much less understood. This line of inquiry is directly addressed in Section 7.

7 Deactivation of ZSM-5 by Pine and Individual Biopolymers

To assess the contributions of the polysaccharide and phenolic components of biomass to the deactivation of ZSM-5 during catalytic fast pyrolysis, upgrading experiments were performed in the Tandem μ -Reactor at 500°C with pine, lignin, and cellulose as feedstocks. The cellulose was obtained from Sigma Aldrich, the lignin was produced at NREL from oak wood, and the pine was provided from Idaho National Lab. More detail on these feedstocks can be found in Section 3.5.

The Tandem μ -Reactor was in the *ex situ* configuration, as detailed in Section 3.2.2.2. For each experiment, twenty successive 0.5 mg samples of biomass were pyrolyzed and upgraded over a 10 mg catalyst bed, resulting in a cumulative biomass:catalyst=2. The ZSM-5 catalyst used for these experiments was provided by Nexceris and had an SAR of 30, with a clay binder. After each biomass sample was pyrolyzed and upgraded, detailed product information was obtained via GC-MS/FID.

In order to have sufficient post-reaction catalyst to perform characterization experiments, 500 mg samples of post-reaction catalyst samples were generated in the Horizontal Packed-bed Reactor, detailed in Section 3.2.3. To generate post-reaction catalyst samples, ten 50 mg boats of each biomass were pyrolyzed and upgraded over a 500 mg catalyst bed, resulting in a final biomass:catalyst=1. After CFP, the catalyst beds were cooled in inert gas flow to below 200°C in order to prevent any oxidation of coke during catalyst extraction.

The elemental and compositional analyses of the feedstocks are shown Table 7.1. The elemental composition of the feedstocks was determined by combustion analysis using a LECO TruSpec®

CHN analyzer. Oxygen was determined by difference. The compositional analysis was performed according to methods published elsewhere [104] [105].

Table 7.1: Composition of feedstocks.

wt%	Pine	Lignin	Cellulose
Inorganics	0.35	0.55	0.04
Extractives	5.32	-	-
Lignin	30.72	93	2.94
Soluble Lignin	3.56	5.75	2.24
Glucan	38.43	0.21	91.65
Xylan	6.35	1.68	1.58
Galactan	2.47	0	0.62
Mannan	16.35	0	1.81
Acetyl	1.54	0.49	-
Total	101.53	95.94	98.65
C	48.56	60.79	41.9
H	6.63	6.71	6.86
N	0.06	0.07	0
O	44.4	31.88	51.2

The cellulose and lignin were relatively pure and they contained 92% glucose sugar and 93% lignin, respectively. The pine contained 38% glucose sugar, 25% other sugars, and 31% lignin. Cellulose had the highest oxygen content (51%) and lignin the lowest (32%), consistent with their composition.

7.1 Deactivation of ZSM-5 by cellulose

To analyze the trends in hydrocarbon formation during CFP of cellulose, the hydrocarbon products from each pyrolyzed sample have been grouped by number of aromatic rings, with benzene, toluene, and p-xylene labeled individually, due to their prominence in the total yield. The resulting trend is shown in Figure 7.1.

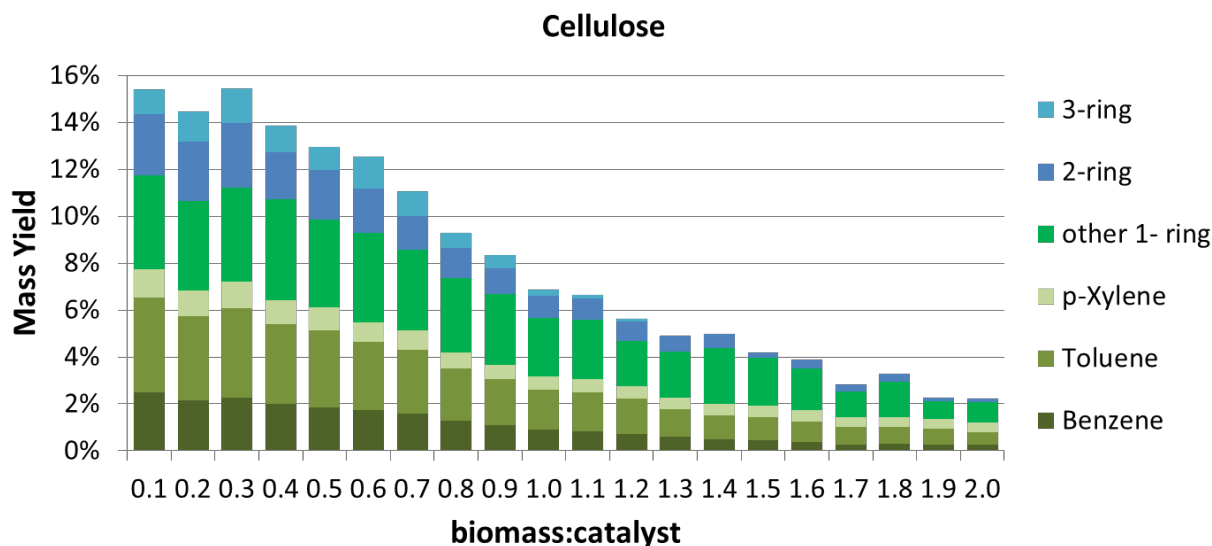


Figure 7.1 The trend of liquid-range hydrocarbon yield during CFP of cellulose over ZSM-5 catalyst as a function of the cumulative biomass:catalyst.

The hydrocarbon production during CFP of pine decays from a maximum yield of ~15% at low biomass:catalyst, down to a minimum of ~2% at biomass:catalyst=2. The yields of 2- and 3-ring aromatic hydrocarbons decrease the fastest with respect to biomass:catalyst. At

biomass:catalyst=2.0, the hydrocarbon products are almost entirely 1-ring aromatics, with only a small fraction of naphthalene being formed and no 3-ring compounds being detected at all. Of benzene, toluene, and xylene (BTX), the yield of benzene decreases most substantially and that of xylenes least. This shows that alkylation reactions are less impacted by deactivation than the ring growth reactions. This in combination with the stark decrease in 2- and 3-ring aromatics, indicates that the 2nd step in catalytic upgrading, the acid-catalyzed deoxygenation and aromatization, is being disrupted. As a result, there is an observed increase in the selectivity to alkylated products such as xylene that are not converted to multi-ring aromatics. Along with liquid-range, aromatic hydrocarbons, light aliphatic hydrocarbon gasses are also produced as a

result of CFP. Figure 7.2 shows the mass yield of 2-, 3-, and 4-carbon hydrocarbon gasses during CFP with cellulose.

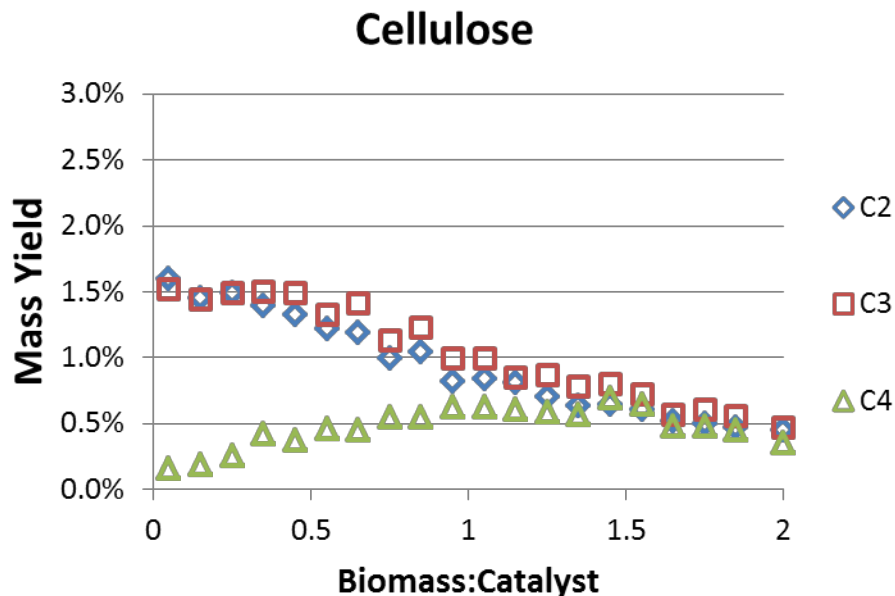


Figure 7.2 Mass yield of light hydrocarbons (2-, 3-, and 4-carbon hydrocarbons) produced during CFP of cellulose with ZSM-5 as a function of the cumulative biomass:catalyst.

The yield of C₂ and C₃ hydrocarbons, primarily ethene and propene, follow a similar trend during CFP of cellulose. Both groups of gasses have a maximum yield (~1.5% mass yield) at low biomass:catalyst and decrease steadily to a minimum at biomass:catalyst=2, similar to the observed aromatic hydrocarbon yield. The C₄ hydrocarbons, mainly isobutene, however, are at a minimum yield during the initial phase of the CFP experiment, and increase in yield with biomass:catalyst until a maximum is reached at biomass:catalyst ~1. Following this maximum, the C₄ hydrocarbons decrease in yield. This suggests that the mechanism of butene production differs from that of ethene and propene.

In methanol-to-gasoline, ethylene is hypothesized to be formed in the aromatic cycle via remethylation reactions of alkylated aromatics, whereas propene and higher olefins are formed via methylation and cracking of other alkenes [106] [107]. The current results suggest that during CFP of cellulose, ethene and propene are formed via a similar mechanism and impacted by catalyst deactivation in a similar manner as aromatics. Butenes, on the other hand, appear to be intermediates whose formation increases as the catalysts deactivated, at the same time as the methylation of aromatics increases in importance compared to aromatization and ring growth.

To analyze the trends in oxygenate yields during CFP of cellulose, the compounds were grouped by functional group and plotted in Figure 7.3.

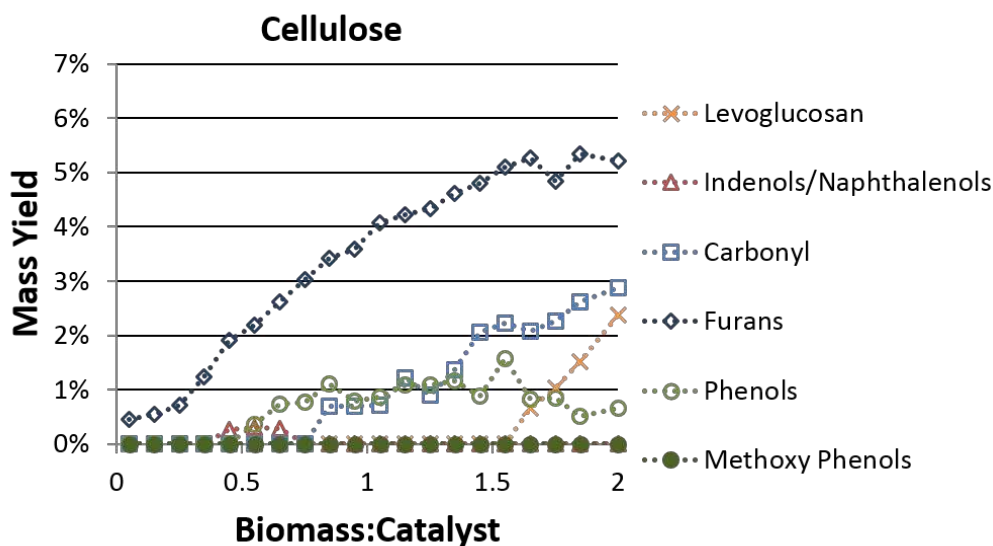


Figure 7.3 Oxygenate formation trends during CFP of cellulose with ZSM-5 catalyst, as a function of the cumulative biomass:catalyst.

The oxygenated species formed during CFP of cellulose, as shown in Figure 7.3, begin with furan and methylfuran formation at low biomass-to-catalyst ratios. Phenol and alkylated phenols,

along with naphthols, begin to form at a biomass:catalyst~0.5, followed by the production of carbonyls, primarily cyclopentenones, which are formed by rearrangements of methylfurans.

Late in the experiment, levoglucosan begins to break through. This indicates that the catalyst is severely deactivated, as levoglucosan is a primary product of uncatalyzed pyrolysis of cellulose.

Unlike the other oxygenate groups, indenols/naphthols and phenols do not continue to increase in yield throughout the experiment, but rather reach a maximum and then decline, as observed in Section 4 during the CFP of pine. The presence of these compounds is surprising, as phenols do not appear in non-catalytic pyrolysis of cellulose, and there is no phenolic component of cellulose.

Phenols have long been observed during CFP of whole biomass, and their origin has been debated. As discussed in Section 4, the phenolic structure of the lignin monomers leads one to infer that it is the source of the intermediate phenolic compounds generated by CFP of whole biomass. However, the observance of aromatic oxygenates during CFP of cellulose, which contains no native aromatics, indicates that phenol, alkylated phenols, and naphthols are generated as a result of a catalytic process during CFP with a partially-deactivated catalyst and not from the partial deoxygenation of aromatic lignin vapors. It has been suggested that the production of phenols and naphthols originates from interactions between the ZSM-5 framework, aromatic intermediates, and steam formed *in situ* during catalytic fast pyrolysis [108]. The higher yield of phenolic compounds during the intermediate stages of catalyst deactivation, compared to low biomass:catalyst may indicate that the phenol-generating interactions with steam are out-competed by aromatization reactions in very fresh catalyst at low biomass:catalyst. Alternatively, the higher yield at intermediate levels of deactivation may mean that the specific

precursors required for phenol production are oxygenated intermediates, which are more abundant with a partially-active catalyst.

7.2 Deactivation of ZSM-5 by lignin

To see the trends in hydrocarbon product yields, during the upgrading of lignin pyrolysis vapors over ZSM-5, the hydrocarbon products were grouped by number of aromatic rings, with benzene, toluene, and xylene singled out due to their prominence in the overall yield. The resulting trend is shown in Figure 7.4.

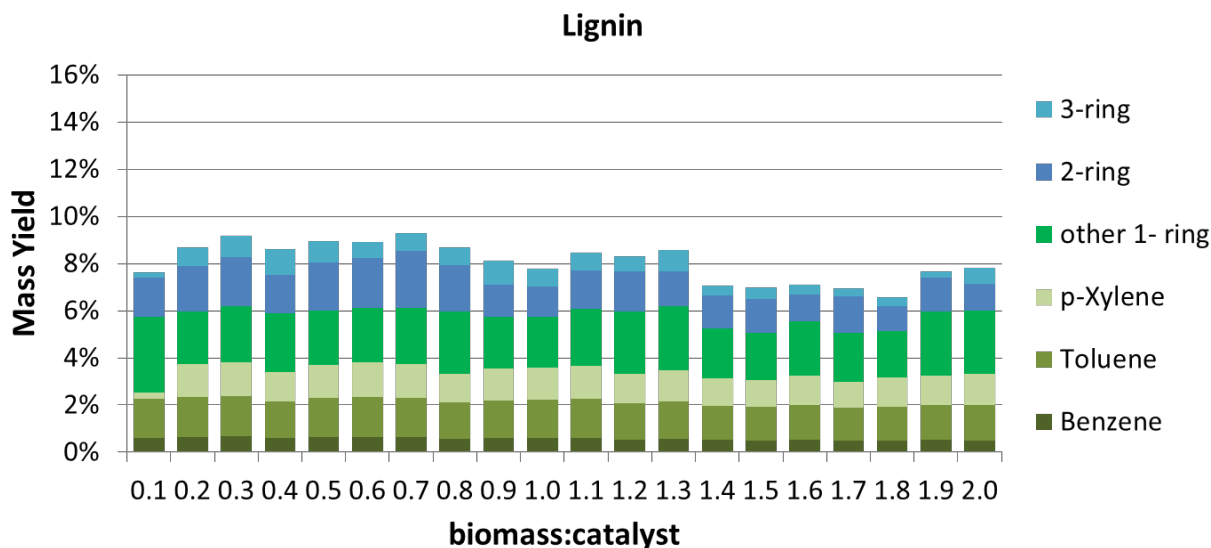


Figure 7.4 Liquid-range hydrocarbon yield trend during CFP of lignin over ZSM-5 catalyst, as a function of the cumulative biomass-to-catalyst ratio.

The most striking feature of Figure 7.4 is the constant nature of the hydrocarbon yield and selectivity. The hydrocarbon products are produced in very similar proportions and yield throughout the course of the experiment, unlike the hydrocarbon yields during the CFP cellulose,

seen in Figure 7.1. 1-ring aromatics account for ~65% of the entire aromatic hydrocarbon products, and roughly half of the 1-ring aromatic yield is composed of toluene and xylene. The aromatization reactions were not affected by continued upgrading. The mass yield of light hydrocarbon gasses produced during CFP is shown in Figure 7.5.

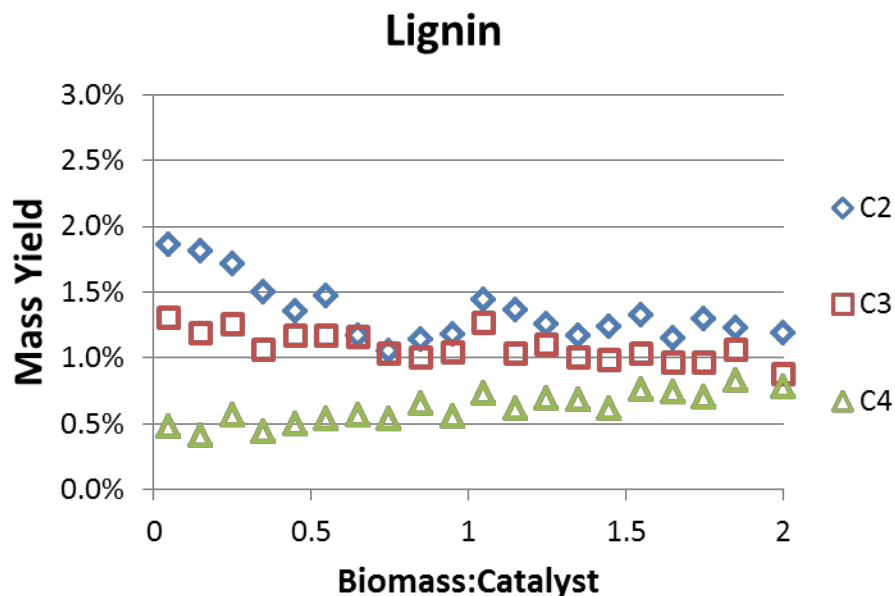


Figure 7.5 Mass yield of light hydrocarbons (2-, 3-, and 4-carbon hydrocarbons) produced during CFP with lignin and ZSM-5 as a function of the cumulative biomass:catalyst.

The yield of C₂ and C₃ hydrocarbons during CFP with lignin shows similarities to the yield of liquid-range products. Unlike the trend seen during CFP with cellulose, the ethyl and propyl hydrocarbons do not have the same initial yield. Initially, from biomass:catalyst= 0.1 to 0.5, the yield of ethene decreased more rapidly than that of propene and was produced at an approximately constant level thereafter. Propene formation, however, decreased slowly during the entire experiment. As seen with cellulose CFP in Figure 7.2, the C₄ hydrocarbon gasses steadily increase in yield throughout the experiment. The catalyst lost the ability to produce

aromatic hydrocarbons more gradually during CFP of lignin than cellulose; hence, butene formation continued to increase through the experiment and no minimum was detected by the end of the experiment. It should be noted that while all alkenes are all expected to be formed from the hydrocarbon pool reactions during cellulose CFP, some alkenes may be formed via cracking of side chains in lignin monomers during lignin CFP.

To analyze the trends in oxygenate yields during the experiment, the oxygenated products were grouped by functional group and plotted in Figure 7.6.

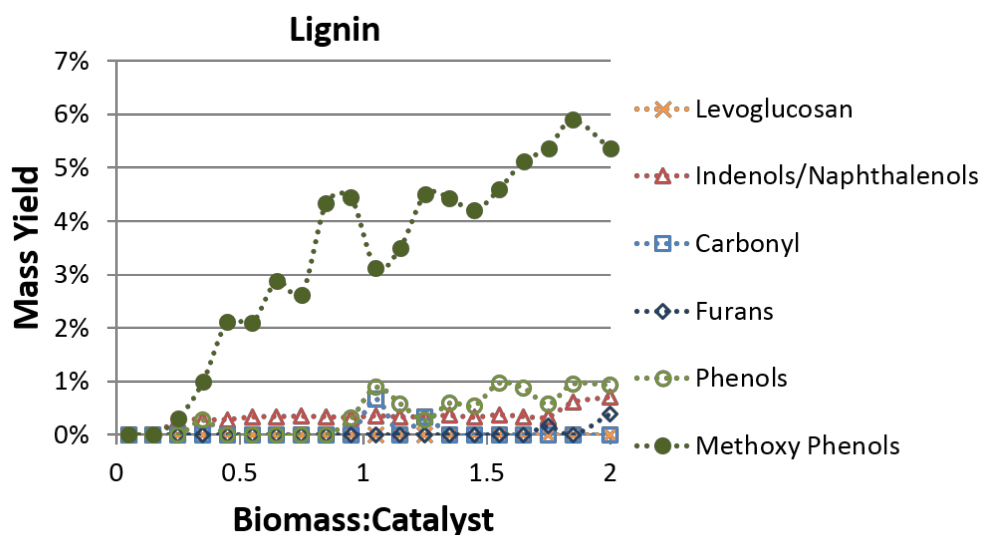


Figure 7.6 Oxygenate yield trends during CFP with lignin over ZSM-5 catalyst, as a function of cumulative biomass-to-catalyst ratio.

From Figure 7.6, it can be seen that the oxygenated species formed during CFP of lignin are almost entirely methoxy phenols, with small amounts of indenols/naphthols and phenols produced. The presence of methoxy-phenols, the primary product of uncatalyzed pyrolysis of

lignin, shows that the CFP of lignin rapidly deactivated the initial cracking step of catalytic upgrading. The primary pyrolysis products of lignin (methoxyphenols) are formed significantly earlier at biomass:catalyst 0.3 than levoglucosan for cellulose, whose formation begins at biomass:catalyst 1.5.

7.3 Deactivation of ZSM-5 by Pine

The deactivation of ZSM-5 by pine pyrolysis vapors was studied via the same process used with lignin and cellulose. Successive 0.5 mg samples of pine were pyrolyzed and upgraded at 500°C over a 10 mg catalyst bed, resulting in a cumulative biomass:catalyst=2. To assess the trends in hydrocarbon yields, the liquid-range hydrocarbon products have been grouped by their number of aromatic rings, with benzene, toluene, and p-xylene listed separately due to their prominence in the yield, and plotted in Figure 7.7.

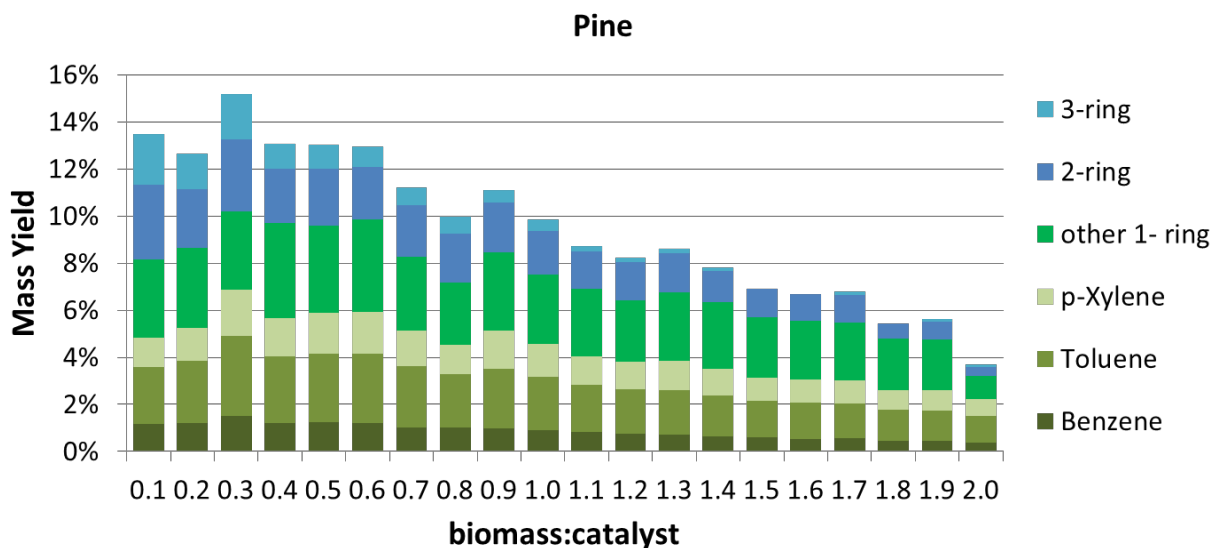


Figure 7.7 Hydrocarbon yield trend during CFP of lignin over ZSM-5 catalyst, as a function of the cumulative biomass-to-catalyst ratio.

In Figure 7.7, at low biomass:catalyst, the yield of hydrocarbons is highest, and at high biomass:catalyst the yield diminishes by approximately two-thirds. This is similar to the trend observed with cellulose, shown in Figure 7.1. As seen with cellulose and lignin, the liquid-range hydrocarbons produced during CFP of pine are primarily 1-ring aromatics. However, a greater yield of 3-ring aromatics was observed during CFP of pine than with either cellulose or lignin. Analogous to the hydrocarbon yield trend observed during CFP of cellulose, 2- and 3-ring aromatics from CFP of pine decrease in yield significantly as the cumulative biomass:catalyst increases. At biomass:catalyst=2, the hydrocarbons are almost entirely 1-ring aromatics, with p-xylene and toluene accounting for ~50% of the total hydrocarbon yield, showing that deactivation is impacting the aromatization step of upgrading. The light hydrocarbons produced during CFP of pine are shown in Figure 7.8.

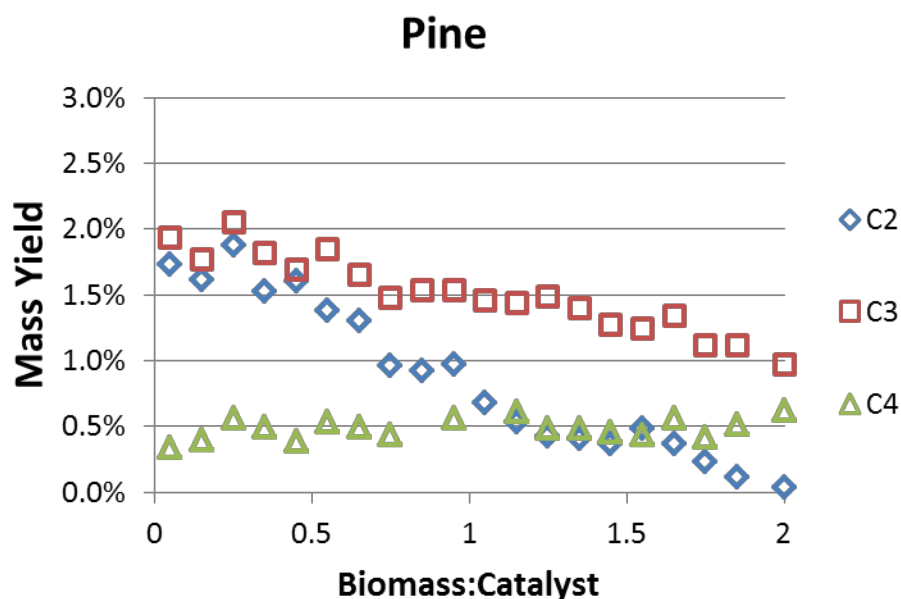


Figure 7.8 Mass yield of light hydrocarbons (2-, 3-, and 4-carbon hydrocarbons) produced during CFP with pine and ZSM-5 as a function of the cumulative biomass:catalyst.

The light hydrocarbons produced during CFP with pine and ZSM-5 show a unique trend, compared to those from the CFP of cellulose and lignin. The C₂ and C₃ hydrocarbons have the same initial yield, as seen with cellulose. However, the C₂ hydrocarbons decrease at a faster rate than the C₃ hydrocarbons. The butyl hydrocarbons remained mostly constant, as a function of biomass:catalyst. The yield of C₄ hydrocarbons continued to rise, similar to the trend seen during CFP of lignin, but at a much more gradual rate.

The trends in oxygenate yields are shown in Figure 7.9, with the oxygenated products grouped by functional group.

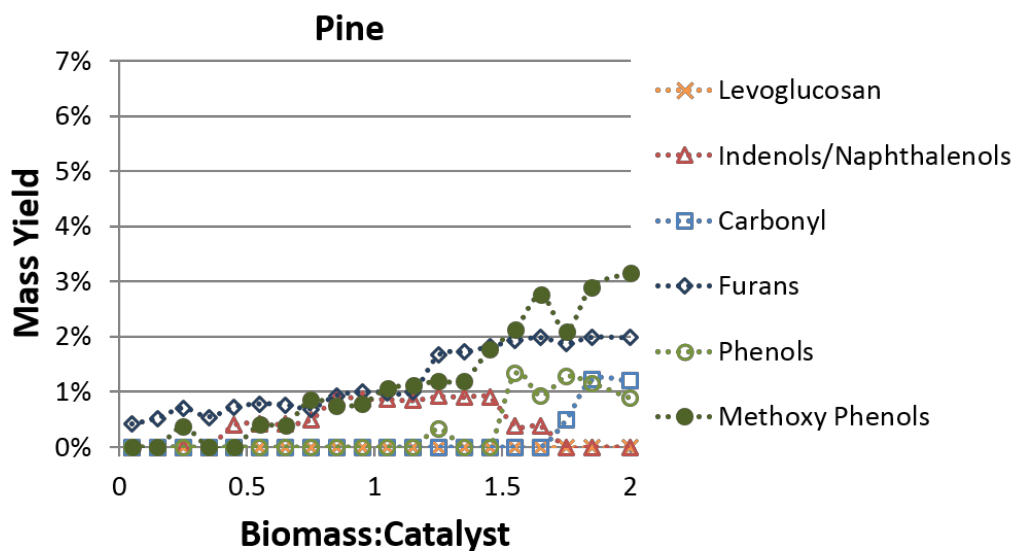


Figure 7.9 Oxygenate yield trends during CFP with lignin over ZSM-5 catalyst, as a function of cumulative biomass-to-catalyst ratio.

The oxygenated species generated during the CFP of pine reflect a composite of those found during CFP of cellulose and lignin. At low biomass:catalyst, furans are the first oxygenates to form. Following this is the introduction of methoxy phenols, as well as indenols and

naphthalenols. The indenols/naphthalenols and phenols both follow a similar trend of reaching a maximum before the end of the experiment, whereas the furans and methoxyphenols, products of uncatalyzed pyrolysis of cellulose and lignin, respectively, continue to be produced in increasing yields as the biomass:catalyst increases. The breakthrough of methoxyphenols during pine CFP is delayed compared to lignin CFP and, similarly, the breakthrough of levoglucosan and formation of carbonyls are delayed compared to cellulose CFP.

7.4 Deactivation trends during CFP of pine and individual biopolymers

To compare broader trends between the three feedstocks, a simplified product grouping was established. The products were grouped as either hydrocarbons or oxygenates, and plotted as a function of biomass:catalyst, shown in Figure 7.10 a)-c). Additionally, Figure 7.10 d) compares the total integrated yields over the course of the experiment.

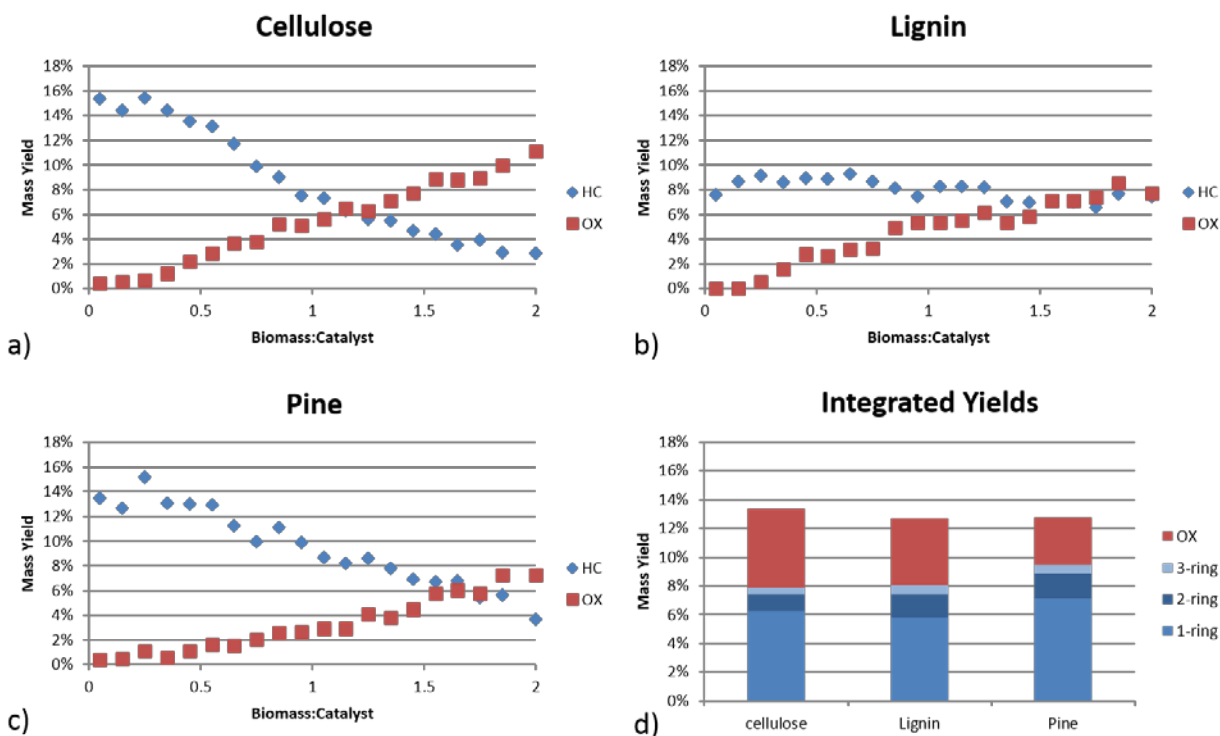


Figure 7.10 a)-c) Deactivation trends from CFP with cellulose, lignin, and pine, with blue markers indicating total yield of hydrocarbon products, and red markers indicating total yield of oxygenated products, as a function of cumulative biomass-to-catalyst ratio. D) integrated yields of hydrocarbon and oxygenates over the course of the experiment.

For all feeds, the catalysts are fully active at low biomass:catalyst and only hydrocarbon products are produced. The deactivation trend for cellulose, Figure 7.10 a), shows that as progressive amounts of cellulose are pyrolyzed and upgraded over the catalyst, increasing the cumulative biomass:catalyst, the yield of hydrocarbons steadily decreases from 15% to 3% and the yield of oxygenates increases from 0.5% to 11%. The hydrocarbon yield and the oxygenate yield are approximately equal at biomass:catalyst=1.15.

During CFP with lignin, Figure 7.10 b), oxygenates begin to form at biomass:catalyst=0.25 and steadily increase in yield until a maximum of ~8% is reached at the end of the experiment. This is similar to the oxygenate trend observed during CFP of cellulose. However, in contrast to the

deactivation trend of cellulose, the hydrocarbon yield remains quite constant, at ~8%, for the duration of the experiment.

During CFP with pine, Figure 7.10 c), the hydrocarbon yield decreases from its maximum of ~14% to a minimum of ~4%, while the oxygenate yield increases up to a maximum of ~8%. This general trend is similar to that observed with cellulose. However, the hydrocarbon yield decreases at a slower rate than seen with cellulose.

The decline in aromatic production during CFP is attributed to the progressive inaccessibility of acid sites due to capping of ZSM-5 pores by coke [51]. The sustained production of hydrocarbons at near-initial yield during CFP with lignin suggests that the ZSM-5 acid sites remain accessible and active despite the increasing yields of oxygenates that is associated with catalyst deactivation.

In part d) of Figure 7.10, the area under the deactivation curves was integrated to represent the bulk properties of the oils had they been condensed throughout the experiment. Despite having the highest initial hydrocarbon yield, CFP of cellulose gave the lowest integrated hydrocarbon yield at cumulative biomass:catalyst of 2 due to the rapid decline in hydrocarbon production throughout the experiment. CFP of cellulose also resulted in the highest total yield of oxygenated species and the highest overall oil yield. The lower, but constant, hydrocarbon yield from CFP of lignin resulted in lignin's integrated hydrocarbon yield being slightly higher than that of cellulose. The integrated hydrocarbon yield from pine was the highest as a result of pine having a higher initial hydrocarbon yield than lignin and a slower decline in yield than observed with cellulose.

For all three feedstocks, the liquid-range hydrocarbons produced were entirely aromatics. The hydrocarbon yield in Figure 7.10 d) is divided to show the contributions from 1-, 2-, and 3-ring aromatics. The 1-ring aromatics are primarily benzene, toluene, and xylene while the 2- and 3-ring aromatics are primarily naphthalene, methylnaphthalene, dimethylnaphthalene, and alkylated fluorenes and anthracenes. The similarities in upgraded hydrocarbon products from all three feedstocks, despite differences in yield, deactivation trend, and oxygenate production, indicate that the hydrocarbon formation occurs via a common pathway, even though the mode of deactivation differs.

Lignin had a higher char yield than cellulose and pine (~40% vs. 1% vs. 15%, respectively) and thus a lower mass of pyrolysis vapors were passed over the catalyst during the lignin CFP experiments than during those of cellulose and pine. To ensure that the trends observed during CFP of cellulose, lignin, and pine were not a result of the varying masses of vapors generated during CFP, the results have been plotted on a vapor basis in Figure 7.11. The x-axis is the ratio of cumulative vapor weight to catalyst bed weight. The data for cellulose and pine have been truncated at the maximum vapor:catalyst achieved during CFP of lignin. The y-axis is the mass yield on a $\text{g/g}_{\text{vapor}}$ basis.

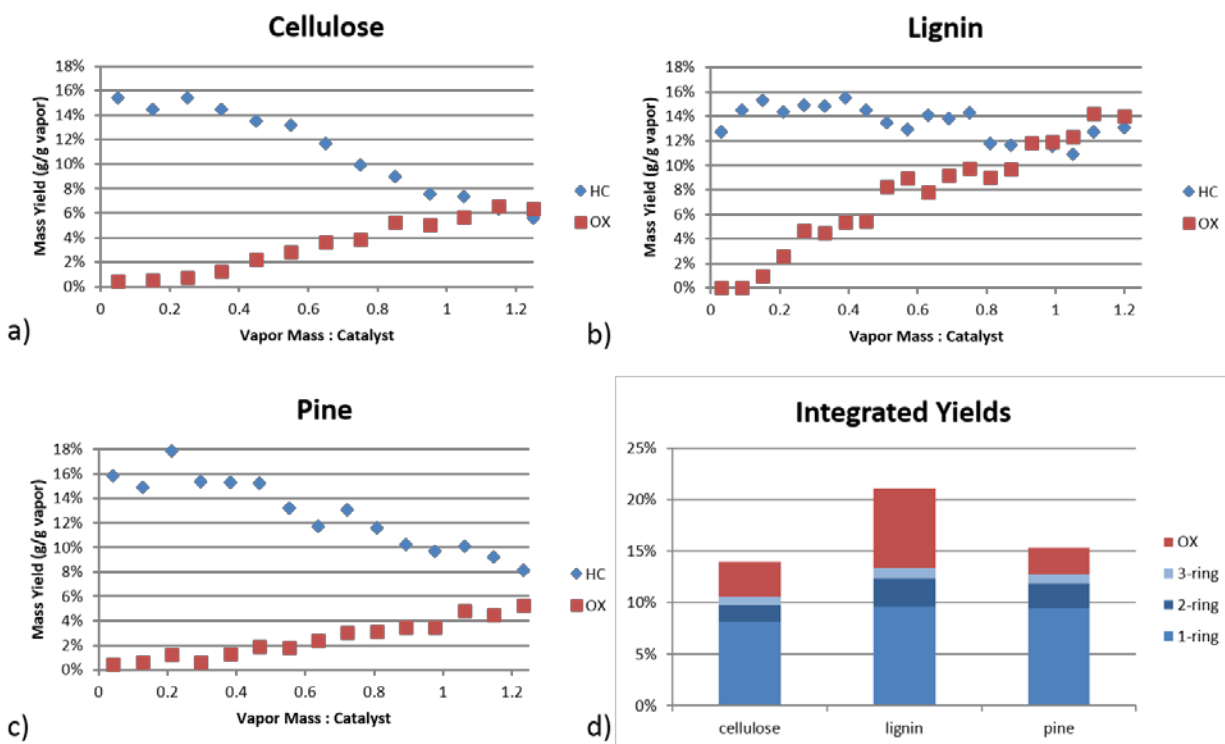


Figure 7.11: Deactivation trends from CFP with a) cellulose, b) lignin, and c) pine on a vapor weight basis. The x-axis is the cumulative ratio of vapor weight to catalyst bed weight. The y-axis is the mass yield of products on a g/g_{vapor} basis. Blue markers indicate the total yield of liquid-range hydrocarbon products, and red markers indicating the total yield of oxygenated products, as a function of cumulative vapor-to-catalyst ratio. Part d) shows the cumulative yield on a g/g_{vapor} basis at 1.2 g_{vapor}/g_{catalyst}.

Figure 7.11 shows that the deactivation trends are still valid on a vapor-weight basis, it also shows that the initial yield of detected liquid-range hydrocarbons is quite comparable for all three biomasses on vapor basis, ~0.16 g hydrocarbons per g pyrolysis vapor. The hydrocarbon yields decrease more rapidly for cellulose and pine and become 6% and 8% at the cumulative vapor:catalyst of 1.2, whereas the hydrocarbon yield remains relatively constant for lignin. The reason for the more constant hydrocarbon yield from lignin CFP is therefore not a result of less pyrolysis vapors being upgraded over the catalyst. The oxygenate mass yield on the other hand increases more rapidly for lignin than for cellulose or pine. This suggests that the aromatization

reactions are impeded more for cellulose than for lignin whereas the cracking and deoxygenation reactions become more impeded for lignin.

In addition to the experiments performed on the Tandem μ -Reactor for product identification and quantification, a set of experiments was performed on the horizontal fixed bed reactor, so that post-reaction catalyst samples could be collected for analysis.

7.5 Post-reaction catalyst analysis

To analyze catalyst that had been coked during upgrading of pine, lignin, and cellulose vapors, samples were generated on the horizontal fixed bed reactor by performing CFP with each feedstock. The post-reaction catalysts and a sample of fresh catalyst were characterized for coke content, NH_3 uptake, and surface area. Details of these characterizations can be found in Section 3.4. The coke on the catalysts, as determined by TGA, is shown in Figure 7.12.

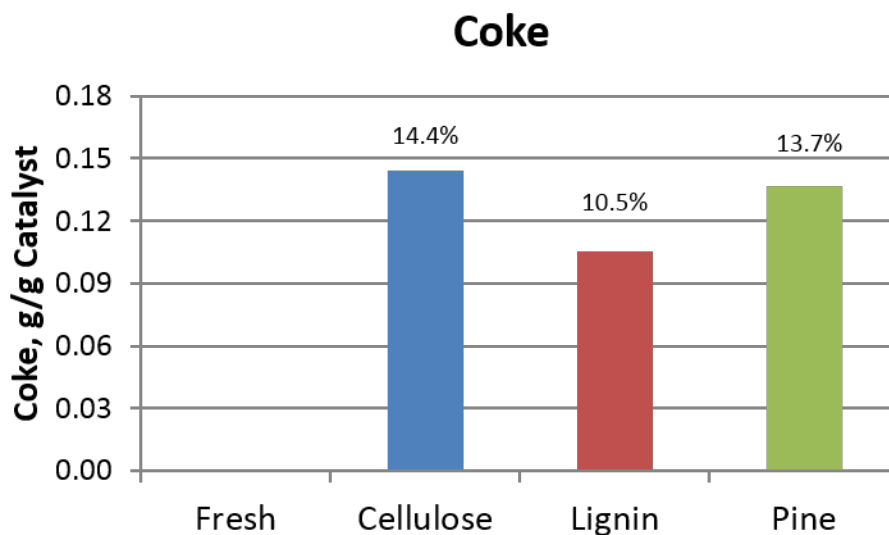


Figure 7.12 Coke, measured by thermogravimetric analysis, present on post-reaction ZSM-5 following CFP of cellulose, lignin, and pine.

CFP of cellulose and pine generated very similar amounts of coke (approximately 14% coke on catalyst) while CFP of lignin generated the least amount of coke at 10.5%). Lower coke formation for lignin agrees with previous studies [29]. The similarities between pine and cellulose are not particularly surprising, as carbohydrates comprise ~ 70 % of pine [15].

The results of the ammonia TPD analysis, Figure 10, show the retention of accessible acid sites on the catalyst.

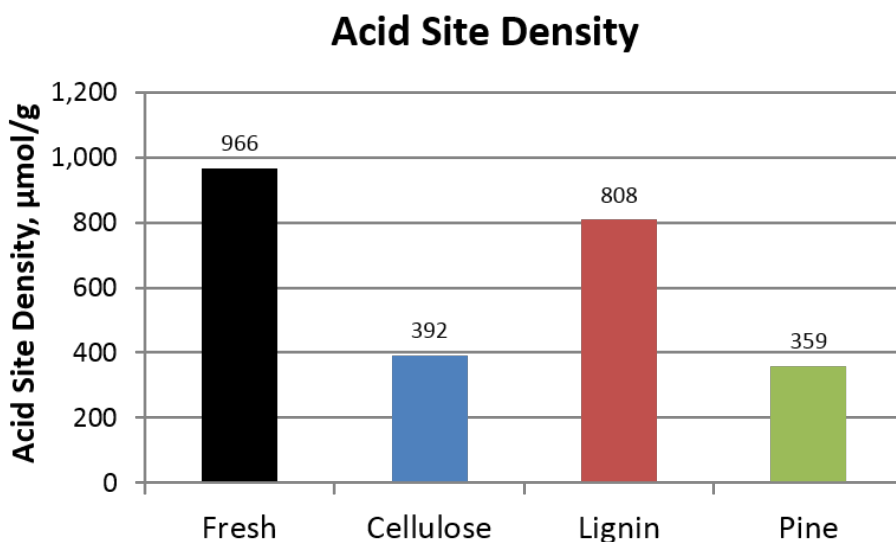


Figure 7.13 Acid site density, as measured by ammonia temperature programmed desorption, accessible on fresh and post-reaction ZSM-5 following CFP of cellulose, lignin, and pine.

Catalysts coked by CFP of cellulose retained the smallest amount of acid sites (37%) compared to fresh catalyst, while the catalyst coked by CFP of lignin retained the highest (84%). The post-reaction catalyst from CFP of pine was comparable to cellulose, retaining 41% of its active sites. Although acid site retention is anticipated to be inversely proportional to coke levels, which

explains the overall trend seen in Figure 7.13, the catalyst coked by lignin retained significantly more of the acid sites than would be expected from the amount of coke.

The surface area measurements of the same post-reaction catalysts are shown in Figure 7.14.

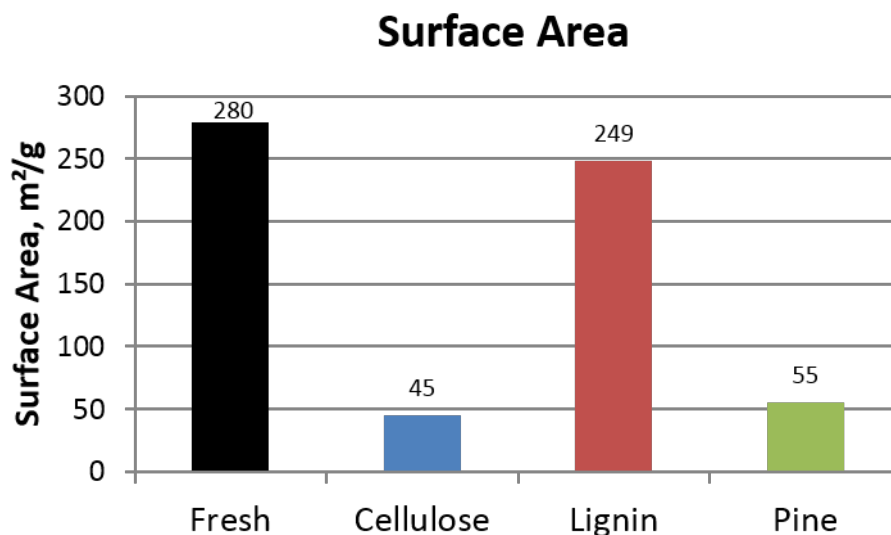


Figure 7.14 Total surface areas (m²/g), measured by nitrogen physisorption and calculated using BET method, on fresh and post-reaction ZSM-5 following CFP cellulose, lignin, and pine.

In Figure 7.14, the catalyst coked by CFP of lignin retained over four times as much surface area as catalysts from the CFP of cellulose and pine (89% vs. 16% and 20%), despite only having ~25% less coke. As seen with the other catalyst characterizations, the catalyst coked by pine closely resembles that of cellulose. The raw isotherms from the physisorption characterization, shown in Figure 7.15, give insight into the surface area that was retained for each catalyst.

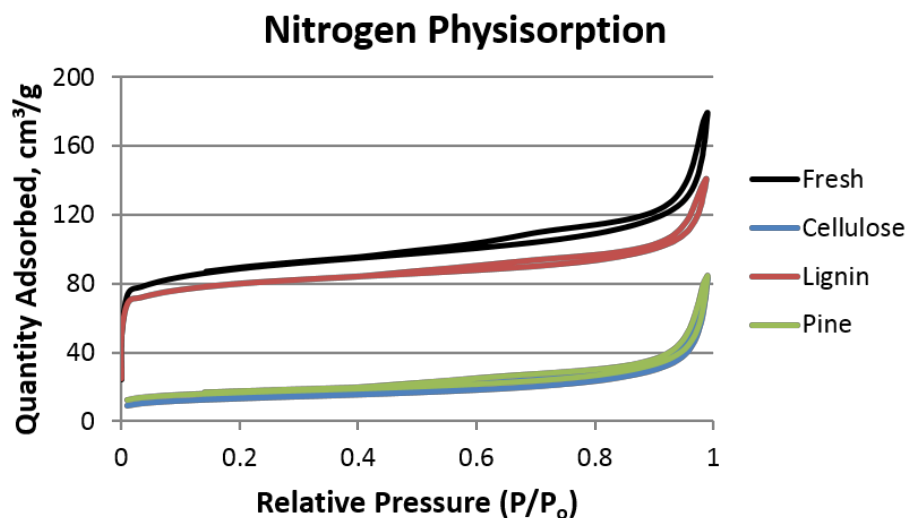


Figure 7.15 Isotherms from nitrogen physisorption on fresh and post-reaction ZSM-5 following CFP of cellulose, lignin, and pine.

Shown at the lowest relative pressures, the micropores are almost entirely eliminated from the ZSM-5 coked by pine and cellulose, which lost 83% and 87% of their micropore volume, respectively. However, the micropore volume was only reduced by 7% in the ZSM-5 coked by lignin. All three catalyst samples retain some of the largest pores, which are filled at the highest relative pressure.

The combination of data in Figure 7.12-Figure 7.15 builds a case that the coking process occurring during the CFP of cellulose is different than the coking process taking place during the CFP of lignin. The coke formed during the CFP of lignin did not significantly block access to the active sites of the catalyst, whereas a steep decline in active sites was observed with the cellulose sample. This can be explained by the hypothesis that coke from lignin is formed primarily by the condensation and coupling of pyrolytic monomers and coke from cellulose by

the formation of multiring aromatics on the active sites. For reference, a schematic of a ZSM-5 catalyst particle with binder is shown in Figure 7.16.

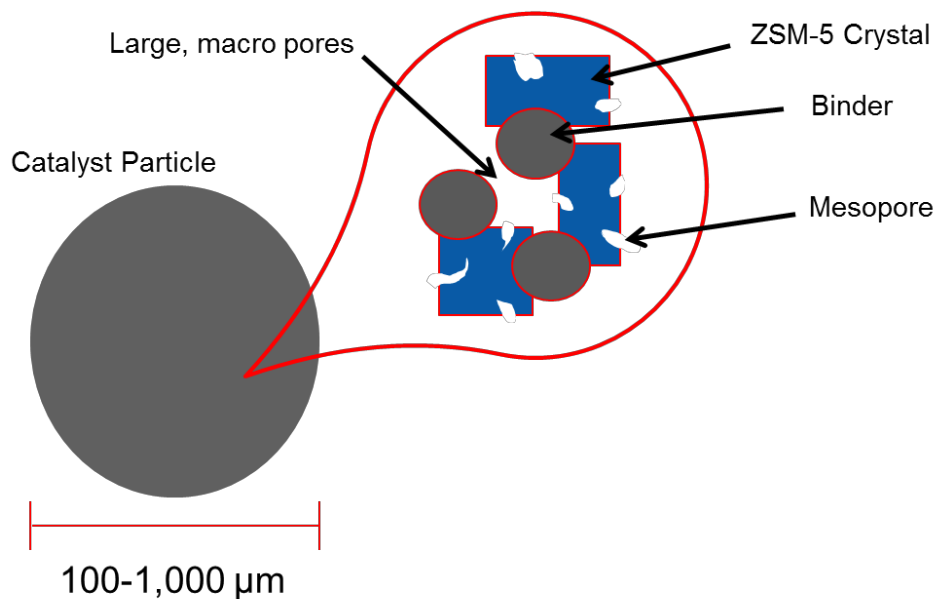


Figure 7.16 Schematic of a ZSM-5 catalyst particle composed of binder and zeolite crystals.

If coke formation was being driven by aromatization reactions, coke would deposit selectively at the site of upgrading on the ZSM-5 crystals capping the pores, blocking access to the acid sites, and reducing the surface area of the catalyst. However, if the coke formation was driven by monomer condensation and coupling, coke would deposit uniformly across the outer surface of the catalyst, including on the surface of the binder, which would cause less pore-blocking per amount of coke than aromatization-driven coke formation.

The results from Figure 7.4 and Figure 7.6, which showed that lignin continued to produce hydrocarbons at the same level throughout the experiment, but with progressively higher amounts of primary vapors being formed, can be explained in this context. Coke was deposited uniformly on the surfaces of binder and ZSM-5 crystal. The catalyst was then no longer able to

provide a suitable surface for cracking reactions. This limited the amount of raw vapors able to enter the zeolite pores and allowed the breakthrough of raw lignin products, as seen in Figure 7.6. However, active sites and micro-pore area were retained to a large extent, which allowed for hydrocarbon formation to continue at relatively constant levels.

In contrast, during CFP of cellulose, the yield of hydrocarbons (Figure 7.1) decreased steadily throughout the experiment. The coke which formed during CFP of cellulose had a direct impact on the upgrading capabilities of the catalyst, and it resulted in significant reduction in pore volume, surface area, and accessible acid sites. This indicates that the CFP of cellulose generated coke on ZSM-5 as an extension of ring-growth reactions during upgrading and formed coke selectively on the ZSM-5 crystals, which lead to the deactivation of the acid-catalyzed aromatization reactions, resulting in reduced aromatics yield, increased alkylation of the aromatics and the generation of intermediate aromatic oxygenates.

The CFP of pine showed similarities to both cellulose and lignin. The hydrocarbon yield from CFP of pine (Figure 7.10 c) does not decrease as rapidly as with cellulose, nor does it remain constant as seen with lignin. The oxygenated species formed during CFP of pine (Figure 7.9) also represent a mixture of lignin- and polysaccharide-derived oxygenates. However, when analyzing the post-reaction catalysts, Figure 7.12-Figure 7.15, it is clear that the ZSM-5 coked by CFP of pine is very similar to the ZSM-5 coked by cellulose. This indicates that during CFP of pine, the biopolymers responsible for the deactivation of the catalyst are the polysaccharide components.

7.6 Section Conclusions

The products of catalytic fast pyrolysis with pine, lignin, and cellulose as well as the characterization of the post-reaction catalysts gave insight into the coking and deactivation process during CFP of whole biomass. Lignin was found to produce an approximately constant yield of liquid-range hydrocarbons throughout the experiment, while cellulose and pine had a high initial hydrocarbon yield which declined rapidly.

The high retention of surface area, microporosity, and accessible acid sites during CFP of lignin, compared to the amount of coke it generated, suggests that ZSM-5 coked primarily via lignin monomer deposition and coupling. This type of coke formation did not have a significant impact on the catalyst activity for hydrocarbon production. However, it led to a deactivation of the cracking capability of the catalyst, resulting in primary pyrolysis vapors being generated at low biomass-to-catalyst ratios. In contrast, ZSM-5 coked by cellulose experienced a large decrease in upgrading activity, accessible acid sites, surface area, and microporosity. This indicates that the coke was forming on the ZSM-5 crystals as an extension of ring-growth reactions during upgrading, and resulted in the deactivation ZSM-5's deoxygenation and aromatization capabilities, leading to a decrease in aromatics and an increase in oxygenated intermediates. The selectivity to alkylated 1-ring aromatics increased and multi-ring hydrocarbons decreased as a result of this type of deactivation. The cumulative results suggest that catalyst deactivation, in the form of decreasing aromatic yield, observed during CFP with whole biomass is primarily caused by the coke generated from the polysaccharide components and not from the lignin component.

8 CFP with metal-modified ZSM-5 in inert and hydrogen atmospheres

The primary objective for this line of research was to decrease yield losses to coke formation, and increase the yield of aromatic hydrocarbons. It is known that biomass has insufficient hydrogen to yield 100% gasoline-range aromatic hydrocarbons, based on stoichiometry, which makes pathways toward low H/C ratio coke precursors more favorable [79]. The hypothesis was that by increasing the reaction-available hydrogen during the CFP of biomass, the favorability towards coke precursors will be reduced, and the yield of desired aromatic hydrocarbons will increase.

For these experiments, the addition of reaction-available hydrogen was achieved by making two adjustments to the standard CFP process. First, the carrier gas used during this series of experiments was 100% hydrogen, supplying the upgrading environment with molecular hydrogen. Secondly, CFP was performed with metal-modified ZSM-5 catalysts, to supply an activating surface for the hydrogen.

The secondary objective was to investigate the broader impact of the catalyst modifications on the upgrading products, catalyst deactivation, and catalyst characteristics during CFP of biomass in both inert and hydrogen atmospheres.

The base catalyst for this study was a ZSM-5 with silica binder and an SAR of 30, procured from Nexceris. Samples of the base catalyst were modified via incipient wetness method with one of the five metals selected: Copper, gallium, nickel, cobalt, and platinum. Each catalyst was loaded such that there was a 1:1 mole ratio of metal:Al₂O₃ in the final catalyst. Details of the catalyst modification are located in Section 3.6.2.

The CFP experiments were carried out in the Pyroprobe Py-GC-MS system, using adjusted temperature set-points. The Pyroprobe reactor and the temperature set-point calibrations are detailed in Sections 3.2.1 and 3.2.1.3, respectively. Prior to each experiment, the catalysts were reduced while loaded in the reactor at 300°C in hydrogen for one hour. During the experiments, successive 10 mg samples of pine were pyrolyzed at 500°C and upgraded over a 10 mg catalyst bed, also at 500°C, achieving a final biomass:catalyst=2. Condensable products were analyzed by the GC-MS at biomass:catalyst= 0.1, 0.2, 0.5, 0.8, 1.1, 1.4, 1.7, and 2.0.

To characterize the changes to the catalysts during upgrading, post-reaction catalyst samples were generated in the Horizontal Packed-bed Reactor, detailed in Section 3.2.3. To generate post-reaction catalyst samples, ten 50 mg boats of pine were pyrolyzed and upgraded over a 500 mg catalyst bed, resulting in a final biomass:catalyst=1. After CFP, the catalyst beds were cooled in inert gas flow to below 200°C, to prevent any oxidation of coke during catalyst extraction.

8.1 Fresh Metal-modified Catalyst Properties

A summary of the characterization of the fresh catalysts is shown in Table 8.1.

Table 8.1 List of catalyst materials that were synthesized and tested for vapor phase upgrading of biomass pyrolysis vapors and their physical properties after reduction at 500°C for metal-promoted ZSM-5 catalysts. Surface area and pore volume as determined by BET analysis of N₂ adsorption isotherms and total acidity as determined by NH₃ TPD. Micropore surface area and pore volume are for pores <2 nm.

Fresh catalysts	Acidity	Total S.A.	Micropore S.A.	Total P.V.	Micropore P.V.
units	μmol/g	m ² /g	cm ² /g	m ³ /g	cm ³ /g
ZSM-5, SAR=30	960	338	284	0.21	0.12
3.3wt% Cu/ZSM-5	854	357	256	0.19	0.11
3.7wt% Ga/ZSM-5	929	364	303	0.12	0.07
3.1wt% Ni/ZSM-5	956	346	242	0.19	0.10
3.1wt% Co/ZSM-5	1001	345	247	0.19	0.10
10.3wt% Pt/ZSM-5	894	327	227	0.18	0.10

The addition of metals to ZSM-5, in general, increased the total surface area of the catalysts and decreased the micropore surface area. This is due to the metal residing on the catalyst's surface, adding surface area, and blocking access to some micropores. The two exceptions to this generalization were the micropore surface area of Ga/ZSM-5, and the total surface area of Pt/ZSM-5. Pt/ZSM-5 had the greatest metal loading, at 10.3 wt%, resulting in a lowered total surface area, and the most significant decrease in micropore surface area. The modification of ZSM-5 with gallium resulted in the largest increase in total surface area, as well as the only increase in micropore surface area.

Metal modification of ZSM-5 decreased the total pore volume and the micropore volume of all catalysts studied. However, the pore volumes of the Ga/ZSM-5 catalyst were reduced substantially, compared to the other catalysts.

Metal modification resulted in a small decrease in total acidity for all catalysts, except Co/ZSM-5, which increased slightly. Overall, the total acidity did not change significantly for any catalyst. However, the distribution of that acidity did change for many of the catalysts, which can be seen in the ammonia TPD signal plots shown in Figure 8.1.

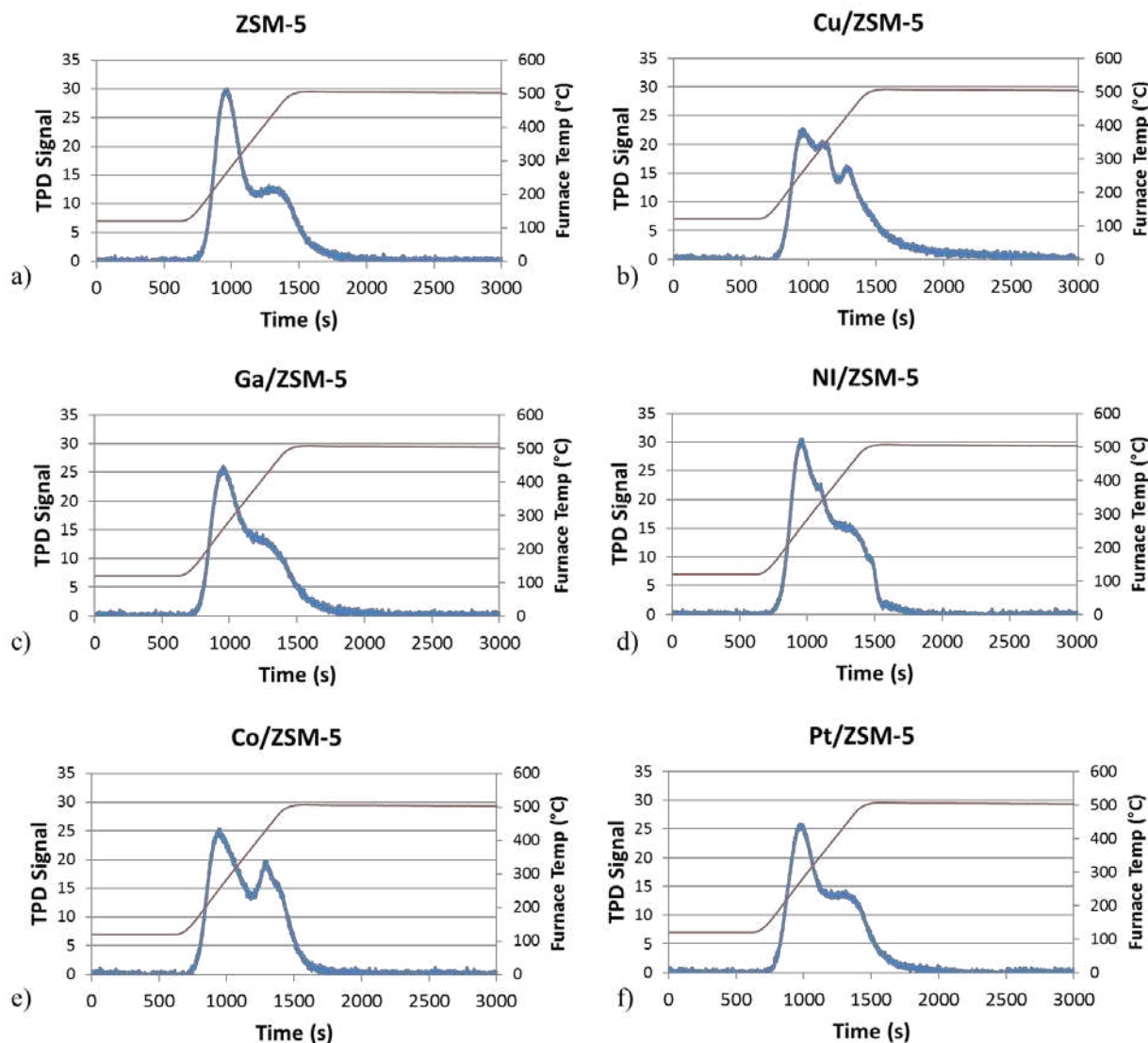


Figure 8.1 Ammonia temperature programmed desorption (TPD) profiles of the fresh catalysts, given by the TCD signal during desorption (shown in blue on the left axis), and the corresponding furnace temperature (shown in red on the right axis).

The plots shown in Figure 8.1 are the TCD signal measured during the desorption of ammonia throughout the NH_3 TPD analysis. A peak at low temperature (120-385°C) correlates with weak acid sites, which allow the adsorbed NH_3 to desorb early in the experiment. These signals are attributed to ammonia bound to weakly acidic sites, such as Lewis acid sites [109]. Peaks

observed at a higher temperature correlate to a stronger acid site, which required higher temperatures, and/or increased time at maximum temperature, for desorption to occur. These strong acid sites, with NH_3 TPD peaks occurring between 370-440°C, were attributed to Brønsted acidity [109]. The Brønsted acid sites are thought to be primarily responsible for the upgrading reactions occurring with ZSM-5, and are therefore of significance [65].

In Figure 8.1 a), the ammonia TPD profile for unmodified ZSM-5 can be seen. It shows that ZSM-5 has a large low-strength acid peak at ~285°C, and a smaller, broad strong acid site peak at ~435°C. This general profile can also be seen in the TPD profiles of Ga/ZSM-5 and Pt/ZSM-5 in Figure 8.1 a) and f). The profile for Ga/ZSM-5 shows a slight increase in the broadness of the strong acid site peak, indicating added acidity from the addition of the metal. Cu/ZSM-5, Ni/ZSM-5, and Co/ZSM-5 all show increased complexity in their ammonia TPD profiles, with notable increases in mid-range and high-strength acid sites, as seen in Figure 8.1 b), d), and e).

To determine the contribution made by the different strength acid sites to the overall NH_3 TPD profile, curve fitting was performed using Gaussian curves. Although more exotic curve-fitting functions have advantages over the Gaussian fit in certain scenarios, the Gaussian has been shown to be sufficient for the deconvolution of ammonia TPD results from ZSM-5 [109]. The curve-fitting for ZSM-5 can be seen in Figure 8.2.

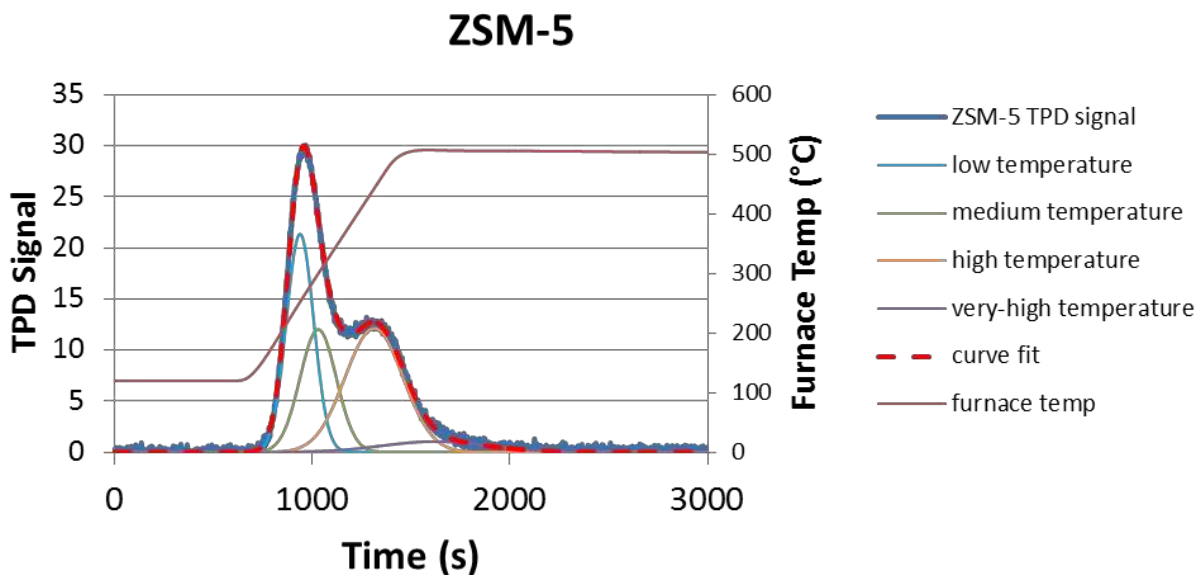


Figure 8.2 Gaussian curve-fitting performed on the Ammonia TPD curve of ZSM-5 to determine the area contribution from acid site strengths.

Deconvolution of the TPD profile is used to identify the contributing components to the overall acidity profile. The high-temperature curve, shown in purple in Figure 8.2, is attributed to Brønsted acidity, and is of interest due to the role of Brønsted acid sites in the pairing and side chain reactions occurring in the hydrocarbon pool, as illustrated in Figure 1.10.

8.2 Catalytic Fast Pyrolysis Reaction Results

To take a broad view of how the addition of metals to ZSM-5 alters the upgrading and catalyst deactivation processes during the CFP of biomass in inert and hydrogen atmospheres, it is useful to analyze the deactivation trend of the catalysts during the experiments. For each biomass pulse pyrolyzed and upgraded over the catalyst in the Py/GC-MS experiments, the products were identified, quantified as a mass yield, and designated as either a “hydrocarbon” or an “oxygenate.” Plotting the hydrocarbon and oxygenate yield for each pulse, as a function of the

biomass:catalyst, then provides a trend for how the catalyst is performing and deactivating. The deactivation trends for CFP in inert atmosphere can be seen in Figure 8.3.

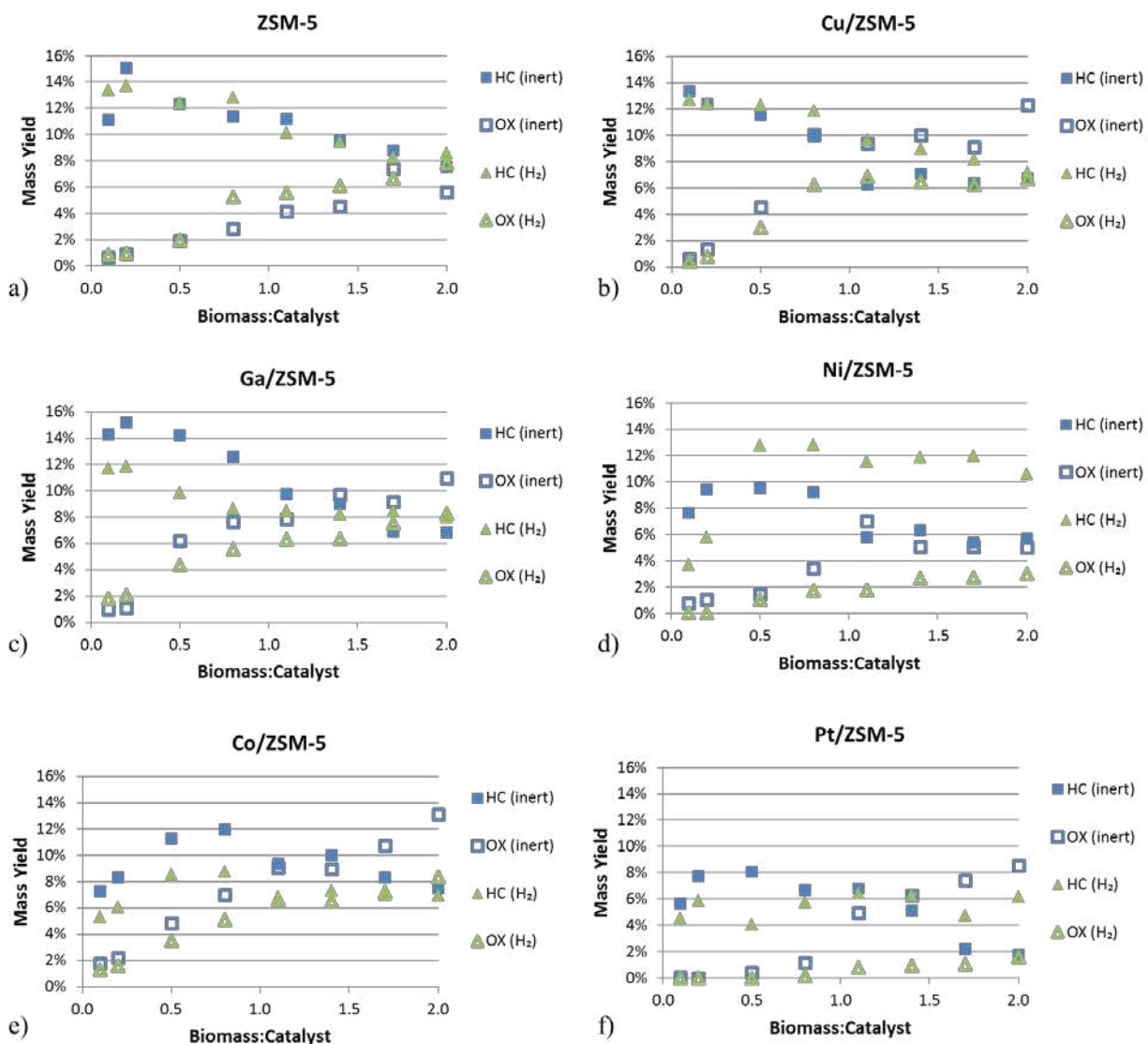


Figure 8.3 The deactivation trends for each catalyst during CFP of pine in inert (blue markers) and hydrogen (green markers) atmospheres. Solid markers indicate total mass yield of hydrocarbons, and hollow markers indicate total mass yield of oxygenates, as a function of the biomass:catalyst.

The deactivation trend of ZSM-5 (Figure 8.3 a) is similar in both hydrogen and inert. In both atmospheres, when the catalyst is fresh, at low biomass:catalyst, the yield of hydrocarbons is high and the yield of oxygenates is low. As the experiment progresses and the cumulative amount of biomass pyrolyzed and upgraded over the catalyst bed increases, the hydrocarbon yield decreases and the oxygenate yield increases. There was very little difference in the performance of unmodified ZSM-5 in inert vs hydrogen, which was anticipated because ZSM-5 does not have sites which can activate hydrogen.

In Figure 8.3, it can be seen that most of the catalysts show some degree of an activation period, observed as an increasing yield of hydrocarbons during the initial pulses of biomass, at low biomass:catalyst. The activation period can be explained by the need to initially form the hydrocarbon pool within the zeolite before maximum catalyst activity can be achieved. Ni/ZSM-5 and Co/ZSM-5, as seen in Figure 8.3 d) and e), exhibited the most pronounced activation periods. During upgrading in both inert and hydrogen, the hydrocarbon yield from Co/ZSM-5 continued to increase through biomass:catalyst=0.8. Co oxides are steam reforming catalysts and have been found effective for example in converting ethanol to hydrogen and carbon dioxide [110]. Co likely initially converted some of the pyrolysis products to light gases, which resulted in a slow build-up of the hydrocarbon pool. Ni/ZSM-5 in a hydrogen atmosphere exhibited the lowest initial hydrocarbon yields and the largest increase in hydrocarbon yield whereas in the inert gas atmosphere, the activation period for Ni/ZSM-5 was much less pronounced. Metallic Ni is a hydrogenation catalyst and the reduced Ni hydrogenated the hydrocarbon pool precursors, which lead to their release into the vapor phase. The observation of catalyst activation periods underscores the value of deactivation experiments, as this effect would not have been noticed had these experiments been performed only at low biomass:catalyst.

The similarity in deactivation profiles in inert and hydrogen is most pronounced with Cu/ZSM-5, Ga/ZSM-5, and Co/ZSM-5, despite the variation in magnitude of the yields. The catalysts' hydrocarbon profiles in hydrogen follow closely with the catalysts' profile in inert, except in magnitude. For all three catalysts, however, the oxygenate profile at high biomass:catalyst deviates in hydrogen, having a more gradual slope.

The two profiles which deviate the most between inert and hydrogen are that of Ni/ZSM-5 and Pt/ZSM-5, shown in Figure 8.3 d) and f), respectively. In the case of Ni/ZSM-5, after the initial activation period, the hydrocarbon yield is considerably more constant in hydrogen, compared to inert. In the case of Pt/ZSM-5, not only is the hydrocarbon yield more stable in hydrogen, but the oxygenate profile has an extremely lower slope.

For a quantifiable comparison of the efficacy of each catalyst at deoxygenation and hydrocarbon production, the integrated mass yields of liquid-range hydrocarbons and oxygenates produced during the entire upgrading experiment have been calculated. Figure 8.4 shows these yields from CFP with each catalyst in a) inert, and b) hydrogen.

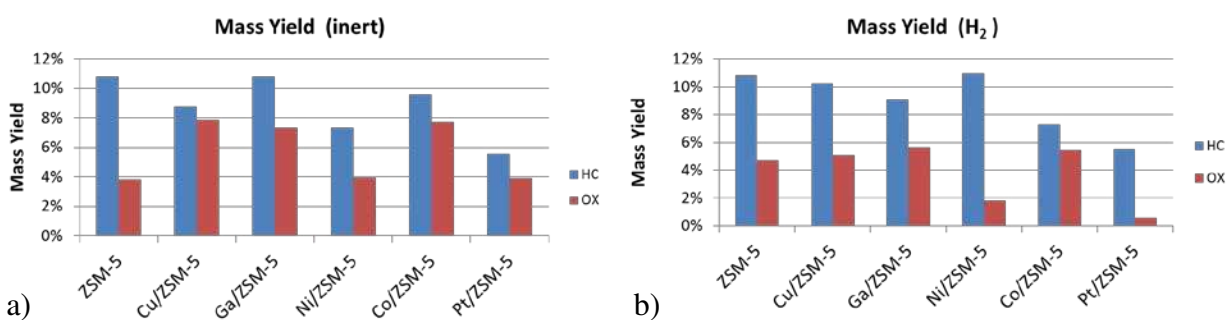


Figure 8.4 Mass yields of liquid-range hydrocarbon and oxygenate products during CFP of pine with various catalysts in a) inert and b) hydrogen.

In inert atmosphere (Figure 8.4 a) the addition of metals to ZSM-5 did not result in enhancements, i.e. higher hydrocarbon yields or lower oxygenate yields, compared to unmodified ZSM-5. CFP with Cu/ZSM-5 and Co/ZSM-5 resulted in both lower hydrocarbon yields and higher oxygenate yields, compared to unmodified ZSM-5. Ni/ZSM-5 and Pt/ZSM-5 catalysts generated oils with approximately the same yields of oxygenated species as unmodified ZSM-5; however, the yield of hydrocarbons was lower for each catalyst.

Ga/ZSM-5 was the only metal-modified catalyst which generated an equal yield of hydrocarbons in inert atmosphere, compared to unmodified ZSM-5. However, in contrast to the observation of several others [88] [54] [89], Ga/ZSM-5 did not result in an increase in aromatic hydrocarbon yield compared to ZSM-5.

CFP with unmodified ZSM-5 gave approximately the same hydrocarbon yield in inert and in hydrogen, as others have reported [87], as did Pt/ZSM-5. Ni/ZSM-5 and Cu/ZSM-5 both showed an increase in hydrocarbon yield during CFP in hydrogen, resulting in both catalysts having comparable yields to unmodified ZSM-5. From Figure 8.3 d), it can be seen that the high total yield of Ni/ZSM-5 in hydrogen is due to the slow rate of deactivation. CFP with Ga/ZSM-5 and Co/ZSM-5 resulted in a lower hydrocarbon yield in hydrogen, compared to their performances in inert.

All metal-modified catalysts yielded less oxygenates during CFP in hydrogen, than in inert.

During CFP in hydrogen, Pt/ZSM-5 and Cu/ZSM-5 had the largest decrease in oxygenate yield compared to inert, resulting in a 3.3 and 2.3 mass % reduction in oxygenate yield, respectively.

Figure 8.5 shows the selectivity of hydrocarbons generated during CFP with each catalyst in (a) inert and (b) hydrogen atmospheres, and provides an overview of the types of hydrocarbons produced.

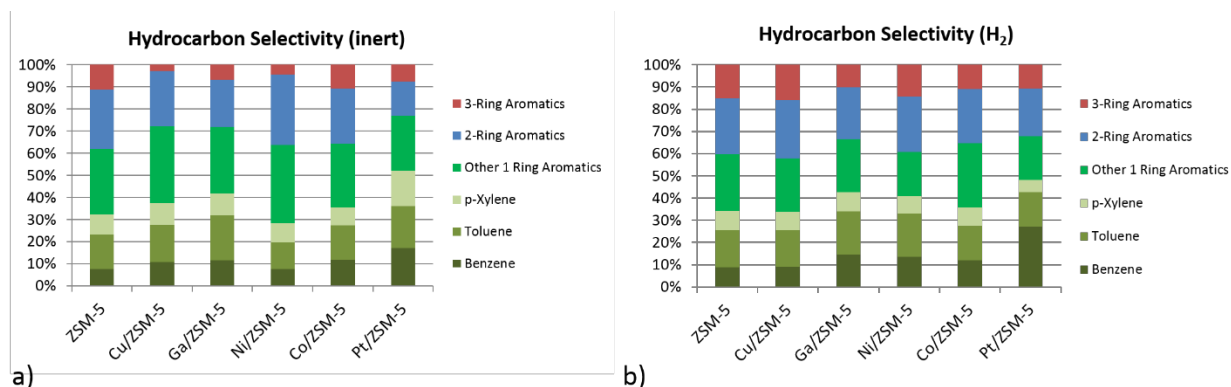


Figure 8.5: Selectivity among liquid-range hydrocarbon products during CFP of pine with metal-modified ZSM-5 in a) inert and b) hydrogen.

All hydrocarbons detected were aromatic in all cases. This shows that there was no significant ring saturation occurring. One-ring aromatics were the most prevalent under all conditions. In general, selectivity towards benzene increased during CFP in the presence of hydrogen, while the selectivity of alkylated 1-ring aromatics, seen most clearly in the “other 1-ring aromatics” category, decreased. The selectivity towards 3-ring aromatics increased in hydrogen for all metal-modified catalysts. It is anticipated that hydrogenation reactions, utilizing the hydrogen atmosphere, decrease the favorability of coke-forming ring-growth reactions, resulting in fewer polyaromatic compounds progressing to coke.

To better determine the impact of the added metals during CFP in inert and hydrogen, the hydrocarbon yield was plotted as a function of the strong acid sites present in the catalysts.

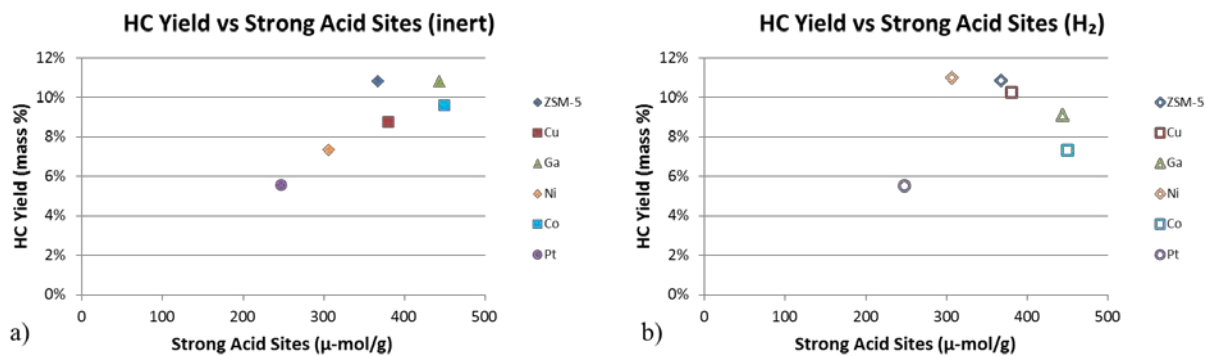


Figure 8.6 The correlation between the density of strong acid sites in each catalyst, and the total hydrocarbon yield during CFP in a) inert and b) hydrogen atmospheres.

In helium, as displayed in Figure 8.6 a), a linear relationship between strong acid site density and aromatic hydrocarbon yield was observed for the metal-modified catalysts. This indicates that the presence of metals is not directly impacting the upgrading reactions during CFP in inert, but rather the yield is only a function of the strong acid sites. However, when the upgrading is performed in the presence of hydrogen (Figure 8.6 b), the trend is noticeably disrupted, indicating that the metals are having a direct impact on upgrading reactions. Ni/ZSM-5 and Cu/ZSM-5 both show an increase in the hydrocarbon yield for their given density of acid sites. Unmodified ZSM-5 and Pt/ZSM-5 were unchanged, while Co/ZSM-5 and Ga/ZSM-5 both gave lower hydrocarbon yields respective to their acid sites, deviating from the trend line established during upgrading in inert atmosphere.

8.3 Post-reaction Catalyst Characterization and Analysis

The post-reaction catalysts were characterized by temperature-programmed oxidation on a TGA to determine the coke yield. Weight loss observed below 250°C was attributed to water loss, and

weight loss observed above 250°C was attributed to coke oxidation. The measured coke yields are shown in Figure 8.7.

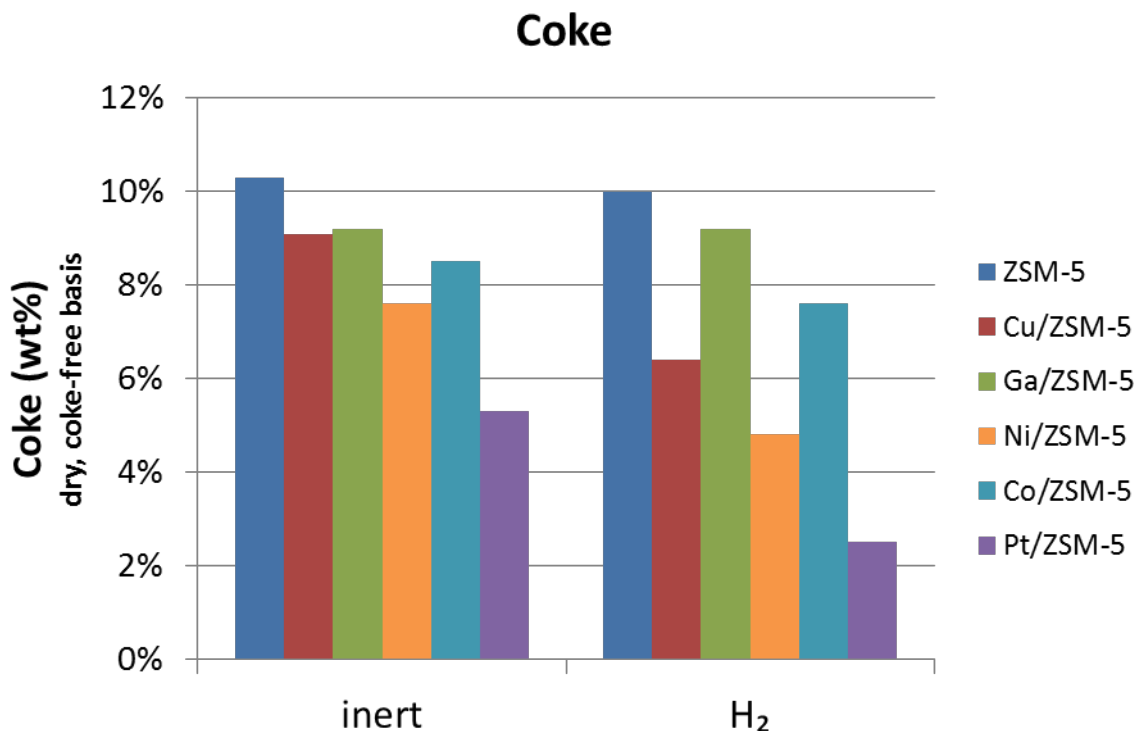


Figure 8.7 Coke present on post-reaction catalysts, following biomass pyrolysis and vapor phase upgrading in inert and H₂-containing environments, as determined by TGA.

No correction was made for possible oxidation of a reduced metal during the TGA analysis. The post-reaction oxidation states were unknown, and therefore could not be accurately accounted for. Theoretically, if none of the metal sites had oxidized during the upgrading, the oxidation during TGA analysis could account for up to 0.84 wt% for the 2⁺ metals (Ni, Pt, Co, Cu) or 1.25 wt% gain for Ga (a 3⁺ metal).

Characterization for coke content showed that all modified catalysts gave lower coke yields, compared to ZSM-5, in both inert and hydrogen. All catalysts also gave the same or lower coke

yields in hydrogen, compared to inert, with Ni/ZSM-5 and Cu/ZSM-5 showing the largest decrease. The relationship between the strong acid sites on the catalysts and the amount of coke generated during upgrading can be seen in Figure 8.8.

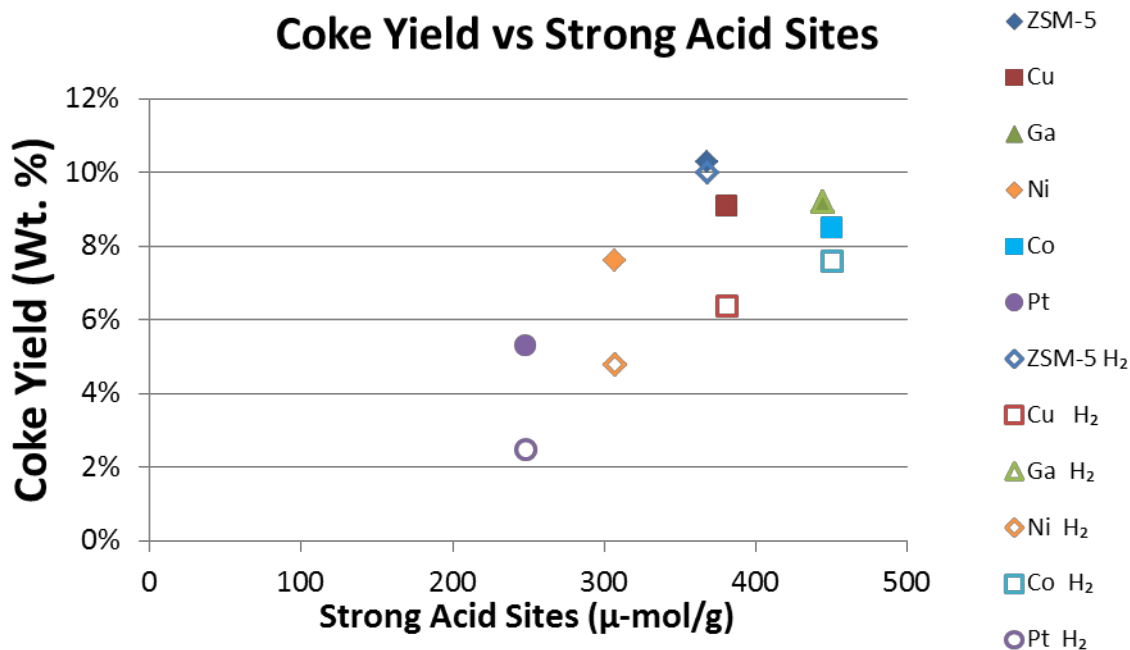


Figure 8.8 Relationship between coke yield on the post-reaction catalysts and the strong acid sites recorded in fresh, reduced catalysts. Solid markers denote values for post-reaction catalysts generated in an inert atmosphere, and hollow markers indicate samples generated in a hydrogen atmosphere.

For most catalysts, the number of strong acid sites correlates strongly with the amount of coke generated during upgrading. With the exception of Ga/ZSM-5, CFP performed in hydrogen resulted in a lower coke yield per unit of strong acid sites.

The correlation between the achieved hydrocarbon yield during Py/GC-MS experiments and the coke yield from the post-reaction catalyst generation experiments, gives some insight into what is occurring during CFP, and is shown in Figure 8.9.

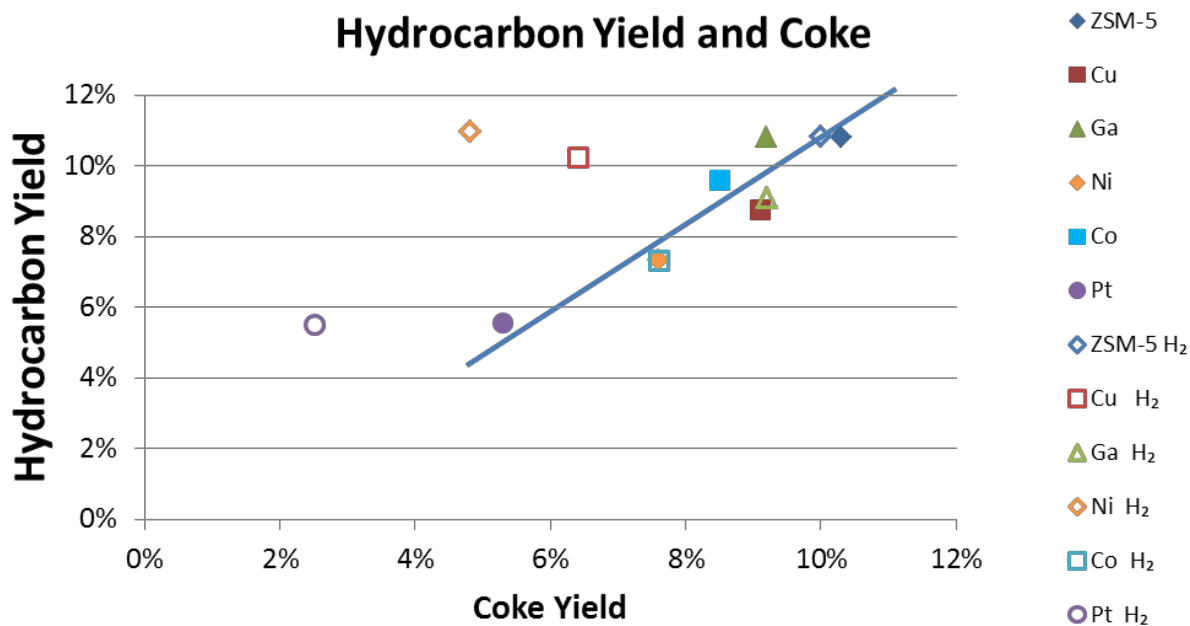


Figure 8.9 Relationship between the hydrocarbon yield generated by each catalyst during CFP and the wt% of coke on the post-reaction catalyst. Solid markers denote values for upgrading in inert and hollow markers denote upgrading performed in hydrogen.

An increase in hydrocarbon production correlated strongly with an increase in coke production during CFP in the inert upgrading atmospheres. This suggests that coke generation is primarily driven by the extension of the ring-growth reactions responsible for the production of aromatic hydrocarbon products. Some of the catalysts, namely ZSM-5, Ga/ZSM-5, and Cu/ZSM-5, followed the same trend in the hydrogen atmosphere as well. However, the correlation did not extend to Pt/ZSM-5, Ni/ZSM-5, and Cu/ZSM-5 in hydrogen, indicating that these metals have an active role in the upgrading reactions when hydrogen is present. Both Ni/ZSM-5 and Cu/ZSM-5 catalysts showed a desirable combination of lowering coke yield while also producing a yield of aromatic hydrocarbons comparable to that of ZSM-5. The Pt/ZSM-5 catalyst also had a significant reduction in coke yield during CFP in hydrogen, but maintained its low hydrocarbon yield. This is likely due to an increase in gasification reactions in the hydrogen atmosphere.

The coke yield can be compared directly to the acidity and surface area retained in the post-reaction catalyst in Table 8.2.

Table 8.2: Post-reaction catalyst analysis results, including coke yield, total acidity retained, and total surface area retained.

Post-reaction catalysts	Coke (wt%)		Acidity Retained		Surface Area Retained	
	Inert	H ₂	Inert	H ₂	Inert	H ₂
ZSM-5	10.3%	10.0%	58.0%	41.3%	31.5%	29.0%
Cu/ZSM-5	9.1%	6.4%	89.9%	79.9%	26.3%	55.6%
Ga/ZSM-5	9.2%	9.2%	48.6%	52.8%	25.7%	26.3%
Ni/ZSM-5	7.6%	4.8%	68.8%	69.5%	34.4%	51.1%
Co/ZSM-5	8.5%	7.6%	82.9%	90.1%	43.3%	51.2%
Pt/ZSM-5	5.3%	2.5%	96.2%	84.4%	94.8%	76.7%

The ZSM-5 and Ga/ZSM-5 catalysts showed the greatest loss of their initial acidity, compared to the other catalysts, for both the reactions run in inert and in the presence of H₂. The acidity retention results are also consistent with the coke measurements, which showed the greatest amounts of coke on ZSM-5 and Ga/ZSM-5. The relationship between acidity retained in the post-reaction catalyst, and coke yield on the catalyst, is shown in Figure 8.10.

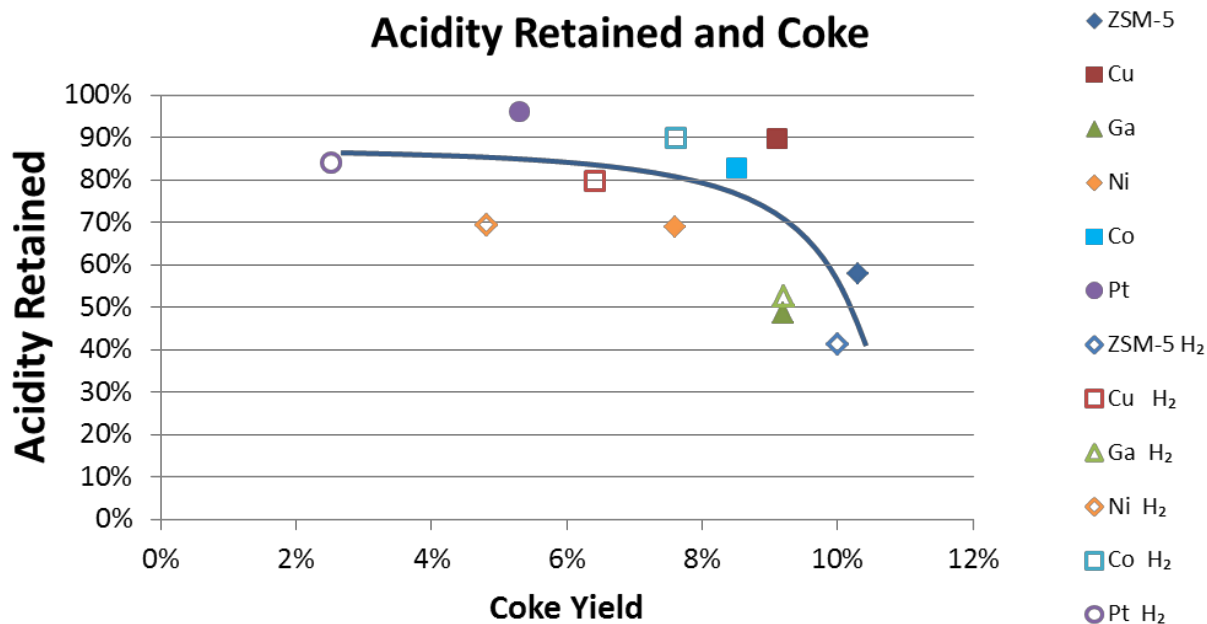


Figure 8.10 Comparison of the acidity retained by each catalyst following CFP, and the amount of coke present on the catalyst. Solid markers denote values from experiments in inert and hollow markers denote results from experiments in hydrogen.

It is reasonable that the highest coke levels would correlate with the lowest number of retained, accessible acid sites, as coke is known to present a physical barrier to the catalyst pores [51].

The Cu/ZSM-5 used for upgrading in inert retains a notable percent of acidity, despite having one of the highest coke yields. Complimentary to this correlation is the comparison of surface area retention and acidity retention, shown in Figure 8.11.

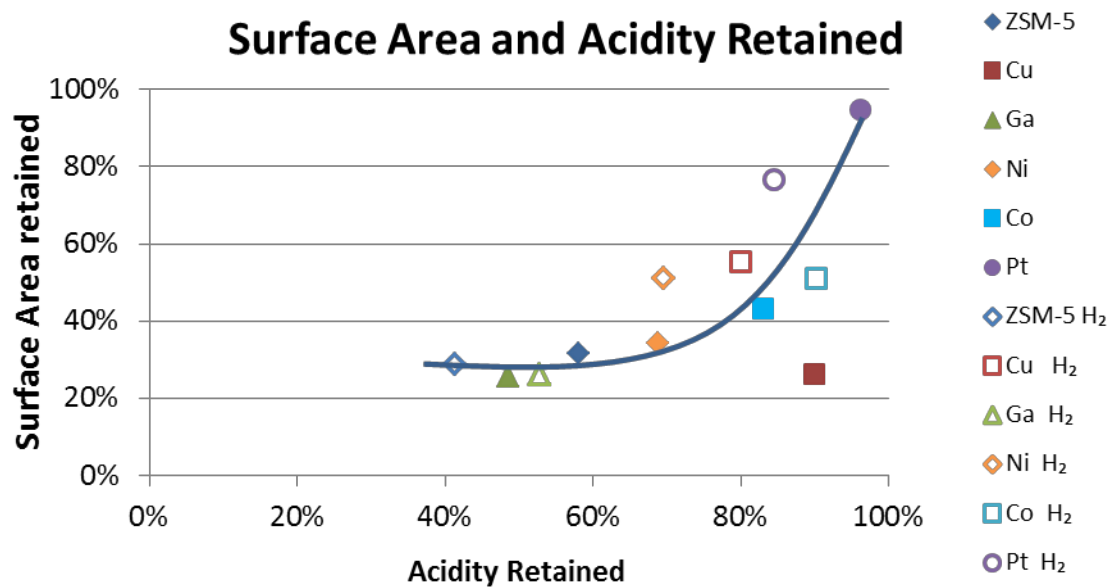


Figure 8.11 Comparison of the surface area retained in the post-reaction catalyst to the acidity retained. Solid markers denote values for upgrading in inert and hollow markers denote upgrading performed in hydrogen.

Acidity and surface area correlate strongly for most of the catalysts, in both atmospheres. This is reasonable, because one would expect that as coke physically obstructs the pores of the catalyst, both the surface area and the acid sites contained in the pores would be lost. The outlier of this trend is the Cu/ZSM-5 used for CFP in inert, which retained a large percentage of its acidity, despite having one of the lowest retentions of surface area. It is possible that the copper became oxidized during the upgrading reactions in helium, which added a small amount of Lewis acidity, inflating the value for acidity retained.

8.4 Section Conclusions

There is a strong linear correlation between the density of strong acid sites in a metal-modified catalyst, and the hydrocarbon yield achieved during CFP in an inert atmosphere. This shows that the primary impact of the metal during upgrading in inert is the strong acid sites it blocks. While

in hydrogen, the metal modifications can result in either a positive impact, such as with Ni/ZSM-5 and Cu/ZSM-5, or a negative impact, as observed with Ga/ZSM-5 and Co/ZSM-5.

No catalyst out-performed unmodified ZSM-5 in terms of hydrocarbon yield. However, Ga/ZSM-5 in inert and Ni/ZSM-5 and Cu/ZSM-5 in hydrogen produced comparable yields to ZSM-5, while reducing coke formation. The results from CFP with Ni/ZSM-5 in hydrogen are of particular significance. The upgrading resulted in an overall oil composition with a more desirable ratio of hydrocarbons to oxygenates, compared to ZSM-5, while maintaining a comparable yield of hydrocarbons.

CFP performed in hydrogen with Ni/ZSM-5, Cu/ZSM-5, and Pt/ZSM-5 resulted not only in an increase in hydrocarbon yield, compared with their yields in helium, but also an increase in the ratio of hydrocarbon yield to coke yield, as anticipated under the initial hypothesis. However, the observed relative increase in hydrocarbon yield did not exceed the base yield set by unmodified ZSM-5. It is theorized that had the CFP experiments been extended, the hydrocarbon yields from these catalysts would exceed that of ZSM-5, by virtue of their slower deactivation rate. This highlights the significance of deactivation-style experiments for catalyst evaluation, as the slow deactivation rates of Ni/ZSM-5 and Pt/ZSM-5, as well as the initial catalyst activation time, seen most prominently with Co/ZSM-5, would not have been discovered in a conventional screening experiment, performed with excess catalyst.

Although this experimental set did not result in an increase in liquid-range aromatic hydrocarbon yield, sufficient promise was shown in oil composition and catalyst longevity by metal-modified ZSM-5 in hydrogen to merit further study.

9 Conclusions and Future Work

9.1 Conclusions

The objective of this work was to further the understanding of catalytic fast pyrolysis (CFP) of biomass by addressing specific gaps in knowledge. Characteristics which impact the efficacy of ZSM-5 during upgrading and the impacts and mode of catalyst deactivation were studied, as well as the results of metal-modifications to ZSM-5 intended to improve the upgrading characteristics and hydrocarbon yield during CFP. Several of the most significant contributions to the understanding of the CFP of biomass with ZSM-5, which are detailed throughout this dissertation, are described below.

The silica-to-alumina ratio (SAR) in ZSM-5 crystals has substantial impact on upgrading ability (Chapter 5): Very low SAR results in rapid deactivation and poor performance. High SAR ZSM-5 lacks sufficient acid sites to completely deoxygenate pyrolysis vapors. SAR30 was found to be the optimal SAR, of the SARs studied, for pure ZSM-5.

Acidity imparted by the binder material can influence the upgrading activity of ZSM-5 in a similar way as the SAR does (Chapter 6): Silica and clay binders were found to be roughly equivalent in upgrading performance on SAR30 ZSM-5. ZSM-5 SAR30 with alumina binder was found to be a poor upgrading catalyst. The results indicate that the added Lewis acidity from the alumina binder impacts the upgrading characteristics of ZSM-5 in a similar way to that of additional Brønsted acid sites.

Intermediate products are formed at moderate levels of catalyst deactivation (Chapter 4):

As the amount of pyrolysis vapors upgraded over the catalyst increases (biomass:catalyst

increases), ZSM-5 loses its effectiveness at deoxygenating pyrolysis vapors. This resulted in a trend of decreasing hydrocarbon yield and increasing primary oxygenate yield. It was found that a series of products is produced at intermediate levels of catalyst deactivation that are not present with very active or very deactivated catalyst. The most pronounced of these products was phenol.

Phenol, an observed oxygenate intermediate product, is a catalytic product of CFP of biomass with ZSM-5 and not a result of incomplete lignin deoxygenation (Chapter 7):

Phenol and methylated phenols were observed during the CFP of cellulose, showing that they are a result of the catalytic upgrading mechanism and not being generated from the partial deoxygenation of phenolic lignin monomers.

There are two distinct types of catalyst deactivation occurring during CFP of biomass with ZSM-5 (Chapter 7): Deactivation caused by the polyphenolic lignin component of biomass inhibits the initial surface cracking reactions and deactivation driven by the cellulose component of biomass inhibits the subsequent deoxygenation and aromatization reactions. Evidence suggests that the coke from lignin was formed by monomer deposition and coupling on the surface of the catalyst. This type of coke did not have a significant impact on the catalyst activity for hydrocarbon production, but resulted in higher yields of unreacted primary vapors. In contrast, cellulose upgrading formed coke as an extension of upgrading reactions, and resulted in the deactivation of upgrading pathways. Coke generated from the cellulose component of biomass is responsible for the decreasing yield of hydrocarbons observed during CFP of whole biomass.

In an inert environment, the primary impact of metal-modification of ZSM-5 results from the blockage of strong acid sites (Chapter 8): There is a linear correlation between the density

of strong acid sites in a metal-modified catalyst and the hydrocarbon yield achieved during CFP in an inert atmosphere. This shows that the primary impact of the metal during upgrading in inert is the blocking of strong acid sites.

In hydrogen, the metal additions can reduce coking (Chapter 8). The metals can activate hydrogen, which results in hydrogenation of coke precursors, which leads to reduced catalyst deactivation. In hydrogen, a reduced coke yield was observed with all metal-modified catalysts, except for Ga/ZSM-5, which had similar coke yields in inert and hydrogen atmospheres.

No metal-modified catalyst out-performed unmodified ZSM-5 on the basis of hydrocarbon yield, either in inert or hydrogen-containing atmospheres (Chapter 8): However, Ga/ZSM-5 in inert and Ni/ZSM-5 and Cu/ZSM-5 in hydrogen produce comparable yields to ZSM-5.

Ni/ZSM-5 in hydrogen is of particular significance, because it yields an oil with a more desirable ratio of hydrocarbons to oxygenates, compared to ZSM-5, while maintaining a comparable yield of hydrocarbons.

9.2 Future Work

The research presented highlights several opportunities for future study. Some of the interesting lines of inquiry that are a direct extension of this work are:

- Further study into the impact of the SAR by performing experiments in which the total number of acid sites in the catalyst beds are kept constant, and not the mass of catalyst.
- Furthermore, the use of an acidic binder, such as alumina, could be explored on a base ZSM-5 with higher SARs, to precisely determine if acidity from the binder impacts the catalytic upgrading in the same fashion.

- The biopolymers study could be furthered by generating catalyst samples at various ratios of pyrolysis vapor mass to catalyst bed weight. This may give additional insight into the two types of deactivation reported.
- The high-quality oil generated by Ni/ZSM-5 was unique and could be significant if the yield was increased. Work done to optimize the metal loading could be beneficial in advancing a modified catalyst that outperforms ZSM-5.
- Modifying ZSM-5 by adding hydrogen-activating metals to the framework. This may reduce the blockage of active sites, and perhaps reduce polyaromatic formation in the micropores.

However, the cumulative work presented here guides one to conclude that the most impactful way to advance catalytic fast pyrolysis technology as a means of renewable hydrocarbon transportation fuel production, would be to investigate catalysts beyond ZSM-5 and other zeolites. ZSM-5 is a first-generation CFP catalyst, and has long been the standard for CFP upgrading catalysts. It has been found to be superior to all other zeolites (such as other zeolite types commonly used in FCC and dewaxing processes), giving the highest overall yield of deoxygenated products and lowest coke formation. Nevertheless, the yields over ZSM-5 are low and the deactivation from coke is rapid. Attempts to optimize and modify ZSM-5 and the operating parameters during CFP have largely failed to result in a meaningful increase in hydrocarbon yield.

My overall recommendation is that catalyst research efforts should move away from ZSM-5 modification and toward alternative catalysts. Of particular interest are metal oxides and bifunctional catalysts. Some examples include molybdenum oxide, which has been shown to fully deoxygenate pine pyrolysis vapors [111], a combination of zirconia and titania, which

showed promise at reducing the oxygen content of biomass pyrolysis vapors [112], Pt on titania support [113], and molybdenum carbide [114].

10 References

- [1] A. J. Ragauskas, C. K. Williams, B. H. Davison, G. Britovsek, J. Cairney, C. A. Eckert, W. J. Frederick, J. P. Hallett, D. J. Leak, C. L. Liotta and others, "The path forward for biofuels and biomaterials," *science*, vol. 311, pp. 484-489, 2006.
- [2] F. Birol and others, "CO2 Emissions from Fuel Combustion Highlights," *International Energy Agency*, vol. 7, 2015.
- [3] B. E. Dale and R. G. Ong, "Energy, wealth, and human development: why and how biomass pretreatment research must improve," *Biotechnology progress*, vol. 28, pp. 893-898, 2012.
- [4] J. R. Regalbuto, "Cellulosic biofuels—got gasoline?," *Science*, vol. 325, pp. 822-824, 2009.
- [5] L. Zhang and G. Hu, "Supply chain design and operational planning models for biomass to drop-in fuel production," *Biomass and bioenergy*, vol. 58, pp. 238-250, 2013.
- [6] K. Tong, M. J. Gleeson, G. Rong and F. You, "Optimal design of advanced drop-in hydrocarbon biofuel supply chain integrating with existing petroleum refineries under uncertainty," *biomass and bioenergy*, vol. 60, pp. 108-120, 2014.
- [7] S. N. Naik, V. V. Goud, P. K. Rout and A. K. Dalai, "Production of first and second generation biofuels: a comprehensive review," *Renewable and Sustainable Energy Reviews*, vol. 14, pp. 578-597, 2010.
- [8] J. L. Easterly and M. Burnham, "Overview of biomass and waste fuel resources for power production," *Biomass and Bioenergy*, vol. 10, pp. 79-92, 1996.
- [9] G. W. Huber, S. Iborra and A. Corma, "Synthesis of transportation fuels from biomass: chemistry, catalysts, and engineering," *Chemical reviews*, vol. 106, pp. 4044-4098, 2006.
- [10] R. D. Perlack, L. L. Wright, A. F. Turhollow, R. L. Graham, B. J. Stokes and D. C. Erbach, "Biomass as feedstock for a bioenergy and bioproducts industry: the technical feasibility of a billion-ton annual supply," 2005.
- [11] N. R. Council and others, *Liquid transportation fuels from coal and biomass: technological status, costs, and environmental impacts*, National Academies Press, 2010.
- [12] R. D. Perlack, L. M. Eaton, A. F. Turhollow Jr, M. H. Langholtz, C. C. Brandt, M. E. Downing, R. L. Graham, L. L. Wright, J. M. Kavkewitz, A. M. Shamey and others, "US billion-ton update: biomass supply for a bioenergy and bioproducts industry," 2011.
- [13] R. D. Perlack, L. L. Wright, A. F. Turhollow, R. L. Graham, B. J. Stokes and D. C. Erbach, "Biomass as feedstock for a bioenergy and bioproducts industry: the technical feasibility of a

billion-ton annual supply," Oak Ridge National Lab TN, 2005.

- [14] P. McKendry, "Energy production from biomass (part 1): overview of biomass," *Bioresource technology*, vol. 83, pp. 37--46, 2002.
- [15] R. C. Pettersen, "The chemical composition of wood," *The chemistry of solid wood*, vol. 207, pp. 57-126, 1984.
- [16] H. Turumtay, "Cell wall engineering by heterologous expression of cell wall-degrading enzymes for better conversion of lignocellulosic biomass into biofuels," *BioEnergy Research*, vol. 8, pp. 1574-1588, 2015.
- [17] M. Verma, S. Godbout, S. Brar, O. Solomatnikova, S. Lemay and J. Larouche, "Biofuels production from biomass by thermochemical conversion technologies," *International Journal of Chemical Engineering*, vol. 2012, 2012.
- [18] D. Leckel, "Diesel production from Fischer- Tropsch: the past, the present, and new concepts," *Energy & Fuels*, vol. 23, pp. 2342-2358, 2009.
- [19] P. McKendry, "Energy production from biomass (part 3): gasification technologies," *Bioresource technology*, vol. 83, pp. 55-63, 2002.
- [20] R. Zhang, R. C. Brown and A. Suby, "Thermochemical generation of hydrogen from switchgrass," *Energy & fuels*, vol. 18, pp. 251-256, 2004.
- [21] G. Chinchin, P. Denny, J. Jennings, M. Spencer and K. Waugh, "Synthesis of methanol: part 1. Catalysts and kinetics," *Applied Catalysis*, vol. 36, pp. 1-65, 1988.
- [22] M. E. Gaffigan, *Biofuels: Potential Effects and Challenges of Required Increases in Production and Use*, DIANE Publishing, 2010.
- [23] S. Czernik and A. Bridgwater, "Overview of applications of biomass fast pyrolysis oil," *Energy & Fuels*, vol. 18, pp. 590-598, 2004.
- [24] A. V. Bridgwater, "Review of fast pyrolysis of biomass and product upgrading," *Biomass and bioenergy*, vol. 38, pp. 68-94, 2012.
- [25] A. V. Bridgwater, "Renewable fuels and chemicals by thermal processing of biomass," *Chemical Engineering Journal*, vol. 91, pp. 87-102, 2003.
- [26] A. Oasmaa, C. Peacocke and others, *A guide to physical property characterisation of biomass-derived fast pyrolysis liquids*, Technical Research Centre of Finland Espoo, 2001.
- [27] D. C. Elliott, "Historical developments in hydroprocessing bio-oils," *Energy & Fuels*, vol. 21, pp. 1792-1815, 2007.

- [28] K. Iisa, R. J. French, K. A. Orton, M. M. Yung, D. K. Johnson, J. ten Dam, M. J. Watson and M. R. Nimlos, "In situ and ex situ catalytic pyrolysis of pine in a bench-scale fluidized bed reactor system," *Energy & Fuels*, vol. 30, pp. 2144-2157, 2016.
- [29] R. French and S. Czernik, "Catalytic pyrolysis of biomass for biofuels production," *Fuel Processing Technology*, vol. 91, pp. 25-32, 2010.
- [30] A. Aho, N. Kumar, K. Eränen, T. Salmi, M. Hupa and D. Y. Murzin, "Catalytic pyrolysis of woody biomass in a fluidized bed reactor: influence of the zeolite structure," *Fuel*, vol. 87, no. 12, pp. 2493-2501, 2008.
- [31] D. J. Mihalcik, C. A. Mullen and A. A. Boateng, "Screening acidic zeolites for catalytic fast pyrolysis of biomass and its components," *Journal of Analytical and Applied Pyrolysis*, vol. 92, pp. 224--232, 2011.
- [32] R. K. Sharma and N. N. Bakhshi, "Catalytic upgrading of fast pyrolysis oil over hzsm-5," *The Canadian Journal of Chemical Engineering*, vol. 71, pp. 383-391, 1993.
- [33] J. D. Adjaye and N. Bakhshi, "Production of hydrocarbons by catalytic upgrading of a fast pyrolysis bio-oil. Part I: Conversion over various catalysts," *Fuel Processing Technology*, vol. 45, pp. 161-183, 1995.
- [34] A. Pattiya, J. O. Titiloye and A. V. Bridgwater, "Fast pyrolysis of cassava rhizome in the presence of catalysts," *Journal of Analytical and Applied Pyrolysis*, vol. 81, pp. 72-79, 2008.
- [35] R. Argauer and G. Landolt, "Crystalline zeolite zsm-5 and method of preparing the same". Patent 3702886, 14 November 1972.
- [36] T. Degnan, G. Chitnis and P. H. Schipper, "History of ZSM-5 fluid catalytic cracking additive development at Mobil," *Microporous and Mesoporous Materials*, vol. 35, pp. 245-252, 2000.
- [37] C. D. Chang and S. S. Grover, "Conversion of methanol to gasoline components". Patent 4058576, 15 November 1977.
- [38] R. J. Quann, L. A. Green, S. A. Tabak and F. J. Krambeck, "Chemistry of olefin oligomerization over ZSM-5 catalyst," *Industrial & engineering chemistry research*, vol. 27, pp. 565-570, 1988.
- [39] G. Woolery, G. Kuehl, H. Timken, A. Chester and J. Vartuli, "On the nature of framework Brønsted and Lewis acid sites in ZSM-5," *Zeolites*, vol. 19, pp. 288-296, 1997.
- [40] D. Coster, A. Blumenfeld and J. Fripiat, "Lewis acid sites and surface aluminum in aluminas and zeolites. A high-resolution NMR study," *Journal of Physical Chemistry*, vol. 98, no. 24, 1994.
- [41] C. Hansch, "The Dehydrocyclization Reaction," *Chemical Reviews*, vol. 53, pp. 353-396, 1953.

- [42] P. Pérez-Uriarte, M. Gamero, A. Ateka, M. Diaz, A. T. Aguayo and J. Bilbao, "Effect of the Acidity of HZSM-5 Zeolite and the Binder in the DME Transformation to Olefins," *Industrial & Engineering Chemistry Research*, vol. 55, pp. 1513-1521, 2016.
- [43] Y. Song, X. Zhu, S. Xie, Q. Wang and L. Xu, "The effect of acidity on olefin aromatization over potassium modified ZSM-5 catalysts," *Catalysis letters*, vol. 97, pp. 31-36, 2004.
- [44] Z. Wan, W. Wu, G. K. Li, C. Wang, H. Yang and D. Zhang, "Effect of SiO₂/Al₂O₃ ratio on the performance of nanocrystal ZSM-5 zeolite catalysts in methanol to gasoline conversion," *Applied Catalysis A: General*, vol. 523, pp. 312-320, 2016.
- [45] K. Thomson, "Reactivity in Zeolite Systems," [Online]. Available: <https://engineering.purdue.edu/~thomsonk/projects.html>. [Accessed 10 7 2017].
- [46] X.-g. Lei, S. Jockusch, M. F. Ottaviani and N. J. Turro, "In situ EPR investigation of the addition of persistent benzyl radicals to acrylates on ZSM-5 zeolites. Direct spectroscopic detection of the initial steps in a supramolecular photopolymerization," *Photochemical & Photobiological Sciences*, vol. 2, pp. 1095-1100, 2003.
- [47] M. Ogura, S.-y. Shinomiya, J. Tateno, Y. Nara, E. Kikuchi and M. Matsukata, "Formation of Uniform Mesopores in ZSM-5 Zeolite through Treatment in Alkaline Solution," *Chemistry letters*, pp. 882-883, 2000.
- [48] J. Jae, G. A. Tompsett, A. J. Foster, K. D. Hammond, S. M. Auerbach, R. F. Lobo and G. W. Huber, "Investigation into the shape selectivity of zeolite catalysts for biomass conversion," *Journal of Catalysis*, vol. 279, pp. 257-268, 2011.
- [49] G. Sastre, C. R. A. Catlow and A. Corma, "Diffusion of benzene and propylene in MCM-22 zeolite. A molecular dynamics study," *The Journal of Physical Chemistry B*, vol. 103, pp. 5187-5196, 1999.
- [50] J. Hargreaves and A. Munnoch, "A survey of the influence of binders in zeolite catalysis," *Catalysis Science & Technology*, vol. 3, pp. 1165-1171, 2013.
- [51] C. Mukarakate, X. Zhang, A. R. Stanton, D. J. Robichaud, P. N. Ciesielski, K. a. D. B. S. Malhotra, E. Gjersing, R. J. Evans, D. S. Heroux and others, "Real-time monitoring of the deactivation of HZSM-5 during upgrading of pine pyrolysis vapors," *Green Chemistry*, vol. 16, pp. 1444-1461, 2014.
- [52] K. Wang, K. H. Kim and R. C. Brown, "Catalytic pyrolysis of individual components of lignocellulosic biomass," *Green Chemistry*, vol. 16, pp. 727-735, 2014.
- [53] K. Wang, J. Zhang, B. H. Shanks and R. C. Brown, "Catalytic conversion of carbohydrate-derived oxygenates over HZSM-5 in a tandem micro-reactor system," *Green Chemistry*, vol. 17, pp. 557-564, 2015.

- [54] Y.-T. Cheng, J. Jae, J. Shi, W. Fan and G. W. Huber, "Production of Renewable Aromatic Compounds by Catalytic Fast Pyrolysis of Lignocellulosic Biomass with Bifunctional Ga/ZSM-5 Catalysts," *Angewandte Chemie*, vol. 124, no. 6, pp. 1416-1419, 2012.
- [55] D. C. Dayton, J. R. Carpenter, A. Kataria, J. E. Peters, D. Barbee, O. D. Mante and R. Gupta, "Design and operation of a pilot-scale catalytic biomass pyrolysis unit," *Green Chemistry*, vol. 17, pp. 4680--4689, 2015.
- [56] E. F. Iliopoulou, S. Stefanidis, K. Kalogiannis, A. Delimitis, A. Lappas and K. Triantafyllidis, "Catalytic upgrading of biomass pyrolysis vapors using transition metal-modified ZSM-5 zeolite," *Applied Catalysis B: Environmental*, vol. 127, pp. 281-290, 2012.
- [57] F. A. Agblevor, S. a. M. O. Beis and N. Abdoulmoumine, "Fractional catalytic pyrolysis of hybrid poplar wood," *Industrial & Engineering Chemistry Research*, vol. 49, pp. 3533-3538, 2010.
- [58] K. Iisa, R. J. French, K. A. Orton, S. Budhi, C. Mukarakate, A. R. Stanton, M. M. Yung and M. R. Nimlos, "Catalytic pyrolysis of pine over HZSM-5 with different binders," *Topics in Catalysis*, vol. 59, pp. 94-108, 2016.
- [59] A. Dutta, A. Sahir, E. Tan, D. Humbird, L. J. Snowden-Swan, P. Meyer, J. Ross, D. Sexton, R. Yap and J. L. Lukas, "Process Design and Economics for the Conversion of Lignocellulosic Biomass to Hydrocarbon Fuels. Thermochemical Research Pathways with In Situ and Ex Situ Upgrading of Fast Pyrolysis Vapors," 2015.
- [60] O. D. Mante, D. C. Dayton, J. Gabrielsen, N. L. Ammitzboll, D. Barbee, S. Verdier and K. Wang, "Integration of catalytic fast pyrolysis and hydroprocessing: a pathway to refinery intermediates and "drop-in" fuels from biomass," *Green Chemistry*, vol. 18, pp. 6123-6135, 2016.
- [61] K. Iisa, R. J. French, K. A. Orton, A. Dutta and J. A. Schaidle, "Production of low-oxygen bio-oil via ex situ catalytic fast pyrolysis and hydrotreating," *Fuel*, vol. 207, pp. 413-422, 2017.
- [62] I. M. Dahl and S. Kolboe, "On the reaction mechanism for propene formation in the MTO reaction over SAPO-34," vol. 20, pp. 329-336, 1993.
- [63] I. M. Dahl and S. Kolboe, "On the reaction mechanism for hydrocarbon formation from methanol over SAPO-34: I. Isotopic labeling studies of the co-reaction of ethene and methanol," *Journal of Catalysis*, vol. 149, pp. 458-464, 1994.
- [64] I. M. Dahl and S. Kolboe, "On the reaction mechanism for hydrocarbon formation from methanol over SAPO-34: 2. Isotopic labeling studies of the co-reaction of propene and methanol," *Journal of Catalysis*, vol. 161, pp. 304-309, 1996.
- [65] D. Lesthaeghe, A. Horre, M. Waroquier, G. B. Marin and V. Van Speybroeck, "Theoretical Insights on Methylbenzene Side-Chain Growth in ZSM-5 Zeolites for Methanol-to-Olefin Conversion,"

Chemistry-A European Journal, vol. 15, pp. 10803-10808, 2009.

- [66] J. F. Haw, W. Song, D. M. Marcus and J. B. Nicholas, "The mechanism of methanol to hydrocarbon catalysis," *Accounts of chemical research*, vol. 36, pp. 317-326, 2003.
- [67] C.-M. Wang, Y.-D. Wang and Z.-K. Xie, "Verification of the dual cycle mechanism for methanol-to-olefin conversion in HSAPO-34: a methylbenzene-based cycle from DFT calculations," *Catalysis Science & Technology*, vol. 4, pp. 2631-2638, 2014.
- [68] K. Hemelsoet, J. Van der Mynsbrugge, K. De Wispelaere, M. Waroquier and V. Van Speybroeck, "Unraveling the Reaction Mechanisms Governing Methanol-to-Olefins Catalysis by Theory and Experiment," *ChemPhysChem*, vol. 14, no. 8, pp. 1526-1545, 2013.
- [69] B. Arstad and S. Kolboe, "The reactivity of molecules trapped within the SAPO-34 cavities in the methanol-to-hydrocarbons reaction," *Journal of the American Chemical Society*, vol. 123, no. 33, pp. 8137-8138, 2001.
- [70] T. R. Carlson, J. Jae and G. W. Huber, "Mechanistic Insights from Isotopic Studies of Glucose Conversion to Aromatics Over ZSM-5," *ChemCatChem*, vol. 1, no. 1, pp. 107-110, 2009.
- [71] F. Bauer and H. G. Karge, "Characterization of coke on zeolites," in *Characterization II*, Springer, 2006, pp. 249-364.
- [72] D. Bibby, N. Milestone, J. Patterson and L. Aldridge, "Coke formation in zeolite ZSM-5," *Journal of Catalysis*, vol. 97, no. 2, pp. 493-502, 1986.
- [73] N. Chen, D. Walsh and L. Koenig, "Fluidized bed upgrading of wood pyrolysis liquids and related compounds," *Prepr. Pap., Am. Chem. Soc., Div. Fuel Chem. (United States)*, vol. 32, no. CONF-870410-, 1987.
- [74] A. Lappas, M. Samolada, D. Iatridis, S. Voutetakis and I. Vasalos, "Biomass pyrolysis in a circulating fluid bed reactor for the production of fuels and chemicals," *Fuel*, vol. 81, pp. 2087-2095, 2002.
- [75] V. Paasikallio, C. Lindfors, E. Kuoppala, Y. Solantausta, A. Oasmaa, J. Lehto and J. Lehtonen, "Product quality and catalyst deactivation in a four day catalytic fast pyrolysis production run," *Green Chemistry*, vol. 16, pp. 3549-3559, 2014.
- [76] J. Jae, R. Coolman, T. Mountziaris and G. W. Huber, "Catalytic fast pyrolysis of lignocellulosic biomass in a process development unit with continual catalyst addition and removal," *Chemical Engineering Science*, vol. 108, pp. 33-46, 2014.
- [77] S. Müller, Y. Liu, M. Vishnuvarthan, X. Sun, A. C. van Veen, G. L. Haller, M. Sanchez-Sanchez and J. A. Lercher, "Coke formation and deactivation pathways on H-ZSM-5 in the conversion of

- methanol to olefins," *Journal of Catalysis*, vol. 325, pp. 48-59, 2015.
- [78] H. S. Cerqueira, C. Sievers, G. Joly, P. Magnoux and J. A. Lercher, "Multitechnique characterization of coke produced during commercial resid FCC operation," *Industrial & engineering chemistry research*, vol. 44, no. 7, pp. 2069-2077, 2005.
- [79] H. Zhang, Y.-T. Cheng, T. P. Vispute, R. Xiao and G. W. Huber, "Catalytic conversion of biomass-derived feedstocks into olefins and aromatics with ZSM-5: the hydrogen to carbon effective ratio," *Energy & Environmental Science*, vol. 4, pp. 2297-2307, 2011.
- [80] A. Corma, G. W. Huber, L. Sauvanaud and P. O'connor, "Processing biomass-derived oxygenates in the oil refinery: catalytic cracking (FCC) reaction pathways and role of catalyst," *Journal of Catalysis*, vol. 247, pp. 307-327, 2007.
- [81] P. R. Patwardhan, D. L. Dalluge, B. H. Shanks and R. C. Brown, "Distinguishing primary and secondary reactions of cellulose pyrolysis," *Bioresource technology*, vol. 102, pp. 5265-5269, 2011.
- [82] W. J. DeSisto, N. Hill, S. H. Beis, S. Mukkamala, J. Joseph, C. Baker, T.-H. Ong, E. A. Stemmler, M. C. Wheeler, B. G. Frederick and others, "Fast pyrolysis of pine sawdust in a fluidized-bed reactor," *Energy & Fuels*, vol. 24, pp. 2642-2651, 2010.
- [83] P. R. Patwardhan, R. C. Brown and B. H. Shanks, "Understanding the fast pyrolysis of lignin," *ChemSusChem*, vol. 4, pp. 1629-1636, 2011.
- [84] M. S. Talmadge, R. M. Baldwin, M. J. Bidy, R. L. McCormick, G. T. Beckham, G. A. Ferguson, S. Czernik, K. A. Magrini-Bair, T. D. Foust, P. D. Metelski and others, "A perspective on oxygenated species in the refinery integration of pyrolysis oil," *Green Chemistry*, vol. 16, pp. 407-453, 2014.
- [85] T. R. Carlson, G. A. Tompsett, W. C. Conner and G. W. Huber, "Aromatic production from catalytic fast pyrolysis of biomass-derived feedstocks," *Topics in Catalysis*, vol. 52, no. 3, pp. 241-252, 2009.
- [86] M. Breyse, E. Furimsky, S. Kasztelan, M. Lacroix and G. Perot, "Hydrogen activation by transition metal sulfides," *Catalysis Reviews*, vol. 44, pp. 651-735, 2002.
- [87] S. Thangalazhy-Gopakumar, S. Adhikari, R. B. Gupta, M. Tu and S. Taylor, "Production of hydrocarbon fuels from biomass using catalytic pyrolysis under helium and hydrogen environments," *Bioresource Technology*, vol. 102, pp. 6742-6749, 2011.
- [88] H. J. Park, Y.-K. Park, J.-S. Kim, J.-K. Jeon, K.-S. Yoo, J.-H. Yim, J. Jung and J. M. Sohn, "Bio-oil upgrading over Ga modified zeolites in a bubbling fluidized bed reactor," *Studies in Surface Science and Catalysis*, vol. 159, pp. 553-556, 2006.

- [89] S. Kelkar, C. M. Saffron, Z. Li, S.-S. Kim, T. J. Pinnavaia, D. J. Miller and R. Kriegel, "Aromatics from biomass pyrolysis vapour using a bifunctional mesoporous catalyst," *Green Chemistry*, vol. 16, pp. 803-812, 2014.
- [90] E. Iliopoulou, S. Stefanidis, K. Kalogiannis, A. Psarras, A. Delimitis, K. Triantafyllidis and A. Lappas, "Pilot-scale validation of Co-ZSM-5 catalyst performance in the catalytic upgrading of biomass pyrolysis vapours," *Green Chemistry*, vol. 16, pp. 662-674, 2014.
- [91] S. Vichaphund, D. Aht-ong, V. Sricharoenchaikul and D. Atong, "Catalytic upgrading pyrolysis vapors of Jatropa waste using metal promoted ZSM-5 catalysts: An analytical PY-GC/MS," *Renewable Energy*, vol. 65, pp. 70-77, 2014.
- [92] F. Melligan, M. Hayes, W. Kwapinski and J. Leahy, "Hydro-pyrolysis of biomass and online catalytic vapor upgrading with Ni-ZSM-5 and Ni-MCM-41," *Energy & Fuels*, vol. 26, pp. 6080--6090, 2012.
- [93] S. Thangalazhy-Gopakumar, S. Adhikari and R. B. Gupta, "Catalytic pyrolysis of biomass over H+ZSM-5 under hydrogen pressure," *Energy & fuels*, vol. 26, pp. 5300-5306, 2012.
- [94] A. Campanella and M. P. Harold, "Fast pyrolysis of microalgae in a falling solids reactor: Effects of process variables and zeolite catalysts," *Biomass and Bioenergy*, vol. 46, pp. 218-232, 2012.
- [95] S. Cheng, L. Wei, X. Zhao, Y. Huang, D. Raynie, C. Qiu, J. Kiratu and Y. Yu, "Directly catalytic upgrading bio-oil vapor produced by prairie cordgrass pyrolysis over Ni/HZSM-5 using a two stage reactor," *AIMS Energy*, vol. 3, pp. 227-240, 2015.
- [96] P. A. Horne and P. T. Williams, "Influence of temperature on the products from the flash pyrolysis of biomass," *Fuel*, vol. 75, no. 9, 1996.
- [97] T. R. Carlson, T. P. Vispute and G. W. Huber, "Green gasoline by catalytic fast pyrolysis of solid biomass derived compounds," *ChemSusChem*, vol. 1, no. 5, pp. 397-400, 2008.
- [98] C. Watanabe, T. Ramus, R. Meijboom and B. Freeman, "A new technique for the rapid characterization of catalysts: Tandem micro-reactor--gas chromatography/mass spectrometry," *Environmental Progress & Sustainable Energy*, vol. 33, pp. 688-692, 2014.
- [99] J. J. Bozell, S. K. Black, M. Myers, D. Cahill, W. P. Miller and S. Park, "Solvent fractionation of renewable woody feedstocks: Organosolv generation of biorefinery process streams for the production of biobased chemicals," *biomass and bioenergy*, vol. 35, pp. 4197-4208, 2011.
- [100] A. R. Stanton, S. Czernik and K. Iisa, "Effect of Biomass Pretreatment Methods on Hydrocarbon Production during Catalytic Fast Pyrolysis of Pine," *American Chemical Society. Abstracts of Papers of the 243rd ACS National Meeting, 25-29 March 2012, San Diego, California*, 2012.

- [101] Z. a. L. S. a. W. Q. Yu, A. Zheng, X. Jun, L. Chen and F. Deng, "Brønsted/Lewis acid synergy in H-ZSM-5 and H-MOR zeolites studied by ^1H and ^{27}Al DQ-MAS solid-state NMR spectroscopy," *The Journal of Physical Chemistry C*, vol. 115, pp. 22320-22327, 2011.
- [102] V. Agarwal, P. J. Dauenhauer, G. W. Huber and S. M. Auerbach, "Ab initio dynamics of cellulose pyrolysis: Nascent decomposition pathways at 327 and 600 C," *Journal of the American Chemical Society*, vol. 134, pp. 14958-14972, 2012.
- [103] M. S. Mettler, S. H. Mushrif, A. D. Paulsen, A. D. Javadekar, D. G. Vlachos and P. J. Dauenhauer, "Revealing pyrolysis chemistry for biofuels production: Conversion of cellulose to furans and small oxygenates," *Energy & Environmental Science*, vol. 1, pp. 5414-5424, 2012.
- [104] J. Sluiter and A. Sluiter, "Summative mass closure," *Laboratory analytical procedure_Review and integration. National renewable energy laboratory*, 2011.
- [105] J. B. Sluiter, R. O. Ruiz, C. J. Scarlata, A. D. Sluiter and D. W. Templeton, "Compositional analysis of lignocellulosic feedstocks. 1. Review and description of methods," *Journal of agricultural and food chemistry*, vol. 58, pp. 9043-9053, 2010.
- [106] M. Bjørgen, S. Svelle, F. Joensen, J. Nerlov, S. Kolboe, F. Bonino, L. Palumbo, S. Bordiga and U. Olsbye, "Conversion of methanol to hydrocarbons over zeolite H-ZSM-5: On the origin of the olefinic species," *Journal of Catalysis*, vol. 249, pp. 195-207, 2007.
- [107] U. Olsbye, S. Svelle, M. Bjørgen, P. Beato, T. V. Janssens, F. Joensen, S. Bordiga and K. P. Lillerud, "Conversion of methanol to hydrocarbons: how zeolite cavity and pore size controls product selectivity," *Angewandte Chemie International Edition*, vol. 51, pp. 5810-5831, 2012.
- [108] C. Mukarakate, J. D. McBrayer, T. J. Evans, S. Budhi, D. J. a. I. K. Robichaud, J. ten Dam, M. J. Watson, R. M. Baldwin and M. R. Nimlos, "Catalytic fast pyrolysis of biomass: the reactions of water and aromatic intermediates produces phenols," *Green Chemistry*, vol. 17, pp. 4217-4227, 2015.
- [109] L. Rodriguez-González, F. Hermes, M. Bertmer, E. Rodriguez-Castellón, A. Jiménez-López and U. Simon, "The acid properties of H-ZSM-5 as studied by NH₃-TPD and Al-MAS-NMR spectroscopy," *Applied Catalysis A: General*, vol. 328, pp. 174-182, 2007.
- [110] H. Song, L. Zhang, R. B. Watson, D. Braden and U. S. Ozkan, "Investigation of bio-ethanol steam reforming over cobalt-based catalysts," *Catalysis Today*, vol. 129, pp. 346-354, 2007.
- [111] K. Murugappan, C. Mukarakate, S. Budhi, M. Shetty, M. R. Nimlos and Y. Román-Leshkov, "Supported molybdenum oxides as effective catalysts for the catalytic fast pyrolysis of lignocellulosic biomass," *Green Chemistry*, vol. 18, pp. 5548-5557, 2016.
- [112] S. Stefanidis, K. Kalogiannis, E. Iliopoulou, A. Lappas and P. Pilavachi, "In-situ upgrading of biomass pyrolysis vapors: catalyst screening on a fixed bed reactor," *Bioresource technology*, vol.

102, pp. 8261-8267, 2011.

- [113] M. B. Griffin, G. A. Ferguson, D. A. Ruddy, M. J. Bidy, G. T. Beckham and J. A. Schaidle, "Role of the support and reaction conditions on the vapor-phase deoxygenation of m-Cresol over Pt/C and Pt/TiO₂ catalysts," *ACS Catalysis*, vol. 6, pp. 2715-2727, 2016.
- [114] D. A. Ruddy, J. A. Schaidle, J. R. Ferrell III, J. Wang, L. Moens and J. E. Hensley, "Recent advances in heterogeneous catalysts for bio-oil upgrading via "ex situ catalytic fast pyrolysis": catalyst development through the study of model compounds," *Green Chemistry*, vol. 16, pp. 454-490, 2014.